Pontifícia Universidade Católica
do Rio de Janeiro

Natasha Barros de Oliveira Hirschfeldt

Stability analysis applied to mechanical, electromagnetic and electromechanical systems with parametric excitation

Dissertação de Mestrado

Dissertation presented to the Programa de Pós–graduação em Engenharia Mecânica of PUC-Rio in partial fulfillment of the requirements for the degree of Mestre em Engenharia Mecânica.

Advisor : Prof. Roberta de Queiroz Lima
Co-advisor: Prof. Rubens Sampaio Filho

Rio de Janeiro
November 2022

Pontifícia Universidade Católica
do Rio de Janeiro

Natasha Barros de Oliveira Hirschfeldt

Stability analysis applied to mechanical, electromagnetic and electromechanical systems with parametric excitation

Dissertation presented to the Programa de Pós–graduação em Engenharia Mecânica of PUC-Rio in partial fulfillment of the requirements for the degree of Mestre em Engenharia Mecânica. Approved by the Examination Committee.

Prof. Roberta de Queiroz Lima
Advisor
Departamento de Engenharia Mecânica – PUC-Rio

Prof. Rubens Sampaio Filho
Co-advisor
Pontifícia Universidade Católica do Rio de Janeiro – PUC-Rio

Prof. Daniel Alves Castello
Universidade Federal do Rio de Janeiro – UFRJ

Prof. Hamilton Faria Leckar
Universidade Federal Fluminense – UFF

Rio de Janeiro, November 24th, 2022

Natasha Barros de Oliveira Hirschfeldt

Bachelor of Science in Mechanical Engineering by the Pontifical Catholic University of Rio de Janeiro (PUC-Rio).

Ficha Catalográfica

Hirschfeldt, Natasha Barros de Oliveira

Stability analysis applied to mechanical, electromagnetic and electromechanical systems with parametric excitation / Natasha Barros de Oliveira Hirschfeldt; advisor: Roberta de Queiroz Lima; co-advisor: Rubens Sampaio Filho. – 2022.

115 f. : il. color. ; 30 cm

Dissertação (mestrado) – Pontifícia Universidade Católica do Rio de Janeiro, Departamento de Engenharia Mecânica, 2022.

Inclui bibliografia

1. Engenharia Mecânica – Teses. 2. Análise de estabilidade. 3. Excitação paramétrica. 4. Teoria de Floquet. 5. Estabilidade de Lyapunov. 6. Sistemas eletromecânicos. I. Lima, Roberta de Queiroz. II. Sampaio Filho, Rubens. III. Pontifícia Universidade Católica do Rio de Janeiro. Departamento de Engenharia Mecânica. IV. Título.

CDD: 621

Acknowledgments

I would like to begin by thanking my advisor Roberta Lima and Professor Rubens Sampaio for the support and guidance during my studies, as well as the other members of the Dynamics and Vibrations laboratory that made the daily life there so welcoming. I wish to specially thank Gustavo Wagner that taught me a lot in the first year of my Master studies and also Héctor Eduardo Goicoechea and Mariana Gomes, that helped me through the final months of it. I also thank Zacharias Kraus and Professor Peter Hagedorn from Technical University Darmstadt (DTU) for the collaboration with our laboratory and the Probral project (88881.143828/2017-01 Edital nº 12/2017) that made their visit to Brazil possible. This study was financed in part by the Coordenação de Aperfeiçoamento de Pessoal de Nível Superior Brasil (CAPES) Finance Code 001. I also acknowledge the financial support given by the Brazilian agencies FAPERJ and CNPq.

I am grateful for my family's support at all times, especially my parents Valéria Barros and Robert Hirschfeldt for always encouraging me to pursue the path of research. The little kid that once said she would become a scientist could not have got to this stage without their help.

Moreover, this dissertation would not be possible without all the time and words of encouragement of my closest friends, especially Luiz Leão, Luiza Goto and Marcella Meirelles. They listened to all of my ideas, plans and engineering talk, giving me all I wanted and needed to get where I am now.

Abstract

Hirschfeldt, Natasha; Lima, Roberta (Advisor); Sampaio, Rubens (Co-Advisor). **Stability analysis applied to mechanical, electromagnetic and electromechanical systems with parametric excitation**. Rio de Janeiro, 2022. 115p. Dissertação de mestrado – Departamento de Engenharia Mecânica, Pontifícia Universidade Católica do Rio de Janeiro.

Parametric excitation is a type of excitation that arises from time-varying coefficients in a system's dynamics. More specifically, this dissertation deals with time-periodic coefficients. This type of excitation has been an extended topic of research from the fields of mechanics and electronics to fluid dynamics. It appears in problems involving dynamical systems, for example, as a way of controlling vibrations in self-excited systems, making this subject worthy of more investigations. By approaching stability in the sense of Lyapunov, this dissertation provides a didactic stability background from basic concepts, such as equilibrium points and phase diagrams, to more advanced ones, like parametric excitation and Floquet theory. The objects of study here are linear systems with time-periodic parameters. Floquet theory is used to make stability statements about the system's trivial solution. Several examples are discussed by making use of a developed numerical procedure to construct stability maps and phase diagrams. The examples presented herein encompass mechanical, electromagnetic and electromechanical systems. By making use of stability maps, several features that can be discussed in stability analysis are approached. Two different strategies to evaluate the stability of the trivial solution are compared: Floquet multipliers and the maximum value of Lyapunov characteristic exponents.

Keywords

Stability analysis; parametric excitation; Floquet theory; Lyapunov stability; electromechanical systems;

Resumo

Hirschfeldt, Natasha; Lima, Roberta; Sampaio, Rubens. **Análise de estabilidade aplicada em sistemas mecânicos, eletromagnéticos e eletromecânicos com excitação paramétrica**. Rio de Janeiro, 2022. 115p. Dissertação de Mestrado – Departamento de Engenharia Mecânica, Pontifícia Universidade Católica do Rio de Janeiro.

Excitação paramétrica se dá a partir de coeficientes variantes no tempo na dinâmica de um sistema. Este tipo de excitação tem sido um amplo tema de pesquisa desde os campos da mecânica e eletrônica até dinâmica de fluidos. Ela aparece em problemas envolvendo sistemas dinâmicos, por exemplo, como uma forma de controle de vibrações em sistemas auto excitados, tornando este assunto digno de mais investigações. Abordando estabilidade no sentido de Lyapunov, esta dissertação fornece uma base didática de estabilidade desde conceitos básicos, como pontos de equilíbrio e planos de fase, até conceitos mais avançados, como excitação paramétrica e teoria de Floquet. Os objetos de estudo aqui são sistemas lineares com parâmetros periódicos no tempo, o que permite usar a teoria de Floquet para fazer afirmações a respeito da estabilidade da solução trivial do sistema. Vários exemplos são discutidos fazendo uso de um procedimento numérico desenvolvido para construir mapas de estabilidade e planos de fase. Os exemplos apresentados abrangem sistemas mecânicos, eletromagnéticos e eletromecânicos. Fazendo uso de mapas de estabilidade, diversas características de análise de estabilidade são abordadas. Duas estratégias diferentes para avaliar a estabilidade da solução trivial são comparadas: multiplicadores de Floquet e valor máximo dos expoentes característicos de Lyapunov.

Palavras-chave

Análise de estabilidade; excitação paramétrica; teoria de Floquet; estabilidade de Lyapunov; sistemas eletromecânicos;

Table of contents

1 Introduction **12**
1.1 Objectives of the dissertation 13
1.2 Dissertation's outline 13

2 Initial concepts **15**
2.1 Resonance 16
2.2 Stability and instability 17
2.2.1 Equilibrium points 18
2.2.2 Phase diagrams 18
2.3 Linearization around equilibrium points 27

3 Stability analysis **31**
3.1 Types of excitation 32
3.1.1 Self-excited systems 32
3.1.2 Parametric systems 33
3.2 Lyapunov stability 36
3.3 Linear time-periodic systems (Floquet theory) 37
3.3.1 Stability maps and parametric resonance 44

4 Stability analysis examples **49**
4.1 SDoF examples: Mathieu's equation 50
4.1.1 Case I: undamped system 50
4.1.2 Case II: damped system 54
4.2 2DoF examples: mechanical and electromagnetic systems 56
4.2.1 Case I: undamped system with one time-periodic coefficient 57
4.2.2 Case II: damped system with two time-periodic coefficients 62
4.2.3 Case III: damped system with one time-periodic coefficient 65

5 Electromechanical systems **73**
5.1 Stability analysis for time-periodic electromechanical systems 74
5.1.1 Electromagnetic loudspeaker 74
5.1.1.1 Case I: undamped autonomous model 75
5.1.1.2 Case II: undamped non-autonomous model with a voltage source 79
5.1.1.3 Case III: undamped non-autonomous model with parametric excitation 80
5.1.1.4 Case IV: damped non-autonomous model with parametric excitation 83

6 Conclusions **85**

A Free vibration and harmonic excitation of a SDoF system **87**
A.1 Response to free vibration 87
A.2 Response to harmonic excitation 91

B Floquet's theorem **96**

C Dynamics of electromagnetic systems **99**

D Dynamics of electromechanical systems **103**
D.1 Example: electromagnetic loudspeaker 103

E Numerical procedure **106**
E.1 General discussions 110

Bibliography **112**

List of figures

Figure 2.1 Undamped SDoF system with an applied external force. 16
Figure 2.2 Stability of an equilibrium point. 18
Figure 2.3 SDoF system with free vibration. 19
Figure 2.4 Phase diagram composed by centers. 21
Figure 2.5 Phase diagram composed by saddles. 22
Figure 2.6 Phase diagram composed by lines. 23
Figure 2.7 Phase diagram composed by stable spirals. 24
Figure 2.8 Phase diagram composed by stable nodes. 24
Figure 2.9 Bifurcation diagram of the linear autonomous system. 26
Figure 2.10 Simple pendulum. 28
Figure 2.11 Simple pendulum's phase diagram. 29

Figure 3.1 SDoF model of an aircraft wing. 32
Figure 3.2 Solution of the SDoF model of an aircraft wing, with $a = 1$, $\phi = 0$, $\omega_n = 2$ and $\xi = -0.1$. 33
Figure 3.3 Pendulum with an oscillating support. 34
Figure 3.4 LC circuit with a time-varying capacitance. 35
Figure 3.5 Stability of a motion in the sense of Lyapunov. 37
Figure 3.6 Transition curves in the $\omega/\omega_n \times \epsilon$ plane, for $p = 1$ and 2. 47

Figure 4.1 Stability maps for the undamped Mathieu's equation with $\delta = 4$ and 9, respectively. 51
Figure 4.2 Stability maps using Λ for the undamped Mathieu's equation for $\delta = 4$ and 9, respectively. 51
Figure 4.3 The maximum value of the LCEs Λ for the undamped Mathieu's equation with $\epsilon = 1$ and $\delta = 4$ and 9, respectively. 52
Figure 4.4 Stability maps for the undamped Mathieu's equation for $\omega = 1, 2, 3$ and 4, respectively. 53
Figure 4.5 Stability maps using Λ for the undamped Mathieu's equation for $\omega = 1, 2, 3$ and 4, respectively. 54
Figure 4.6 Phase diagrams for the undamped Mathieu's equation for $\omega = 1, 2, 3$ and 4, respectively, for $\delta = 4$ and $\epsilon = 2$. 55
Figure 4.7 Stability maps for the damped Mathieu's equation with $b = 0.1$ and $\omega = 1$ and 3, respectively. 56
Figure 4.8 Stability maps for the damped Mathieu's equation with $b = 0.5$ and $\omega = 1$ and 3, respectively. 56
Figure 4.9 Stability maps using Λ for the damped Mathieu's equation with $b = 0.1$ and $\omega = 1$ and 3, respectively. 57
Figure 4.10 Stability maps using Λ for the damped Mathieu's equation with $b = 0.5$ and $\omega = 1$ and 3, respectively. 57
Figure 4.11 2DoF mechanical system with its electromagnetic equivalent system for case I. 58
Figure 4.12 Stability map for the 2DoF system with $k = k_2 = k_3 = 1$. 59
Figure 4.13 Stability map for the 2DoF system with $k = k_2 = k_3 = 1$ using Λ. 60

Figure 4.14 $\omega \times \Lambda$ plot for the system with $k = k_2 = k_3 = 1$. 60
Figure 4.15 Phase diagrams for $y_1 \times \dot{y}_1$ with $\omega = 1.5$, $k = k_2 = k_3 = 1$ and $\epsilon = 0.3$, where the start points are marked with red dots and the numerical approximations at the final time are marked with black dots. 61
Figure 4.16 Phase diagrams for $y_2 \times \dot{y}_2$ with $\omega = 1.5$, $k = k_2 = k_3 = 1$ and $\epsilon = 0.3$, where the start points are marked with red dots and the numerical approximations at the final time are marked with black dots. 61
Figure 4.17 2DoF mechanical system with its electromagnetic equivalent system for case II. 62
Figure 4.18 Stability map for the 2DoF system with $k = k_2 = 1$ and $b_1 = b_2 = 0.1$. 63
Figure 4.19 Stability map for the 2DoF system with $k = k_2 = 1$ and $b_1 = b_2 = 0.1$ using Λ. 63
Figure 4.20 $\omega \times \Lambda$ plot for the system with $k = k_2 = 1$ and $b_1 = b_2 = 0.1$. 64
Figure 4.21 Numerical approximations with $\epsilon = 0.3$ and $\omega = 4$. 65
Figure 4.22 Phase diagrams with $\epsilon = 0.3$ and $\omega = 4$. 65
Figure 4.23 2DoF mechanical system with its electromagnetic equivalent system for case IV. 66
Figure 4.24 Stability map in the $\omega \times \epsilon$ plane for the 2DoF system with $k_1 = 3$, $k = 1$ and $b = 0.2$. 67
Figure 4.25 Stability map in the $\omega \times \epsilon$ plane for the 2DoF system with $k_1 = 3$, $k = 1$ and $b = 0.2$ using Λ. 68
Figure 4.26 $\omega \times \Lambda$ plot for the system with $k_1 = 3$, $k = 1$ and $b = 0.2$. 69
Figure 4.27 Phase diagrams with $\omega = 1$. 69
Figure 4.28 Phase diagrams with $\omega = \Delta$. 70
Figure 4.29 Numerical approximations of the system's response with $\epsilon = 0.3$ and $\omega = 1$. 70
Figure 4.30 Numerical approximations of the system's response with $\epsilon = 0.3$ and $\omega = \Delta$. 71
Figure 4.31 Phase diagrams with $\omega = 2\omega_2$. 71
Figure 4.32 Numerical approximations of the system's response with $\epsilon = 0.3$ and $\omega = 2\omega_2$. 72

Figure 5.1 Electromagnetic loudspeaker. 75
Figure 5.2 Numerical approximations when $\omega = \omega_{1,2} = 3$. 80
Figure 5.3 Electromagnetic loudspeaker's stability map in the $\omega \times \epsilon$ plane. 81
Figure 5.4 Electromagnetic loudspeaker's stability map in the $\omega \times \epsilon$ plane using Λ. 82
Figure 5.5 $\omega \times \Lambda$ plot for the electromagnetic loudspeaker with $\kappa = 8$, $\rho = 1$ and $\epsilon = 0.3$. 82
Figure 5.6 Electromagnetic loudspeaker's stability map in the $\omega \times \rho$ plane using Λ for $\epsilon = 0.3$. 83
Figure 5.7 Electromagnetic loudspeaker's stability map in the $\omega \times b$ plane using Λ. 84
Figure 5.8 Electromagnetic loudspeaker's stability map in the $r \times b$ plane using Λ. 84

Figure A.1 Solution of the undamped SDoF system. 88
Figure A.2 Effect of damping on the solution for free vibration. 91
Figure A.3 SDoF system with an applied external force. 91
Figure A.4 Solution of the undamped SDoF system with an external harmonic force, where $y_0 = v_0 = 0$, $\omega = \omega_n = 2$ and $f_0 = 1$. 94
Figure A.5 Effect of damping on the particular solution. 95

Figure C.1 2DoF electromagnetic system. 101

1
Introduction

The topic of stability analysis is of great interest when dealing with dynamic systems, with applications in simple systems such as pendulums and circuits to more complex ones such as ships and helicopters. This study not only provides additional knowledge of a system's behaviour through time, but can also be a way of finding possible improvements in terms of performance [1; 2; 3]. This study can be applied to time-invariant or time-variant systems, where the latter is the main object of study in this dissertation. The time-variant systems of most interest here are the parametrically excited ones. Parametric excitation is a type of excitation that arises from time-varying coefficients in a system's dynamics. More specifically, this dissertation deals with time-periodic coefficients.

Stability analysis is widely made in purely mechanical systems [4] as well as in purely electromagnetic ones [5]. A classic example of its applicability in parametrically excited systems is the Mathieu's equation, a differential equation capable of describing several real world problems. In the mechanical realm, Mathieu's equation can describe, for example, a pendulum with an oscillating support [6]. Meanwhile, in the electromagnetic realm it can describe an LC circuit with time-periodic capacitance [5]. Thus, there is a wide range of applications to stability analysis. By fully comprehending its use in the types of systems aforementioned, one can apply it to systems with both origins, called an electromechanical system. Thereby, the final goal in this dissertation is to apply stability analysis to electromechanical systems, more specifically, with time-periodic coefficients.

Electromechanical systems have two different natures: mechanical and electromagnetic [7; 8; 9; 10]. This means that the energies present in these systems also have distinct origins, mechanical (such as kinetic and potential energies) and electromagnetic (such as magnetic and electrical energies) [11; 12]. This class of system is characterized by the mutual interaction between its subsystems, meaning that the dynamics of the mechanical subsystems influence the dynamics of the electromagnetic subsystems as well as the inverse [13; 14; 15; 16; 17]. This mutual interaction is only possible through coupling elements that provide a way of exchanging energy among the subsystems. For

some linear electromechanical systems, these coupling terms appear in the equations of motion through gyroscopic and circulatory terms, matrices G and N, respectively, as it will be discussed latter on. For an accurate description of electromechanical system dynamics, it is not sufficient to describe each subsystem separately. Thus, it is necessary to take into account parameters of both mechanical and electromagnetic natures [18; 19]. To obtain their equations of motion it is possible to use, for example, energetic methods such as the Lagrangian method [8; 10]. Afterwords, it is possible to make a stability analysis for this type of system.

1.1 Objectives of the dissertation

This dissertation aims to make use of numerical simulations to evaluate the stability of a parametrically excited system's trivial solution by using Floquet theory. It is presented a step by step description of how to apply the theory to this type of system. The simulations were made by making use of the software *MatLab*, but the presented numerical procedure is given in a general form that provides a guide for the reader to implement it using other simulation softwares. Two different strategies to evaluate the stability of the trivial solution are presented: Floquet multipliers and the maximum value of Lyapunov characteristic exponents.

Following the introduction of the needed stability analysis concepts and the numerical procedure used to address stability, this theory and computational process are applied to several examples. Them being purely mechanical systems as well as purely electromagnetic systems, where the final goal is to apply this theory and computational process to an electromechanical system: the electromagnetic loudspeaker. More specifically, Floquet theory is going to be used to analyse the stability of its trivial solution when the system has a time-periodic coefficients.

1.2 Dissertation's outline

The dissertation is divided as follows. Chapter 2 introduces the ideas of resonance and instability, two concepts that are frequently confused. The basics of the resonance phenomenon are addressed in appendix A in more details. Some topics that are needed for a full understanding of stability are also discussed in the chapter. They are: equilibrium points, phase diagrams and linearization of nonlinear systems around equilibrium points.

Chapter 3 starts by discussing different types of excitation through examples. They are: self-excited systems and parametric systems. Externally excited systems have been treated in previous sections. Thereafter, the concept of stability according to Lyapunov is presented and stability analysis for linear time-periodic systems is dealt with, where Floquet theory is discussed. The concept of parametric resonance is also tackled. The chapter finishes by presenting stability maps, a very useful tool in studies involving stability analysis, as well as an approximation method to obtain the transition curves that separates unstable from stable regions. Floquet's theorem is given in details in appendix B.

In chapter 4, Floquet theory is applied first to the well known Mathieu's equation, for undamped and damped cases. After that, several examples of two degrees of freedom systems are also analyzed. Floquet theory is used to make stability statements of these examples' trivial solution while also making use of stability maps and phase portraits. The chapter's goal is to show how existing parametric excitation influences the stability of their trivial solution. This is accomplished by changing the elements of the system where there appears this type of excitation for different scenarios of two degrees of freedom systems. These scenarios include the association of purely mechanical systems with the purely electromagnetic systems that can be described by the same differential equations. Appendix C shows how to obtain the equations of motion of purely electromagnetic systems, where an example is given so the reader can compare the found dynamics with the examples in chapter 4.

Floquet theory is then applied in chapter 5 to electromechanical systems by making use of a system called electromagnetic loudspeaker, where different scenarios for this system are given. The consequences of existing time-periodic parameters in electromechanical systems are then discussed. Appendix D makes an introduction to electromechanical systems by discussing how to obtain their dynamics.

A summary is presented in chapter 6 of what was done in the dissertation as well as possible ways of continuing with this study. Also, the developed numerical procedure used throughout the dissertation is given in appendix E, where a step by step description of how to make stability statements of a system's trivial solution using Floquet theory and stability maps is shown.

2
Initial concepts

To start this study, take a linear system with n degrees of freedom (nDoF) in the general form of second order differential equations

$$M\ \ddot{y}(t)\ +\ [D+G]\ \dot{y}(t)\ +\ [K+N]\ y(t)\ =\ f, \tag{2-1}$$

where the response vector is $y(t) \in \mathbb{R}^n$ for $t > 0$, written as $y(t) = [y_1(t) \quad y_2(t) \quad ... \quad y_n(t)]^T$, with initial conditions $y(0) = y_0,\ \dot{y}(0) = v_0$, and $f \in \mathbb{R}^n$ represents external forces. The size of all the coefficient matrices is $n \times n$, but they have different features. These matrices have the following properties [20]:

- M is the *mass matrix*, that is symmetric ($M = M^T$) and positive definite ($M > 0$);
- K is the *stiffness matrix*, that is symmetric ($K = K^T$) and positive semi-definite ($K \geq 0$);
- D is the *damping matrix*, that is symmetric ($D = D^T$) and positive semi-definite ($D \geq 0$);
- G is the *gyroscopic matrix*, that is skew-symmetric ($G = -G^T$);
- N is the *circulatory matrix*, that is skew-symmetric ($N = -N^T$).

Equation (2-1) can be rewritten as

$$\ddot{y} = h(y, \dot{y}, t), \tag{2-2}$$

where y and its derivatives depend on time. A system is *autonomous* or *time-invariant* when there is no explicit dependency on time in equation (2-2), meaning that the coefficient matrices and external forces do not depend on time explicitly. Otherwise, it is called a *non-autonomous* or *time-variant* system [3].

Next, two fundamental concepts when dealing with dynamic systems are going to be discussed in this chapter: *resonance* and *instability*. Resonance occurs when the system's response is analyzed for a situation where there exists an imposed excitation, known as *forced response*. This phenomenon is briefly presented in section 2.1 and more discussions about this topic are given in appendix A. Afterwords, the idea of instability is introduced in section 2.2 when dealing with the *free response* of linear time-invariant systems [2].

2.1 Resonance

As previously mentioned, the resonance phenomenon appears when there is a forced response, meaning that an imposed excitation is applied to the system. Appendix A provides further content about resonance and how to obtain the solutions of mass-spring and mass-spring-damper systems, with free and forced vibrations.

Take here a single degree of freedom (SDoF) system with an applied external force, as depicted in figure 2.1. This system is composed by a mass m and a spring with stiffness coefficient k. The external force is harmonic of the form $f(t) = f_0 \cos(\omega t)$, where f_0 is its amplitude and ω, its frequency.

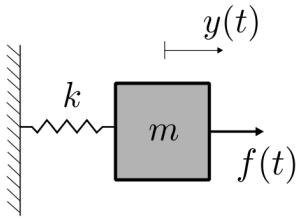

Figure 2.1: Undamped SDoF system with an applied external force.

The system's equation of motion is

$$\ddot{y}(t) + \omega_n^2 y(t) = F_0 \cos(\omega t), \tag{2-3}$$

where $\omega_n = \sqrt{k/m}$ is the natural frequency and $F_0 = f_0/m$. The initial conditions are $y(0) = y_0,\ \dot{y}(0) = v_0$. The total response $y(t)$ is the sum of an homogeneous solution $y_h(t)$, found by taking the system with free vibration, and by a particular solution $y_p(t)$, found by considering the applied external force. The response $y(t) = y_h(t) + y_p(t)$ can then be fully obtained by making use of the initial conditions.

The proposed particular solution is taken in the same form as the forcing term, being

$$y_p(t) = Y_0 \cos(\omega t), \tag{2-4}$$

where Y_0 is the amplitude of the forced response. By substituting this into equation (2-3), one gets that for the case where the natural frequency and the excitation frequency are not the same ($\omega \neq \omega_n$), the particular solution is

$$y_p(t) = \frac{F_0}{\omega_n^2 - \omega^2} \cos(\omega t).$$

The total solution $y(t)$ is a sum of the homogeneous and particular solutions, given by

$$y(t) = \frac{v_0}{\omega_n}\,\sin(\omega_n t) + \left(y_0 - \frac{F_0}{\omega_n^2 - \omega^2}\right)\,\cos(\omega_n t) + \frac{F_0}{\omega_n^2 - \omega^2}\,\cos(\omega t), \qquad (2\text{-}5)$$

where the provided initial conditions were already used as discussed in appendix A. It is possible to notice through equation (2-5) that the solution's amplitude becomes larger as the excitation frequency approaches the natural frequency, once the denominator of $\frac{F_0}{\omega_n^2 - \omega^2}$ becomes very small. When these values are equal ($\omega = \omega_n$) the previous solution does not apply anymore, once the proposed particular solution in equation (2-4) for this situation is also a solution for the homogeneous one. For this case, the particular solution must be of the form

$$y_p(t) = t\,Y_0\,\sin(\omega t).$$

Substituting this in the equation of motion, one can use the initial conditions to obtain the system's response for $\omega = \omega_n$, that is

$$y(t) = \frac{v_0}{\omega}\,\sin(\omega t) + y_0\,\cos(\omega t) + \frac{F_0}{2\omega}\,t\,\sin(\omega t).$$

By analyzing this result, one can see that for this given frequency the solution's amplitude grows indefinitely with a linear dependency on time. This is the definition of the *resonance phenomenon*.

2.2 Stability and instability

Now that the concept of resonance was briefly covered, the meaning of stability and instability will be discussed [20]. For a first intuition, take figure 2.2, where the behaviour of a pink ball in three different cases is going to be discussed. Take the case on the left, where if the ball is placed slightly to one of its sides, it will tend to come back to its rest position, the bottom of the "valley", considered a *stable* position. Now take the case in the middle of the same figure, where the ball is placed at the top of a hill. If the ball is perfectly placed at the peak, it will remain still, but if the ball is placed slightly to one of its sides, it will distance itself from the rest position indefinitely. This is considered an *unstable* position. The last case is considered *neutral*, where the ball would be on a smooth flat surface, neither returning to or distancing itself indefinitely from the original position.

These concepts have different applications depending on the system under analysis: whether it is a linear or nonlinear system, with free or forced vibration. In the remaining of this section, some basic concepts needed for stability analysis are addressed for linear time-invariant systems with free vibration.

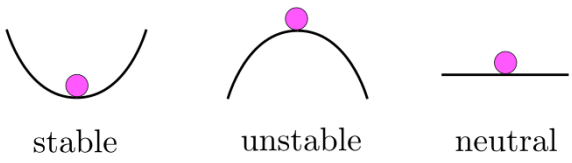

Figure 2.2: Stability of an equilibrium point.

2.2.1 Equilibrium points

Take equation (2-2) for a linear autonomous system. It can be rewritten as

$$\ddot{y} = h(y, \dot{y}), \tag{2-6}$$

where y and its derivatives depend on time. An *equilibrium point*, also called *fixed point*, is a point that satisfies

$$\begin{aligned} y(t) &= \text{constant} = y_{eq}, \\ \dot{y}(t) &= 0, \\ \ddot{y}(t) &= 0. \end{aligned} \tag{2-7}$$

This means that the particle is not moving, thus it is said to be stationary and can also be called a *stationary point*. To obtain these equilibrium points, one must find the trio $(y, \dot{y}, \ddot{y}) = (y_{eq}, 0, 0)$ that satisfy the equations of motion of the given system. It is possible to obtain none, one or even more than one equilibrium point for a given differential equation.

It is of interest now to discuss what happens to the particle at points that are not the equilibrium ones. If it is slightly moved from an equilibrium point, does the particle return to this position or continues to distance itself from it? If the former holds, the equilibrium point is said to be *stable*, while if the latter is true, the equilibrium point is said to be *unstable*. To define which of these cases hold, one can analyze *phase diagrams*.

2.2.2 Phase diagrams

Phase diagrams are graphs that allow one to evaluate the stability of an arbitrary number of solutions of a given dynamic system by plotting their trajectory in a phase plane [21]. Let us rewrite the second order differential

equation (2-6) in the form of two first order differential equations by doing

$$\begin{aligned} x &= \dot{y}, \\ \dot{x} &= h(y, \dot{y}). \end{aligned}$$

This leads to a simple way of obtaining phase diagrams. The goal of this approach is to evaluate stability without having to fully integrate the equations of motion. To exemplify this, take the SDoF system with free vibration in figure 2.3 [2; 20]. The system is composed by a mass m, a damper with damping coefficient b and a spring with stiffness coefficient k.

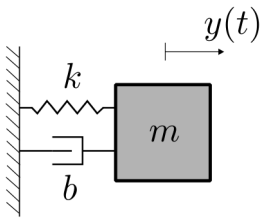

Figure 2.3: SDoF system with free vibration.

For this example, equation (2-1) reads

$$m\ddot{y}(t) + b\dot{y}(t) + ky(t) = 0, \tag{2-8}$$

with initial conditions taken as $y(0) = y_0,\ \dot{y}(0) = v_0$. Next, the equilibrium points for different scenarios are going to be obtained as well as phase diagrams for each one of them [22; 23]. Equation (2-8) can be rewritten in the form of equation (2-6) as

$$\ddot{y} = h(y, \dot{y}) = -\frac{b\dot{y}}{m} - \frac{ky}{m}.$$

If there is no damping in the system, meaning that we are dealing with a mass-spring system, the dynamics is given by

$$\ddot{y} = -\frac{ky}{m}. \tag{2-9}$$

Now, take the definition in equation (2-7) to classify a point as an equilibrium one. One can obtain it for this example by finding the trio $(y, \dot{y}, \ddot{y}) = (y_{eq}, 0, 0)$ satisfying the equation of motion (2-9). Thus, the equilibrium point y_{eq} for this system is

$$\begin{aligned} 0 &= h(y_{eq}, 0) = -\frac{ky_{eq}}{m}, \\ y_{eq} &= 0. \end{aligned}$$

To obtain the general form of the phase diagram, we can write the second order differential equation as two first order differential equations by doing

$$\begin{cases} x_1 = y \\ x_2 = \dot{y} \end{cases} \rightarrow \begin{cases} \dot{x}_1 = x_2 \\ \dot{x}_2 = \ddot{y} = -\dfrac{k}{m} x_1 \end{cases}$$

Dividing one equation by the other and integrating, one gets

$$\begin{aligned} \frac{\dot{x}_2}{\dot{x}_1} &= \frac{-\dfrac{k}{m}\, x_1}{x_2} \\ \int -\frac{k}{m}\, x_1\, dx_1 &= \int x_2\, dx_2 \\ -\frac{k}{m}\, \frac{x_1^2}{2} + c_1 &= \frac{x_2^2}{2} + c_2 \\ m\dot{y}^2 + ky^2 &= \text{constant}, \end{aligned}$$

that is a general form of an ellipse in the phase plane $y \times \dot{y}$. Taking $m = 1$ and $k = 1$, it becomes a circle given by

$$\dot{y}^2 + y^2 = \text{constant},$$

where the constant value depends on the initial conditions provided to the system. Figure 2.4 shows a schematic phase diagram for this case. The curves in the phase diagram for this linear time-invariant system are called *centers*. The circle's radius is defined by the square root of the right-hand side of the obtained relation, found by using the initial conditions in the integration process.

The blue arrows in figure 2.4 show the direction the particle follows in the phase paths. When the velocity $\dot{y}$ (the rate of change of the displacement y) is positive, the displacement is towards the right, increasing y. Meanwhile, the particle goes to the opposite direction when $\dot{y}$ is negative, decreasing y. Therefore, the phase diagram of the present example follows the clockwise direction.

The closed curves in the phase diagram represent periodic solutions around the equilibrium point, that is then said to be a stable one. The equilibrium point found before is depicted in figure 2.4 as a filled red circle, used to represent that it is a stable equilibrium point.

Another interesting approach is by making use of the concept of energy [23]. For example, take the equation of motion in (2-9)

$$m\ddot{y} + ky = 0.$$

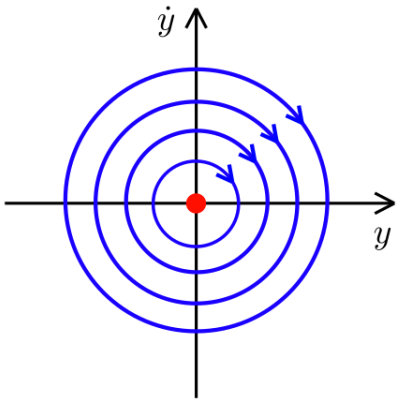

Figure 2.4: Phase diagram composed by centers.

Multiplying this by the velocity $\dot{y}$, one gets

$$\begin{aligned} m\ddot{y}\dot{y} + ky\dot{y} &= 0, \\ m\,\frac{d}{dt}\left(\frac{\dot{y}^2}{2}\right) + k\,\frac{d}{dt}\left(\frac{y^2}{2}\right) &= 0, \\ \frac{d}{dt}\left(\frac{1}{2}m\dot{y}^2 + \frac{1}{2}ky^2\right) &= 0, \end{aligned}$$

that are, respectively, the kinetic and potential energies. The system is conservative and, since the derivative is null, the sum of the energies must be equal to a constant. This results in

$$m\dot{y}^2 + ky^2 = \text{constant},$$

the same relation found before. Taking $m = 1$ and $k = 1$, this relation is describing circles, representing different energy levels that are defined by the circles' radius.

Moving on to another example, the situation changes if the system's dynamics is

$$m\ddot{y} - ky = 0,$$

that has the same equilibrium point as the last example. Taking $m = 1$ and $k = 1$, the curves are now described by

$$\dot{y}^2 - y^2 = \text{constant}.$$

Figure 2.5 shows the phase diagram for this case. The curves seen in the phase diagram for this linear time-invariant system are called *saddles*. The solutions are non-periodic and their directions are shown in the figure, found by following a reasoning analogous to the previous example. The equilibrium point is given as a red unfilled circle to represent that it is an unstable one, once the particle tends to distance itself from this point.

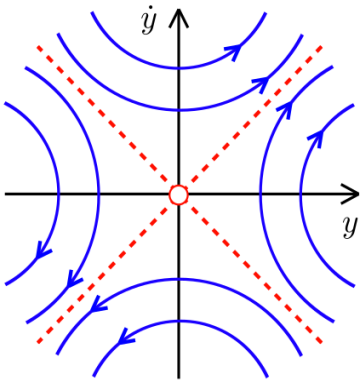

Figure 2.5: Phase diagram composed by saddles.

Continuing now with another example, if there is no stiffness in equation (2-8), meaning the system is only composed by a mass and a damper, the equation of motion is

$$\ddot{y} = -\frac{b\dot{y}}{m}. \tag{2-10}$$

Taking the definition in equation (2-7), one can finding the trio $(y, \dot{y}, \ddot{y}) = (y_{eq}, 0, 0)$ satifying the equation of motion (2-10) to obtain the equilibrium point, that is

$$0 = h(y_{eq}, 0).$$

This means that all points are equilibrium points, since $h(y_{eq}, 0) = 0$ for all values of y. Writing the second order differential equation as two first order differential equations, one obtains

$$\begin{cases} x_1 = y \\ x_2 = \dot{y} \end{cases} \rightarrow \begin{cases} \dot{x}_1 = x_2 \\ \dot{x}_2 = \ddot{y} = -\dfrac{b\dot{y}}{m} = -\dfrac{bx_2}{m} \end{cases}$$

Dividing one by the other,

$$\begin{aligned} \frac{\dot{x}_2}{\dot{x}_1} &= \frac{-\dfrac{b\,x_2}{m}}{x_2} = -\frac{b}{m}, \\ \int b\,dx_1 &= \int -m\,dx_2, \\ bx_1 + c_1 &= -mx_2 + c_2, \\ m\dot{y} + by &= \text{constant}. \end{aligned}$$

This means that the curves in the phase diagram are defined by *lines*. Making $m = 1$ and $b = 1$, for example,

$$\dot{y} + y = \text{constant}.$$

Figure 2.6 shows the corresponding phase diagram. The direction the

lines take are shown in the figure and they are towards the equilibrium points, which are then stable. The solutions are non-periodic and there are no oscillations around the equilibrium points.

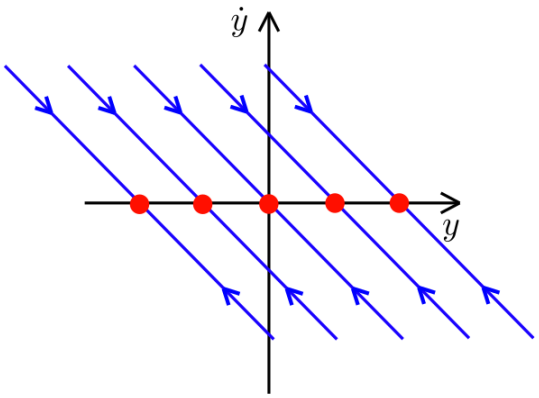

Figure 2.6: Phase diagram composed by lines.

Now, for a mass-damper-spring system, the equation of motion is

$$\ddot{y} = -\frac{b\dot{y}}{m} - \frac{ky}{m}.$$

Using equation (2-7), the equilibrium point is obtained as

$$\begin{aligned} 0 &= h(y_{eq}, 0) = -\frac{ky_{eq}}{m}, \\ y_{eq} &= 0. \end{aligned}$$

For this system, take $m = 1$ and $k = 1$. The phase diagrams differ depending on the value of the damping b. For example, with $b = 1$ (when the system is underdamped), the curves in the phase diagram of this linear time-invariant system are called *stable spirals* or *stable focus*. They have oscillatory solutions and the direction of the phase path is towards the equilibrium point, which is then stable, as seen in figure 2.7. Meanwhile, for $b = 3$ (when the system is overdamped) the curves in the phase diagram of this linear time-invariant system are called *stable nodes*. They represent non-periodic solutions with direction towards the equilibrium point, that is also stable, as seen in figure 2.8.

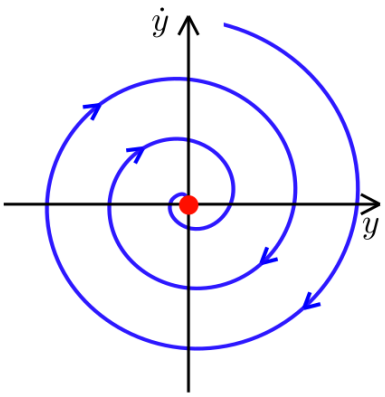

Figure 2.7: Phase diagram composed by stable spirals.

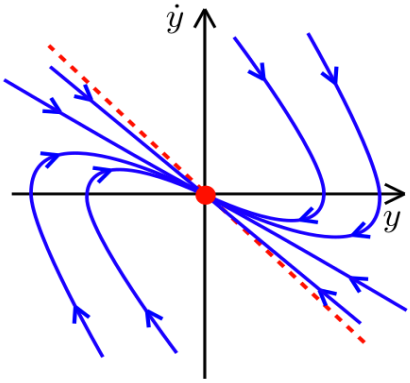

Figure 2.8: Phase diagram composed by stable nodes.

The examples shown until this point contained SDoF systems composed by a mass, a spring and/or a damper. Take now a generalization of this linear autonomous system in the first order form [22; 24]

$$\begin{bmatrix} \dot{x}_1(t) \\ \dot{x}_2(t) \end{bmatrix} = \begin{bmatrix} a_{11} & a_{12} \\ a_{21} & a_{22} \end{bmatrix} \begin{bmatrix} x_1(t) \\ x_2(t) \end{bmatrix},$$

$$\dot{x}(t) = A\,x(t),$$

where matrix A, composed by a_{ij}, is known as the coefficient matrix.

Solutions of the form $x = ue^{\lambda t}$ are wanted, where λ are the eigenvalues and u the respective eigenvectors. Substituting this in the above equation, the eigenvalue problem (EVP) that must be solved is $Au = u\lambda$, that leads to the

characteristic equation $\det[A - \lambda I] = 0$. Thus,

$$\begin{aligned} \det \begin{bmatrix} a_{11} - \lambda & a_{12} \\ a_{21} & a_{22} - \lambda \end{bmatrix} &= 0, \\ \lambda^2 - \mathrm{tr}(A)\lambda + \det(A) &= 0, \end{aligned}$$

where $\mathrm{tr}(A) = a_{11} + a_{22}$ is the trace of the coefficient matrix and $\det(A) = a_{11}a_{22} - a_{12}a_{21}$, its determinant. Solving for λ,

$$\lambda_{1,2} = \frac{\mathrm{tr}(A) \pm \sqrt{[\mathrm{tr}(A)]^2 - 4\,\det(A)}}{2}.$$

This relation makes it possible to draw a graphic to represent the types of curves obtained in phase diagrams in terms of the obtained trace and determinant, given in figure 2.9. This type of diagram is called a *bifurcation diagram* [24]. It provides important features: the light blue area represents the oscillatory responses; the remaining area of the graphic represents the non-oscillatory responses and the dark blue curve ($[\mathrm{tr}(A)]^2 = 4\,\det(A)$) is the limit between oscillatory and non-oscillatory responses.

Thus, it is possible to know the nature of the behaviour by analyzing the mentioned trace and determinant [22; 24], once they determine what happens to the obtained eigenvalues. The different possible ones are:

- $\det(A) > 0$ and $\mathrm{tr}(A) = 0$: for this situation, the eigenvalues assume purely imaginary values. This correspond to the case of *centers*, periodic solutions around the equilibrium point that is then stable;
- $\det(A) < 0$: this situation provides two purely real eigenvalues, one positive and another one negative. This correspond to the case of *saddles*, that have non-periodic solutions and an unstable equilibrium point;
- $\det(A) = 0$: here, the eigenvalue assumes a null value, corresponding to the case of *lines*, that can have stable or unstable equilibrium points;
- $\det(A) > 0$ and $[\mathrm{tr}(A)]^2 < 4\,\det(A)$: for this case, both eigenvalues are complex values with real part equal to $\mathrm{tr}(A)/2$. That is divided in two cases:
  - If $\mathrm{tr}(A) > 0$, the system's response is said to be unbounded, meaning that its amplitude increases indefinitely with time. This corresponds to the case of a *unstable spirals* (or *unstable focus*);
  - If $\mathrm{tr}(A) < 0$, it corresponds to the case of *stable spirals* (or *stable focus*), that have oscillatory solutions with direction towards the equilibrium point;

– $\det(A) > 0$ and $[\mathrm{tr}(A)]^2 > 4\det(A)$: here, the eigenvalues are two purely real numbers. It can also be divided in two cases:

  – If $\mathrm{tr}(A) > 0$, both eigenvalues are positive and, as time goes by, the solution's amplitude increases indefinitely. This situation corresponds to the case of *unstable nodes*;
  – If $\mathrm{tr}(A) < 0$, both eigenvalues are negative. These situation corresponds to the case of *stable nodes*.

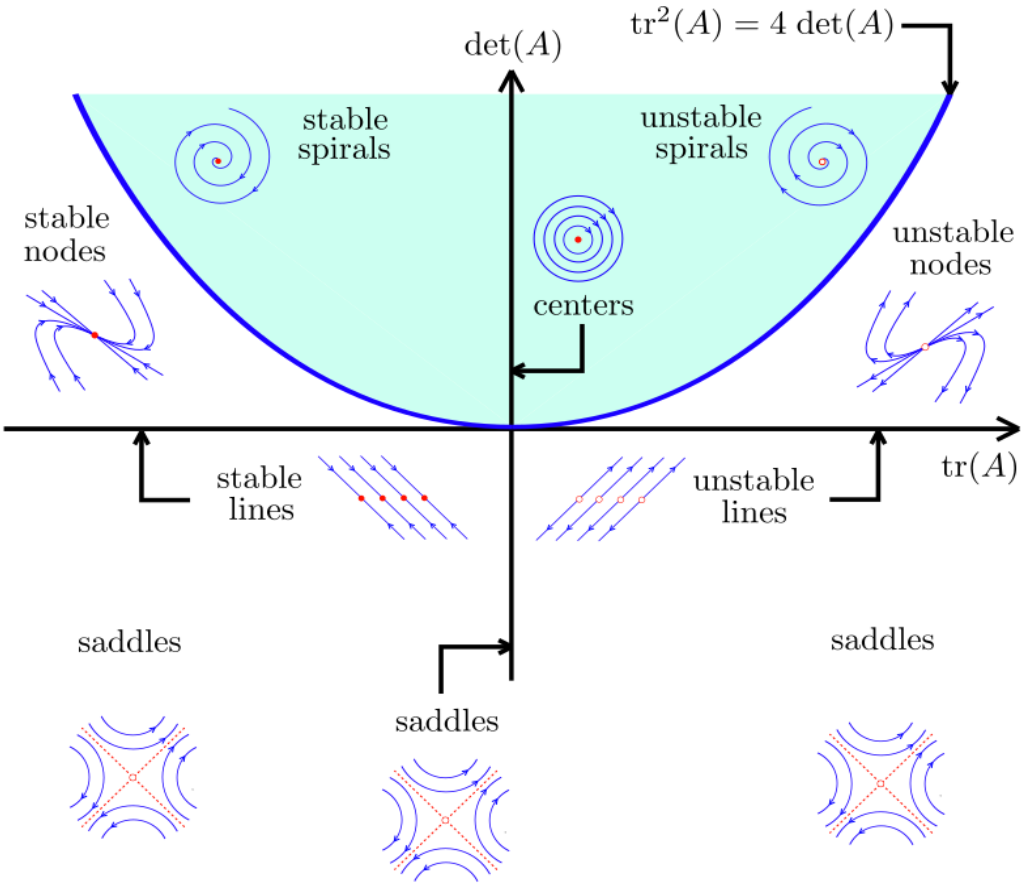

Figure 2.9: Bifurcation diagram of the linear autonomous system.

So far, the analysis was restricted to the free vibration of linear autonomous systems for simplification. Phase diagrams for this type of system are easy to obtain and visualize. Meanwhile, the visualization of phase diagrams for linear non-autonomous cases can be quite tricky due to the explicit dependency on time, thus it is not going to be treated at this point [21]. This topic is left for chapter 4, where several examples are treated and phase diagrams for this type of system, discussed.

2.3 Linearization around equilibrium points

Given a nonlinear system with equations of motion in the form of (2-6), it is possible to linearize its dynamics around equilibrium points by making use of Taylor's expansion into series [25]. By doing so, the discussions in section 2.2.2 can be applied to the neighbourhood of such points.

Take a function $h(y)$ infinitely differentiable. Its expansion into an infinite sum of terms is

$$h(y) = h(y_0) + \left.\frac{dh}{dy}\right|_{y_0} (y - y_0) + \left.\frac{d^2h}{dy^2}\right|_{y_0} \frac{(y-y_0)^2}{2!} + \left.\frac{d^3h}{dy^3}\right|_{y_0} \frac{(y-y_0)^3}{3!} + \dots \quad (2\text{-}11)$$

If we truncate this series, an approximation around point y_0 for the function $h(y)$ is obtained. The greater the number of terms used in the truncation, the more accurate will be the approximation around the given point. For example, if a linear approximation is wanted, equation (2-11) becomes

$$h(y) = h(y_0) + \left.\frac{dh}{dy}\right|_{y_0} (y - y_0).$$

If h is a function of two variables, y and $\dot{y}$ for example, its linear approximation around the point $(y_{eq}, \dot{y}_{eq})$ is

$$h(y, \dot{y}) \cong h(y_{eq}, \dot{y}_{eq}) + \left.\frac{\partial h}{\partial y}\right|_{y_{eq},\, \dot{y}_{eq}} (y - y_{eq}) + \left.\frac{\partial h}{\partial \dot{y}}\right|_{y_{eq},\, \dot{y}_{eq}} (\dot{y} - \dot{y}_{eq}).$$

This last approximation is now going to be used for a nonlinear system with equations of motion in the form of (2-6). Knowing that an equilibrium point is one satisfying equation (2-7), the linearization around an equilibrium point $(y_{eq},\ \dot{y}_{eq} = 0,\ \ddot{y}_{eq} = 0)$ is

$$\ddot{y} = h(y, \dot{y}) \cong h(y_{eq}, 0) + \left.\frac{\partial h}{\partial y}\right|_{y_{eq},\, \dot{y}_{eq}=0} (y - y_{eq}) + \left.\frac{\partial h}{\partial \dot{y}}\right|_{y_{eq},\, \dot{y}_{eq}=0} (\dot{y} - 0).$$

Since $h(y_{eq}, 0) = \ddot{y}_{eq} = 0$, the linearized function can be written as

$$\ddot{\chi} = \left.\frac{\partial h}{\partial y}\right|_{y_{eq},\, \dot{y}_{eq}=0} (\chi - y_{eq}) + \left.\frac{\partial h}{\partial \dot{y}}\right|_{y_{eq},\, \dot{y}_{eq}=0} (\dot{\chi} - 0).$$

To exemplify this, let us take a classical example of a simple pendulum and linearize it around its equilibrium points [23; 24]. This system is shown in figure 2.10. Gravity acceleration is taken as g, the pendulum's length is l_0 and its mass, m. Taking $g/l_0 = \omega_0^2$, the pendulum's dynamics is

$$\ddot{\theta} + \omega_0^2 \sin(\theta) = 0. \quad (2\text{-}12)$$

For our purpose here, it is useful to present this equation of motion in the form

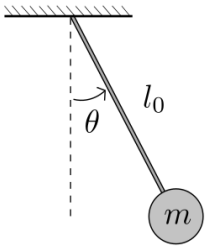

Figure 2.10: Simple pendulum.

$$\ddot{\theta} = h(\theta, \dot{\theta}) = -\omega_0^2 \sin(\theta).$$

Knowing (2-7), the system's equilibrium points are $\theta_{eq} = n\pi,\ n \in \mathbb{Z}$. Intuitively, one expects that when the pendulum is at its lower point, meaning $\theta = 0,\ 2\pi,\ 4\pi, ...$, the equilibrium positions are stable. Since the system is not damped, the mass tends to oscillate periodically around these positions if one moves it slightly to one of its sides. Meanwhile, when the pendulum is at its highest point, meaning $\theta = \pi,\ 3\pi,\ 5\pi, ...$, the equilibrium positions are unstable. The mass does not return to this position if one moves it slightly to one of its sides.

Let us verify this by taking the equilibrium points $\theta_{eq} = 0$ and $\theta_{eq} = \pi$. The other ones would result in the same conclusions since they merely represent more revolutions. For $\theta_{eq} = 0$ the following derivatives are needed:

$$\begin{aligned} \left.\frac{\partial h}{\partial \theta}\right|_{\theta_{eq}=0} &= -\omega_0^2\ \cos(\theta)|_{\theta_{eq}=0} = -\omega_0^2, \\ \left.\frac{\partial h}{\partial \dot{\theta}}\right|_{\theta_{eq}=0} &= 0. \end{aligned}$$

Thus, linearizing the equation of motion around this equilibrium point gives

$$\begin{aligned} \ddot{\chi} &= \left.\frac{\partial h}{\partial \theta}\right|_{\theta_{eq}=0} (\chi - \theta_{eq}) + \left.\frac{\partial h}{\partial \dot{\theta}}\right|_{\theta_{eq}=0} (\dot{\chi} - 0), \\ \ddot{\chi} &= -\omega_0^2(\chi - 0) + 0. \end{aligned}$$

Supposing $\omega_0^2 = 1$, this results in

$$\ddot{\chi} + \chi = 0,$$

which results in a center in the phase diagram, as done in the previous section and depicted in figure 2.4.

For the equilibrium point $\theta_{eq} = \pi$, the same procedure can be followed

by first obtaining the derivatives

$$\begin{aligned}\left.\frac{\partial h}{\partial \theta}\right|_{\theta_{eq}=\pi} &= -\omega_0^2 \ \cos(\theta)|_{\theta_{eq}=\pi} = \omega_0^2, \\ \left.\frac{\partial h}{\partial \dot{\theta}}\right|_{\theta_{eq}=\pi} &= 0.\end{aligned}$$

Then, the linearization around $\theta_{eq} = \pi$ is given by

$$\begin{aligned}\ddot{\chi} &= \left.\frac{\partial h}{\partial \theta}\right|_{\theta_{eq}=0} (\chi - \theta_{eq}) + \left.\frac{\partial h}{\partial \dot{\theta}}\right|_{\theta_{eq}=0} (\dot{\chi} - 0), \\ \ddot{\chi} &= \omega_0^2(\chi - \pi) + 0.\end{aligned}$$

Supposing once again $\omega_0^2 = 1$, this results in

$$\ddot{\chi} - \chi = -\pi.$$

Furthermore, by making the change of variables $\varphi = \chi - \pi$, one gets

$$\ddot{\varphi} - \varphi = 0,$$

which results in a saddle around $\theta_{eq} = \pi$ in the phase diagram, as shown in the previous section and depicted in figure 2.5.

Thus, the simple pendulum's motion is given by a nonlinear differential equation that can be linearized around its equilibrium points to evaluate stability in their neighbourhoods. Figure 2.11 shows the phase diagram for this system, where it is possible to see the stable and unstable equilibrium points as well as the different phase paths.

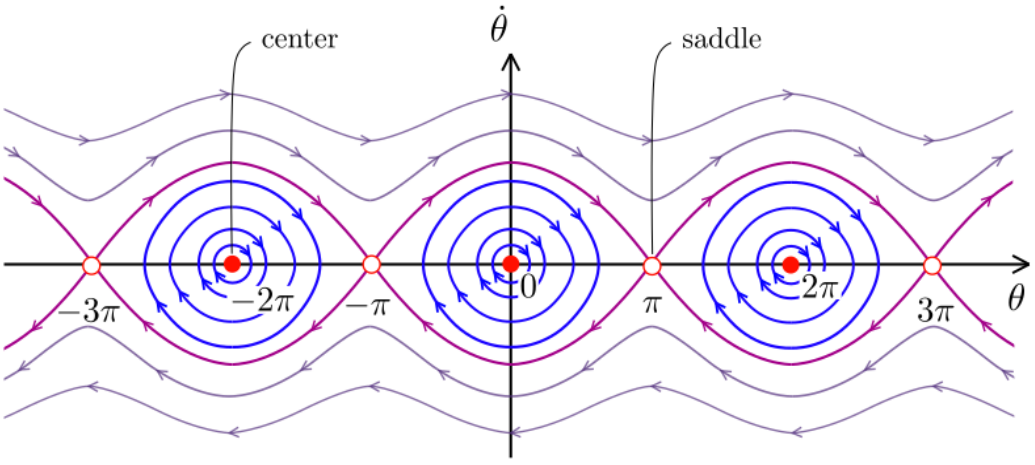

Figure 2.11: Simple pendulum's phase diagram.

For an intuitive perspective, imagine the pendulum is slightly placed out of its equilibrium point $\theta = 0$ (the vertical downward point). The pendulum's mass is then oscillating with a periodic motion in the vertical position. If now we slightly place it out of the equilibrium point $\theta = \pi$ (the vertical upward point), the mass will fall from this vertical position, following the phase path that leads it far from this equilibrium position.

Linear differential equations are quite particular cases to the vast world of equations, where many problems actually involve nonlinear formulations. However, obtaining solutions and/or phase diagrams for this type of system sometimes is not so trivial. Therefore, linearization around equilibrium points is of great interest in stability analysis. By doing so, one is able to make stability statements in the neighbourhood of such points by using previous knowledge of linear systems, as in section 2.2.2 for example. This makes it possible to better understand the behaviour of nonlinear systems around these equilibrium positions.

3
Stability analysis

In the previous chapter, we saw that phase diagrams are used to describe a system's solution given an initial state. On top of that, they can provide a set of solutions for different initial states [24]. Using this approach is simple when dealing with linear autonomous systems, but it is not trivial to apply this in other cases, such as nonlinear systems. To do so, one can use the already presented process of linearization around equilibrium points, making it possible to use the found linear differential equations to evaluate the behaviour of the original nonlinear system in the vicinity of such points.

Furthermore, evaluating phase diagrams for non-autonomous systems can also be challenging due to the explicit dependency of time. Thus, this chapter begins by presenting two different types of excitations while providing examples of each one. Afterwords, *stability of an equilibrium* is addressed by introducing the concept of stability in the sense of Lyapunov [2; 24; 26]. For the type of system that is of interest in this dissertation, meaning linear time-periodic systems, stability analysis of the trivial solution is then address. Criteria for stability classification of the zero solution of systems with parametric excitation are given. More specifically, Floquet theory is presented, a theory that provides a way of making stability statements about the trivial solution of linear systems with time-periodic coefficients [26; 27; 28].

The phenomenon of parametric resonance is also discussed and a perturbation method is used to obtain the curves that separates the unstable from the stable regions in stability maps, where the Mathieu's equation is used to exemplify its application.

3.1 Types of excitation

Now that the needed basic concepts from the previous chapter are clear, this section will introduce through some examples two different types of excitations that have not yet been addressed. They are: self-excitation and parametric excitation.

3.1.1 Self-excited systems

Self-excitation happens due to the interaction between the internal elements of a dynamic system [24]. This type of excitation can occur, for example, in rotating shafts due to the friction between internal components, also called internal damping [2; 4]. Another example of self-exciting oscillation is the vibration of an aircraft wing [2; 20], illustrated in figure 3.1. This last one is going to be analyzed in more details.

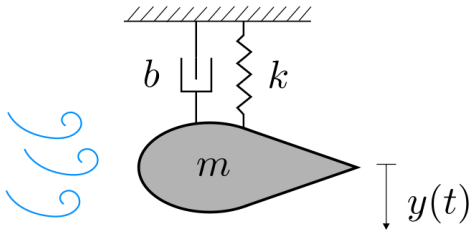

Figure 3.1: SDoF model of an aircraft wing.

The simplest aircraft wing model can be given as a SDoF system with equation of motion [20]

$$m\ddot{y} + b\dot{y} + ky = \beta\dot{y},$$

where m is its mass, b is the damping and k the stiffness of the aircraft wing. The right-hand side of this equation represents the aerodynamic forces that are imposed to the system, where β is a constant. This dynamics can be rewritten as

$$m\ddot{y} + (b - \beta)\dot{y} + ky = 0.$$

Two cases can be addressed: $b > \beta$ and $b < \beta$. If the former is true, the system's solution is given by one of the three cases of damped SDoF systems in appendix A. However, if the latter proceeds, then the damping ratio $\xi = \dfrac{(b-\beta)}{2m\omega_n}$ assumes a negative value, which leads to a solution in the form

$$y(t) = a\, e^{-\xi\omega_n t} \sin(\omega_d t + \phi).$$

where $\omega_d = \omega_n\sqrt{1-\xi^2}$. Since $\xi < 0$ for all $t > 0$, the system's response increases indefinitely with time, making it unstable. This behaviour can be seen in figure 3.2, where $y(t)$ is plotted for $a = 1$, $\phi = 0$, $\omega_n = 2$ and $\xi = -0.1$. This situation is also called flutter instability, a phenomenon that can happen to several engineering projects and that is unwanted.

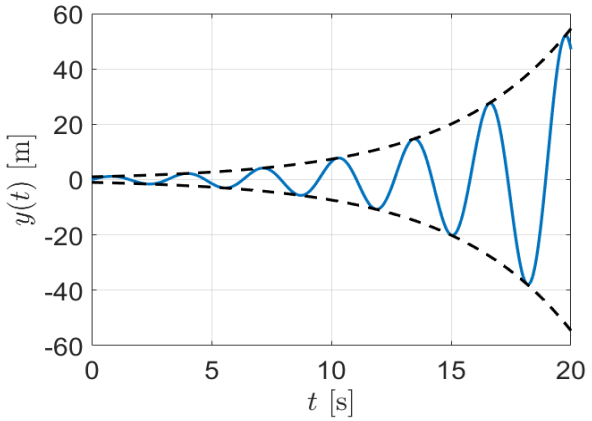

Figure 3.2: Solution of the SDoF model of an aircraft wing, with $a = 1$, $\phi = 0$, $\omega_n = 2$ and $\xi = -0.1$.

3.1.2 Parametric systems

A system is said to be *parametrically excited* when it has time-varying coefficients in its equations of motion. A common way of finding parametric excitation in literature is when parameters are not only time dependent, but are also periodic, called time-periodic coefficients. At the beginning of chapter 2, it was seen that, if equation (2-2) had a direct dependency on time, the system is said to be time-variant or non-autonomous. Therefore, parametric systems are non-autonomous systems.

An important feature of parametrically excited systems is that the phenomenon of *parametric resonance* may occur for some excitation frequencies [29; 30; 31]. This frequencies are dependent on the natural frequencies of the undamped system without parametric excitation [4; 3] , as discussed in more details in section 3.3.1.

A well known example of parametric excitation is in systems that can be described by the second order differential equation

$$\ddot{y} + b(t)\,\dot{y} + k(t)\,y = 0, \tag{3-1}$$

where $k(t) = k(t+T)$ and $b(t) = b(t+T)$ with $T > 0$, meaning that these coefficients are periodic. Taking the undamped case,

$$\ddot{y} + k(t)\, y = 0.$$

The generalization given by this equation is known as *Hill's equation* and it appears in several studies of real dynamic systems. A special case of a system that can be described by this equation is

$$\ddot{y} + [\delta + \epsilon \cos(\omega t)]\ y = 0, \tag{3-2}$$

called *Mathieu's equation* [22; 27; 32; 33], where δ, ϵ and ω are constant parameters. Since there are no dissipation terms, this equation is also known as *undamped Mathieu's equation.*

As an example, take a pendulum with an oscillating support, depicted in figure 3.3 [2; 29; 34]. This system is composed by a mass m and a rod of length l_0 with negligible mass. Gravity acceleration is taken as g and the vertical oscillation of the pendulum's support is $u_v(t) = u_a\cos(\omega t)$, where u_a is its amplitude and ω, its frequency.

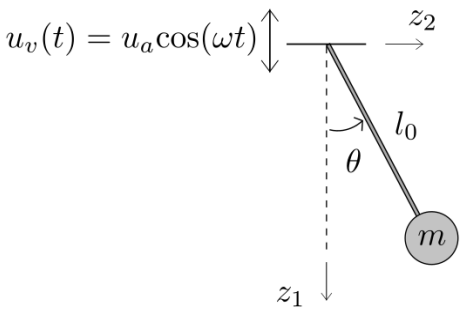

Figure 3.3: Pendulum with an oscillating support.

The general form of Mathieu's equation can be found by making use of, for example, Lagrange's method [6]. By knowing that $z_1 = l_0\cos(\theta)$ and $z_2 = l_0\sin(\theta)$, the kinetic energy T and potential energy V are

$$\begin{aligned} T &= \frac{1}{2}m\,\dot{z}_2^2 + \frac{1}{2}m\,(\dot{z}_1 - \dot{u}_v)^2 = \frac{m}{2}\left[l_0^2\dot{\theta}^2 - 2l_0\dot{\theta}\dot{u}_v\sin(\theta) + \dot{u}_v^2\right], \\ V &= -mg(z_1 - u_v) = -mg[l_0\cos(\theta) - u_v] \end{aligned}$$

Thus, the Lagrange function is

$$L = T - V = \frac{m}{2}\left[l_0^2\dot{\theta}^2 - 2l_0\dot{\theta}\dot{u}_v\sin(\theta) + \dot{u}_v^2\right] + mg[l_0\cos(\theta) - u_v].$$

By using the formula for this case with no dissipative terms

$$\frac{d}{dt}\left(\frac{\partial L}{\partial \dot{\theta}} - \frac{\partial L}{\partial \theta}\right) = 0,$$

one obtains the equation of motion as being

$$\ddot{\theta} + \frac{(g - \ddot{u}_v)}{l_0} \sin(\theta) = 0.$$

Linearizing this equation around its equilibrium point at the lowest position as done in section 2.3, one can write

$$\ddot{\theta} + \left[\omega_0^2 - \frac{u_a\, \omega^2}{l_0} \cos(\omega t)\right] \theta = 0,$$

where $g/l_0 = \omega_0^2$. This equation has the form of equation (3-2). The pendulum in this situation is said to be parametrically excited, where the excitation is provided through a stiffness term.

The form of Mathieu's equation does not only appear in mechanical systems, it may also be applicable to oscillatory electrical circuits [5; 29]. Take for example an LC circuit with a time-varying capacitance, as seen in figure 3.4.

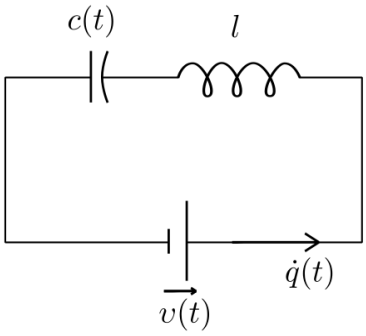

Figure 3.4: LC circuit with a time-varying capacitance.

The system is taken with no resistance or voltage source ($\upsilon = 0$). Taking q as the charge in the circuit, l the inductance and a capacitance that varies periodically with time as in $c(t) = c_0/(1 + a\, \cos(\omega t))$, it is possible to take $\omega_{lc} = (l\, c_0)^{-1/2}$ [5]. This system is described by the differential equation

$$\begin{aligned} l\ddot{q} &+ \frac{1}{c(t)}\, q = 0, \\ \ddot{q} &+ \left[\omega_{lc}^2 + \omega_{lc}^2\, a\, \cos(\omega t)\right]\, q = 0, \end{aligned}$$

that also has the form of the undamped Mathieu's equation. Further information about obtaining the equations of motion of purely electromagnetic system is provided in appendix C.

Those two examples are some of the many systems that can be described by Mathieu's equation. This differential equation is deeply studied until today and having a clear understanding of the systems that can be described by this

equation is of great interest in stability analysis studies. Therefore, this is going to be discussed in several sections and in more details in section 4.1.

Systems with parametric excitation are the ones of interest in this dissertation. Next, the idea of stability used throughout this dissertation is presented so stability for this type of system can be addressed.

3.2 Lyapunov stability

Stability studies are widely used in many fields, from fluid dynamics to stability of structures and electronics. However, its concept may vary depending on the object of study being dealt with. This section will introduce the definition of stability used for the rest of the dissertation, that is *stability according to Lyapunov* [2; 22; 24; 26].

It is important to highlight the fact that stability as defined here is a property assigned to the solution of a system. A differential equation may have both stable and unstable solutions [6; 26], once they are unique for given initial conditions.

Take equation (2-2) and write it as a first order differential equation in the generic form

$$\dot{x} = w(x,t). \tag{3-3}$$

where $x = [x_1 \ x_2 \ \dots \ x_{2n}]^T$ and $w = [w_1 \ w_2 \ \dots \ w_{2n}]^T$. A solution of this system is unique for given initial conditions $x(0) = x_0$. To start the task of defining stability, take a known solution x^* with initial conditions x_0^*. This solution is said to be *stable* in the sense of Lyapunov if

$$\forall \epsilon > 0 \ \ \exists \delta > 0 \ \text{ such that } \ |x_0 - x_0^*| < \delta \ \Rightarrow \ |x - x^*| < \epsilon, \ \ \forall t \geq 0,$$

where $|\cdot|$ is the norm of a vector, for example the Euclidean norm $|x| = \sqrt{x_1^2 + x_2^2 + \cdots + x_{2n}^2}$. The solution x^* is thus considered stable if x stays arbitrarily close to x^* (meaning that $|x - x^*|$ stays smaller than an arbitrarily small ϵ) for all times, given that the initial condition x_0 is sufficiently close to the initial condition x_0^*. A schematic representation of this definition is depicted in figure 3.5.

If the solution is stable and also

$$|x_0 - x_0^*| < \delta \ \Rightarrow \ \lim_{t\to\infty} |x - x^*| = 0,$$

it is said to be *asymptotically stable*.

If there exists an $\epsilon > 0$ for an arbitrarily small $|x_0 - x_0^*|$ that results in $|x - x^*| > \epsilon$ for some time t, the solution x^* is said to be *unstable* in the sense of Lyapunov.

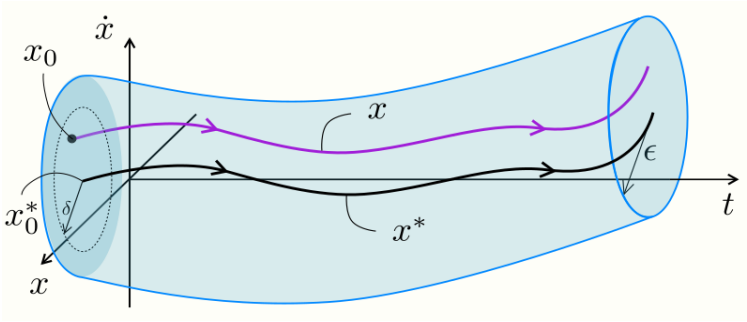

Figure 3.5: Stability of a motion in the sense of Lyapunov.

This concept of stability concerns stability of motions in general. However, the solution of interest here is an equilibrium position, that is, a stationary position. More specifically, the dissertation deals with stability of the *trivial solution*, an equilibrium position such that it is zero for all times ($x = [0\ 0\ \ldots\ 0]^T$).

3.3 Linear time-periodic systems (Floquet theory)

After this introduction to how stability is approached, recall that the main focus of the dissertation is to make stability analysis for linear time-periodic systems, where the stability of the trivial solution is of interest.

To continue, it is necessary to introduce some initial concepts to investigate the stability of the trivial solution of this type of system [27; 28]. Take the first order linear differential equation for the homogeneous case in the generic form

$$\dot{x}(t) = A(t)\, x(t), \tag{3-4}$$

where $x(t) = [y(t)\ \ \dot{y}(t)]^T \in \mathbb{R}^{2n}$. $A(t) \in \mathbb{C}^{2n\times 2n}$ is the coefficient matrix, that is time-periodic with period T, which means that for $T > 0$, $A(t) = A(t+T)$ for every $t \in \mathbb{R}$. For a set of linear independent solutions $(x_1(t), x_2(t), ..., x_{2n}(t))$ of this equation, it is possible to define

$$\Phi(t) = [\ x_1(t) \quad x_2(t) \quad \ldots \quad x_{2n}(t)\ ],$$

called the *fundamental matrix*, a non-singular matrix where its columns are composed by the linear independent solutions of (3-4).

If the coefficient matrix A did not vary with time, we would be dealing with linear time-invariant systems, already discussed in previous sections. For these autonomous systems, it is known that the solution is given by a linear combination of

$$u_i\ e^{\lambda_i\, t}, \tag{3-5}$$

where λ_i and u_i are, respectively, the eigenvalues and eigenvectors of the constant coefficient A. However, when dealing with time-periodic systems as seen in section 3.1.2, the solutions cannot be obtained with the same approach due to the time dependency of the coefficient matrix $A(t)$. The solution for a linear time-periodic system must be of the form

$$x_i(t) = p_i(t)e^{\varrho_i\, t}, \tag{3-6}$$

where $p_i(t)$ are time-periodic [3; 28; 35] and ϱ_i are constant values that are going to be treated at the end of this section.

Next, *Floquet's theorem* is enunciated [1; 3; 27; 28; 35], a theorem that provides a form for the fundamental matrix of systems with time-periodic coefficients described by (3-4). This form allows one to make stability statements about the trivial solution's stability, as discussed in details latter on in this section. Appendix B shows this theorem in more details while also providing several important features that lead to it.

Theorem 3.1 (Floquet's theorem) *The fundamental matrix* $\Phi(t)$ *with* $\Phi(0) = I$ *has a Floquet normal form*

$$\Phi(t) = Q(t)e^{Bt}, \tag{3-7}$$

where $Q \in C^1(\mathbb{R})$ *is a* T*-periodic* $(Q(t) = Q(t+T))$ *invertible matrix for all* t *and* $B \in \mathbb{C}^{2n\times 2n}$ *is a constant matrix given by* $B = \dfrac{1}{T}\, ln(\Phi(T))$.

For linear systems with constant coefficients, as treated in chapter 2 with SDoF systems, stability is addressed by evaluating the eigenvalues of the constant coefficient matrix A [26]. As previously said, this same approach cannot be applied for the type of system being dealt with, meaning time-periodic systems, due to the time dependency of the coefficient matrix $A(t)$. Floquet's theorem provides a way of doing such analysis. The solutions of equation (3-4) are products of periodic functions with e^{Bt} and thus it is possible to determine stability through the eigenvalues of the constant matrix B.

As an example, take a linear system with coefficient matrix [36]

$$A(t) = \begin{bmatrix} -1 + \frac{3}{2}\cos^2(t) & 1 - \frac{3}{2}\cos(t)\sin(t) \\ -1 - \frac{3}{2}\sin(t)\cos(t) & -1 + \frac{3}{2}\sin^2(t) \end{bmatrix}. \tag{3-8}$$

First, let us show that

$$\Phi(t) = \begin{bmatrix} x_1(t) & x_2(t) \end{bmatrix} = \begin{bmatrix} e^{t/2}\cos(t) & e^{-t}\sin(t) \\ -e^{t/2}\sin(t) & e^{-t}\cos(t) \end{bmatrix}$$

is the fundamental matrix of this system, meaning that the system's response is given by the general form of

$$\Phi(t) = \begin{bmatrix} \cos(t) & \sin(t) \\ -\sin(t) & \cos(t) \end{bmatrix} \begin{bmatrix} e^{t/2} & 0 \\ 0 & e^{-t} \end{bmatrix}. \tag{3-9}$$

By direct substitution it is possible to conclude that $\Phi(0) = I$. The columns of the fundamental matrix are the linear independent solutions of the analyzed system. Thus, take the first column $x_1(t)$ of $\Phi(t)$ to find its derivative, that is

$$\begin{aligned} x_1(t) &= \begin{bmatrix} x_{11} \\ x_{21} \end{bmatrix} = \begin{bmatrix} e^{t/2}\cos(t) \\ -e^{t/2}\sin(t) \end{bmatrix}, \\ \dot{x}_1(t) &= \begin{bmatrix} \dot{x}_{11} \\ \dot{x}_{21} \end{bmatrix} = \begin{bmatrix} \frac{1}{2}e^{t/2}\cos(t) - e^{t/2}\sin(t) \\ -\frac{1}{2}e^{t/2}\sin(t) - e^{t/2}\cos(t) \end{bmatrix}. \end{aligned}$$

The goal is to show that this derivative is obtained by multiplying the coefficient matrix $A(t)$ by $x_1(t)$, concluding then that this is indeed a solution of the given system. Thus,

$$A(t)\, x_1(t) = \begin{bmatrix} \left(-1 + \frac{3}{2}\cos^2(t)\right) e^{t/2}\cos(t) - \left(1 - \frac{3}{2}\cos(t)\sin(t)\right) e^{t/2}\sin(t) \\ \left(-1 - \frac{3}{2}\sin(t)\cos(t)\right) e^{t/2}\cos(t) + \left(-1 + \frac{3}{2}\sin^2(t)\right) e^{t/2}\sin(t) \end{bmatrix}$$

that simplifying leads to

$$A(t)\, x_1(t) = \begin{bmatrix} \frac{1}{2}e^{t/2}\cos(t) - e^{t/2}\sin(t) \\ -\frac{1}{2}e^{t/2}\sin(t) - e^{t/2}\cos(t) \end{bmatrix} = \dot{x}_1(t).$$

The same can be done for $x_2(t)$. Finding its derivative, one gets

$$\begin{aligned} x_2(t) &= \begin{bmatrix} x_{12} \\ x_{22} \end{bmatrix} = \begin{bmatrix} e^{-t}\sin(t) \\ -e^{-t}\cos(t) \end{bmatrix}, \\ \dot{x}_2(t) &= \begin{bmatrix} \dot{x}_{12} \\ \dot{x}_{22} \end{bmatrix} = \begin{bmatrix} -e^{-t}\sin(t) + e^{-t}\cos(t) \\ -e^{-t}\cos(t) - e^{-t}\sin(t) \end{bmatrix}. \end{aligned}$$

Then,

$$A(t)\, x_2(t) = \begin{bmatrix} \left(-1 + \frac{3}{2}\cos^2(t)\right) e^{-t}\sin(t) + \left(1 - \frac{3}{2}\cos(t)\sin(t)\right) e^{-t}\cos(t) \\ \left(-1 - \frac{3}{2}\sin(t)\cos(t)\right) e^{-t}\sin(t) + \left(-1 + \frac{3}{2}\sin^2(t)\right) e^{-t}\cos(t) \end{bmatrix}$$

that simplifying leads to

$$A(t)\, x_2(t) = \begin{bmatrix} -e^{-t}\sin(t) + e^{-t}\cos(t) \\ -e^{-t}\cos(t) - e^{-t}\sin(t) \end{bmatrix} = \dot{x}_2(t).$$

Therefore, it is possible to conclude that $\Phi(t)$ is indeed the system's fundamental matrix.

One can also find that

$$\begin{aligned}\log\left(\Phi(t)\right) &= \log\left(\begin{bmatrix} e^{t/2}\cos(t) & e^{-t}\sin(t) \\ -e^{t/2}\sin(t) & e^{-t}\cos(t) \end{bmatrix}\right) \\ &= \log\left(\begin{bmatrix} \cos(t) & \sin(t) \\ -\sin(t) & \cos(t) \end{bmatrix}\begin{bmatrix} e^{t/2} & 0 \\ 0 & e^{-t} \end{bmatrix}\right) \\ &= \log\left(\begin{bmatrix} \cos(t) & \sin(t) \\ -\sin(t) & \cos(t) \end{bmatrix}\right) + \log\left(\begin{bmatrix} e^{t/2} & 0 \\ 0 & e^{-t} \end{bmatrix}\right).\end{aligned}$$

By continuing the calculations in the example, one may obtain the constant matrix B by using its definition $B = \frac{1}{T}\ln(\Phi(T))$ in theorem 3.1. Thereafter, stability of the trivial solution could be addressed through its eigenvalues. However, obtaining the matrix B explicitly is not a simple task and some times it is not even possible to obtain it analytically. For the example being carried out here, the calculation of the logarithm of a rotation matrix would be necessary, a not so simple task (this calculation is provided, for example, in [27]).

Therefore, numerical approximations of the fundamental matrix are widely used in stability analysis. To achieve so, another important definition in stability analysis for time-periodic systems is the *monodromy matrix* R, defined as being

$$\Phi(t+T) = \Phi(t)\ R. \tag{3-10}$$

The existence of such matrix is proved in appendix B. Substituting the relation (3-10) into equation (3-7),

$$Q(t+T)e^{B(t+T)} = Q(t)e^{Bt}R.$$

Recalling that $Q(t)$ is periodic with period T leads to

$$\begin{aligned}Q(t+T)e^{Bt}e^{BT} &= Q(t)e^{Bt}R, \\ e^{BT} &= R.\end{aligned}$$

The monodromy matrix R is a non-singular constant matrix and its eigenvalues are denoted $\gamma_i,\ i = 1, ..., 2n$, called *Floquet multipliers*. Making use of Floquet multipliers is an usual way to make stability statements about the system's trivial solution. For example, if the magnitude of an eigenvalue of R is greater then 1, it means that an eigenvalue of B has positive real part, making the solution's amplitude increase indefinitely with time. It is thus unbounded and therefore unstable.

Since the monodromy matrix is time-independent, take the case where $R = \Phi^{-1}(0)\Phi(T)$ with initial conditions $\Phi(0) = I$ to go accordingly to

Floquet's theorem. The monodromy matrix is resumed to

$$R = \Phi(T). \tag{3-11}$$

Therefore, Floquet theory makes use of the Floquet multipliers of a linear time-periodic system in the form of equation (3-4) to evaluate the stability of its zero solution. These stability statements are [3; 26; 27]:

- If $|\gamma_i| \leq 1$ for all i, the trivial solution of equation (3-4) is *stable*;
- If $|\gamma_i| < 1$ for all i, the trivial solution of equation (3-4) is *asymptotically stable*;
- For other cases, the trivial solution of equation (3-4) is *unstable*.

The monodromy matrix for the last example with coefficient matrix (3-8) is now going to be found to exemplify this. The fundamental matrix evaluated at $t = 0$ is $\Phi(0) = I$, as one can conclude by simple substitution. Evaluating the fundamental matrix at $t = T$,

$$\Phi(T) = \Phi(2\pi) = \begin{bmatrix} e^{\pi} & 0 \\ 0 & e^{-2\pi} \end{bmatrix}.$$

Thus, the monodromy matrix is

$$R = \Phi(T) = \Phi(2\pi) = \begin{bmatrix} e^{\pi} & 0 \\ 0 & e^{-2\pi} \end{bmatrix}.$$

To obtain the Floquet multipliers, one must solve the eigenvalue problem $Ru = \gamma u$, that leads to

$$\det(R - \gamma I) = \begin{bmatrix} e^{\pi} - \gamma & 0 \\ 0 & e^{-2\pi} - \gamma \end{bmatrix} = 0,$$
$$(e^{\pi} - \gamma)(e^{-2\pi} - \gamma) = 0.$$

The roots are $\gamma_1 = e^{\pi}$ and $\gamma_2 = e^{-2\pi}$, the Floquet multipliers. Since $|\gamma_1| > 1$, the trivial solution is unstable.

Floquet multipliers depend only on the coefficient matrix $A(t)$ and are independent of the basis chosen for the set of solutions [25; 35]. To prove this, take $\Phi(t)$ and $\Phi^*(t)$ as two different fundamental matrices. Since a fundamental matrix cannot be singular, there exists a non-singular constant matrix V from which

$$\Phi^*(t) = \Phi(t)V$$

is valid. Being T the period, one gets that

$$\begin{aligned}\Phi^*(t+T) &= \Phi(t+T)V \\ &= \Phi(t)RV \\ &= \Phi^*(t)V^{-1}RV \\ &= \Phi^*(t)W,\end{aligned}$$

where $W = V^{-1}RV$. It is possible to use determinant properties to obtain

$$\begin{aligned}\det[W-\gamma I] &= \det[V^{-1}RV-\gamma I] \\ &= \det[V^{-1}(R-\gamma I)V] \\ &= \det[V^{-1}V]\,\det[R-\gamma I] \\ &= \det[R-\gamma I],\end{aligned}$$

meaning that W and R have the same eigenvalues. Therefore the Floquet multipliers do not depend on the basis of the set of solutions.

Theorem 3.1 also leads to an important result: there exists a time-periodic transformation capable of transforming a time-periodic system into an autonomous system [27; 28]. Taking equation (3-7) and substituting it in the known relation $\dot{\Phi}(t) = A(t)\Phi(t)$, one gets

$$\begin{aligned}\dot{Q}(t)e^{Bt} + Q(t)Be^{Bt} &= A(t)Q(t)e^{Bt}, \\ \dot{Q}(t) + Q(t)B &= A(t)Q(t).\end{aligned}$$

Multiplying this by a vector $\nu(t)$ results is

$$\dot{Q}(t)\nu(t) + Q(t)B\nu(t) = A(t)Q(t)\nu(t). \tag{3-12}$$

Now, take the transformation

$$x(t) = Q(t)\nu(t)$$

and substitute this into equation (3-4), getting

$$\dot{Q}(t)\nu(t) + Q(t)\dot{\nu}(t) = A(t)Q(t)\nu(t). \tag{3-13}$$

Using equations (3-12) and (3-13), one has that

$$\dot{\nu}(t) = B\nu(t),$$

a system with constant coefficients. This is also known as *Lyapunov-Floquet transformation*. This result implies that the relation $x(t) = Q(t)\nu(t)$ transforms a system described by $\dot{x}(t) = A(t)x(t)$ with a time-periodic coefficient matrix

into a system described by $\dot{\nu}(t) = B\nu(t)$ with a constant coefficient matrix [27; 28].

Nevertheless, as discussed previously, finding analytical solutions for these cases can be a tiring process depending on the dynamics and sometimes not even possible to solve analytically. Thus, numerical methods are widely used in stability analysis. The numerical procedure followed in this dissertation is given in details in appendix E, where some important remarks regarding it are discussed. The process of finding the monodromy matrix and using the Floquet multipliers to evaluate stability is called *Floquet analysis* [28].

Let us now introduce a final definition that is going to be used throughout this dissertation. The characteristic exponents or Floquet exponents (ϱ_i) are the eigenvalues of matrix B [35], that can be defined as

$$\gamma_i = e^{\varrho_i \, T},$$

where γ_i are the Floquet multipliers. The *Lyapunov characteristic exponents* (LCEs) μ_i can be expressed as the real part of such Floquet exponents [28; 35]. They can also be obtained directly by the Floquet multipliers [28; 35] as

$$\mu_i = \frac{1}{T} \ln|\gamma_i|. \tag{3-14}$$

Taking the type of solution for the system given in its general form by equation (3-6), it is possible to categorize stability just as it was done for the Floquet multipliers. The trivial solution is stable when $\mu_i \leq 0$ for all i and asymptotically stable when all the LCEs are strictly negative, once the response will eventually damp out as time goes by. For an unstable trivial solution, at least one of the LCEs is a positive number.

Take the example used throughout this section that has a solution with the general form of equation (3-9): it has an LCE $\mu_1 = 1/2$ and another one $\mu_2 = -1$. Since μ_1 is a positive value, the trivial solution is considered unstable, as it was also concluded by the use of the Floquet multipliers.

It is sufficient for the largest LCE to be positive so that the trivial solution is unstable. This value is denoted Λ, meaning $\Lambda = \max(\mu_i), \;\; i = 1, ..., 2n$ [1; 28]. One of the benefits of using Lyapunov characteristic exponents is that stabilizing and destabilizing effects can be seen in stability maps and in the $\omega \times \Lambda$ plane, as discussed further on in chapter 4. Another advantage is that the use of LCEs offers a stability criterion that allows one to compare autonomous and time-periodic systems, as done in [28].

3.3.1 Stability maps and parametric resonance

After understanding how to determine stability of the trivial solution of linear time-periodic systems, it would be useful to do so for a given range of parameters that compose the system. The tool capable of doing this is called *stability map*. Stability maps are plots capable of graphically show stable and unstable regions for given range of parameters. The boundary between these two types of behavior are known as *transition curves* [2; 3; 4; 5; 6; 24; 32; 33].

To obtain these plots, one may use numerical or analytical methods [3; 6; 26; 32; 33]. Perturbation methods are widely used to address transition curves and the *Lindstedt-Poincaré technique* is going to be used to obtain such curves [22; 26]. The Lindstedt-Poincaré technique is an interesting approach for the objective here. The transition curves obtained from this method uses directly the fact that periodic solutions occur for parameter values placed right at this boundary, thus providing the parameters values that result in *periodic behavior*. The process to search for transition curves is done here as it was in [22; 26].

To exemplify this procedure, one can make use of the well known Mathieu's equation, given by (3-2). To proceed, take this equation in the form $\ddot{y}+\omega_n^2\left(1+\epsilon\cos(\omega t)\right)y=0$, where $\omega_n^2=\delta$ and the excitation amplitude is now given by $\omega_n^2\epsilon$. Taking the dimensionless time τ by making $\omega t=2\tau$, one gets

$$y''+\left(\sigma+\eta\cos(2\tau)\right)y=0, \tag{3-15}$$

where $y''=d^2y/d\tau^2$, $\sigma=\left(2\omega_n/\omega\right)^2$ and $\eta=\epsilon\left(2\omega_n/\omega\right)^2$. Here, $\epsilon<<1$ is assumed, meaning that the approximations obtained further on are only valid for small amplitudes of excitation.

The transition curves in the $\sigma\times\eta$ plane correspond to the pairs of parameters that result in periodic solutions, thus approximate solutions can be obtained by finding pairs (σ,η) that makes this true. The Lindstedt-Poincaré procedure starts by taking the following expansion for σ and y:

$$\sigma = p^2+\eta\sigma_1+\eta^2\sigma_2+\dots \tag{3-16}$$

$$y(\tau) = y_0+\eta y_1+\eta^2 y_2+\dots \tag{3-17}$$

where σ_1, σ_2, $\dots$ are unknown constants that are going to be obtained. Substituting the expansions (3-16) and (3-17) into equation (3-15) one gets

$$\begin{aligned}&(y_0''+\eta y_1''+\eta^2 y_2''+\dots)+\\&\quad+\left(p^2+\eta\sigma_1+\eta^2\sigma_2+\dots+\eta\cos(2\tau)\right)(y_0+\eta y_1+\eta^2 y_2+\dots)=0.\end{aligned}$$

Grouping terms of equal power of η,

$$\begin{aligned} y_0'' + p^2 y_0 &= 0, \\ y_1'' + p^2 y_1 &= -(\sigma_1 + \cos(2\tau))y_0, \\ y_2'' + p^2 y_2 &= -(\sigma_1 + \cos(2\tau))y_1 - \sigma_2 y_0, \\ &\vdots \end{aligned}$$

Take now the two sets of initial conditions $y(0) = 1,\ y'(0) = 0$ and $y(0) = 0,\ y'(0) = 1$. Using them in the equation regarding y_0, one gets that its solutions must be in the form

$$y_0 = \cos(p\,\tau) \tag{3-18}$$

and

$$y_0 = \frac{1}{p}\sin(p\,\tau), \tag{3-19}$$

respectively for the two sets of initial conditions.

Let us find the first approximation for $p = 0$. By the first set of initial conditions, $y_0 = \cos(0) = 1$ in equation (3-18), one gets

$$y_1'' = -\sigma_1 - \cos(2\tau).$$

To obtain periodic solutions through this relation, σ_1 must be taken as 0. Integrating this equation for $\sigma_1 = 0$ leads to

$$y_1 = \frac{1}{4}\cos(2\tau) + a,$$

where a is a constant. Substituting y_1 in the equation due respect to y_2,

$$y_2'' = -\sigma_2 - \frac{1}{8} - a\cos(2\tau) - \frac{1}{8}\cos(4\tau),$$

that for periodic solutions must have $\sigma_2 = -1/8$. Substituting $\sigma_1 = 0$ and $\sigma_2 = -1/8$ in equation (3-16), one gets

$$\sigma = -\frac{1}{8}\eta^2 + O(\eta^3),$$

where $O(\eta^3)$ corresponds to orders higher than the second one in the approximation for σ. However, for $p = 0$, it is not possible to obtain a non-trivial periodic solution for the second set of initial conditions. Therefore, $p = 0$ does not lead to transition curves.

Moving on to the approximation for $p = 1$, equation (3-18) corresponding to the first set of initial conditions means that we begin the procedure with

$y_0 = \cos(\tau)$. This leads to

$$\begin{aligned} y_1'' + y_1 &= -\left(\sigma_1 + \cos(2\tau)\right)\, \cos(\tau), \\ &= -\left(\sigma_1\, \cos(\tau) + \cos(2\tau)\, \cos(\tau)\right), \\ &= -\left(\sigma_1 + \frac{1}{2}\right)\, \cos(\tau) - \frac{1}{2}\, \cos(3\tau), \end{aligned}$$

that must have $\sigma_1 = -1/2$. Thus

$$y_1'' + y_1 = -\frac{1}{2}\, \cos(3\tau),$$

which solution is

$$y_1 = \frac{1}{16}\left(\cos(3\tau) - \cos(\tau)\right).$$

Substituting the just found y_1 in the equation due respect to y_2 gives us

$$y_2'' + y_2 = -\left(\frac{1}{32} + \sigma_2\right) + \frac{1}{16}\, \cos(3\tau) - \frac{1}{32}\, \cos(5\tau),$$

that must have σ_2 as $-1/32$. Substituting $\sigma_1 = -1/2$ and $\sigma_2 = -1/32$ in equation (3-16),

$$\sigma = 1 - \frac{1}{2}\eta - \frac{1}{32}\eta^2 + O(\eta^3).$$

Beginning now with (3-19), $y_0 = \sin(\tau)$ for $p = 1$, the process leads to

$$\begin{aligned} y_1'' + y_1 &= -\left(\sigma_1 + \cos(2\tau)\right)\, \sin(\tau), \\ &= -\left(\sigma_1\, \sin(\tau) + \cos(2\tau)\, \sin(\tau)\right), \\ &= -\left(\sigma_1 - \frac{1}{2}\right)\, \sin(\tau) - \frac{1}{2}\, \sin(3\tau), \end{aligned}$$

that must have $\sigma_1 = 1/2$ for periodic solutions. Thus

$$y_1'' + y_1 = -\frac{1}{2}\, \sin(3\tau),$$

which solution is

$$y_1 = \frac{1}{16}\left(\sin(3\tau) - \sin(\tau)\right).$$

Substituting the just found y_1 in the equation due respect to y_2,

$$y_2'' + y_2 = -\left(\frac{1}{32} - \sigma_2\right) - \frac{1}{32}\, \sin(5\tau),$$

that must have σ_2 as $1/32$. Substituting $\sigma_1 = -1/2$ and $\sigma_2 = 1/32$ in equation (3-16), one gets

$$\sigma = 1 + \frac{1}{2}\eta + \frac{1}{32}\eta^2 + O(\eta^3).$$

The same procedure can be done for other values of p. For example, for

$p = 2$ this process leads to

$$\sigma = 4 + \frac{5}{48}\eta^2 + O(\eta^3).$$
$$\sigma = 4 - \frac{1}{48}\eta^2 + O(\eta^3).$$

Before, the stability of the trivial solution was dependent on ω_n, ω and ϵ. With the change to dimensionless time, the stability is only dependent on σ and η. Recalling now that $\sigma = (2\omega_n/\omega)^2$ and $\eta = \epsilon\,(2\omega_n/\omega)^2$, one can plot the obtained curves in the $\omega/\omega_n \times \epsilon$ plane, shown in figure 3.6 for $p = 1$ and 2. The areas outside these transition curves are the stable regions, while the areas inside them are the unstable regions.

Since this is only valid for small values of ϵ, as this parameter increases the approximations no longer hold. If higher order terms in σ were used, better approximations would be obtained. However, this would lead to even longer calculations that require algebraic manipulation in computers.

It is possible to see that the unstable areas arise from $\omega/\omega_n = 2/p,\ p \in \mathbb{N}_+$. For $p = 1$, $\omega/\omega_n = 2$; for $p = 2$, $\omega/\omega_n = 1$; for $p = 3$, $\omega/\omega_n = 2/3$ and so on. These frequencies are known as *critical frequencies*. In the just seen example of Mathieu's equation, a small parameters approximation method to obtain these critical frequencies was used. By doing so, it is possible not only to obtain these frequencies, but it also provides a way of obtaining the boundaries between stable and unstable regions.

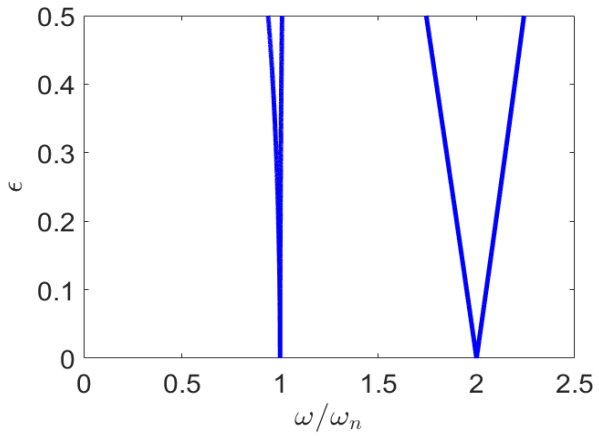

Figure 3.6: Transition curves in the $\omega/\omega_n \times \epsilon$ plane, for $p = 1$ and 2.

As discussed in previous sections, for systems with applied external forces, where the excitation is provided by a periodic input, the resonance phenomenon occurs when the excitation frequency equals the system's natural frequency. The response's amplitude grows without bound as it approaches this

value. Meanwhile, for time-periodic systems *parametric resonance* [2; 3; 28] occurs for several excitation frequencies. Such frequencies depend on the natural frequencies of the undamped system without parametric excitation.

One can conclude that parametric resonance occurs when the excitation frequency approaches

$$\omega_{crit,\,p} = \frac{2\,\omega_n}{p}, \quad p \in \mathbb{N}_+, \tag{3-20}$$

where $\omega_{crit,\,p}$ are the critical frequencies, which depend on the natural frequencies ω_n of the undamped system without parametric excitation. For MDoF systems, parametric resonance may also occur at

$$\omega_{crit,\,p} = \frac{|\omega_r \pm \omega_l|}{p}, \quad p \in \mathbb{N}_+ \ \text{ for } \ r \neq l, \tag{3-21}$$

with ω_r and ω_l representing, respectively, the r-th and l-th natural frequencies of the undamped system without parametric excitation. The index p can be seen as the order of the parametric resonance.

Parametric resonance is thus a phenomenon that can result in large response amplitudes even for small excitation frequencies. For critical frequencies originated from (3-20), the effect is always destabilizing [28]. However, for some of the critical frequencies originated from the combination of natural frequencies in (3-21), a stabilizing effect can be obtained. This is where *parametric anti-resonance* occurs, that, differently from the parametric resonance, does not result in instability. Parametric anti-resonance can actually be used as a way of doing vibration control [2; 3]. By strategically setting the excitation frequency to be the one corresponding to the parametric anti-resonance, self-excited systems can have their vibration totally extinguished. An example of this phenomenon is given in chapter 4. This could be widely used in control vibration in rotating machinery to higher their efficiency, as discussed in [4].

Therefore, instability for parametrically excited systems occurs in several excitation frequency intervals. These unstable regions can be seen clearly through stability maps, where stable and unstable regions are shown for different pairs of parameters. However, notice that until this point only an undamped system was treated. A logical doubt that could follow this is: what are the effects of damping in stability maps? The damping shrinks the unstable areas, as it is going to be discussed in more details in the next chapter.

Even though an approximation method was briefly discussed, this dissertation deals from now on with numerical approximations, where the followed numerical procedure is given in appendix E, used in the next chapter to discuss in more details the Mathieu's equation as well as several examples of 2DoF systems.

4
Stability analysis examples

This chapter's goal is to provide several examples of systems with time-periodic coefficients to exemplify the use of Floquet theory. First, single degree of freedom (SDoF) systems that can be described by Mathieu's equations are going to be dealt with, embracing both undamped and damped cases. These equations are capable of describing several real world system and are widely studied until today in stability analysis. A good comprehension of their applications and implications is of great interest in the stability studies, being a first step into this topic.

Afterwords, examples of two degrees of freedom (2DoF) systems are going to be discussed. The goal is to analyze the stability of the trivial solution of these 2DoF systems using Floquet theory and see how parametric excitation influences stability. In the examples, purely mechanical systems and purely electromagnetic systems that can be described by the differential equations are shown.

To do a complete analysis of these systems, stability maps using different parameters are plotted for each example. Two different strategies to evaluate the stability of trivial solutions are compared: Floquet multipliers and the maximum value of Lyapunov characteristic exponents (Λ). Phase diagrams are also shown so the general behaviour of the numerical approximations can be discussed. Furthermore, plots in the $\omega \times \Lambda$ plane are shown for more details into the analysis. The numerical procedure followed here is given in appendix E in details.

4.1 SDoF examples: Mathieu's equation

A brief introduction to Mathieu's equation was present in section 3.1 as well as in 3.3.1. Now, stability analysis of the trivial solution of systems that can be described by this equation is going to be made by using Floquet theory. Stability maps using Floquet multipliers and the maximum value of LCEs as well as phase diagrams are going to be discussed. Both the undamped and damped Mathieu's equations are going to be dealt with in this section.

4.1.1 Case I: undamped system

As seen in section 3.1, a special case of a system that can be described by equation (3-1) is

$$\ddot{y} + [\delta + \epsilon \cos(\omega t)]\ y = 0,$$

known as Mathieu's equation. Writing it in its two-dimensional first order form,

$$\begin{bmatrix} \dot{y} \\ \ddot{y} \end{bmatrix} = \begin{bmatrix} 0 & 1 \\ -[\delta + \epsilon \cos(\omega t)] & 0 \end{bmatrix} \begin{bmatrix} y \\ \dot{y} \end{bmatrix}, \tag{4-1}$$

where δ, ϵ and ω are parameters of the system.

It is possible to use the numerical procedure in appendix E to obtain stability maps for this equation. An usual stability map for systems that can be described by this equation is obtained by varying the values of excitation frequency ω and amplitude ϵ. This allows one to use different values of δ, where for each one of its values a $\omega \times \epsilon$ plane can be plotted. Figure 4.1 shows these stability maps with a grid of 0.005 for the undamped Mathieu's equation with $\delta = 4$ and 9, where the dark blue area represents the unstable regions and the light blue area, the stable regions.

The stability maps in this plane provide the frequency vicinities where instability takes place for each fixed value of δ. As seen in section 3.3.1, the critical frequencies where parametric resonance occurs depend on the natural frequencies of the undamped system without parametric excitation. By taking $\epsilon = 0$, the equation becomes

$$\ddot{y} + \delta y = 0.$$

Thus, for this example, the natural frequency is

$$\omega_{n,\,\delta} = \sqrt{\delta}.$$

For both of the proposed systems, these frequencies are, in rad/s,

$$\omega_{n,\,\delta=4} = 2 \ \text{ and } \ \omega_{n,\,\delta=9} = 3.$$

By using equation (3-20) with the just obtained natural frequencies, it is possible to say where the "tongues" of instability start forming. For example, by taking $\delta = 4$, the critical frequencies are: 4, 2, 1 and so on. In the vicinities of these frequencies, instability behaviour takes place.

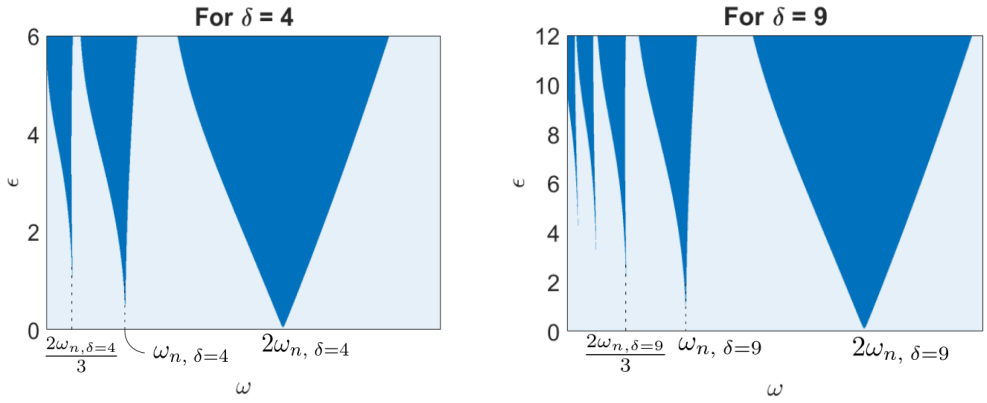

Figure 4.1: Stability maps for the undamped Mathieu's equation with $\delta = 4$ and 9, respectively.

It is also possible to make use of the maximum value of the Lyapunov characteristic exponents (Λ) to evaluate the stability of the trivial solution. The stability maps in figure 4.1 are also plotted in the $\omega \times \epsilon$ plane, with a grid of 0.05. The values of Λ for each pair of excitation frequency and excitation amplitude are obtained. The more red is the region of the map, the higher is the value of Λ. The difference between the two forms of plotting these stability maps is that a gradient of values of Λ is obtained, disposed in different colors through the color bars.

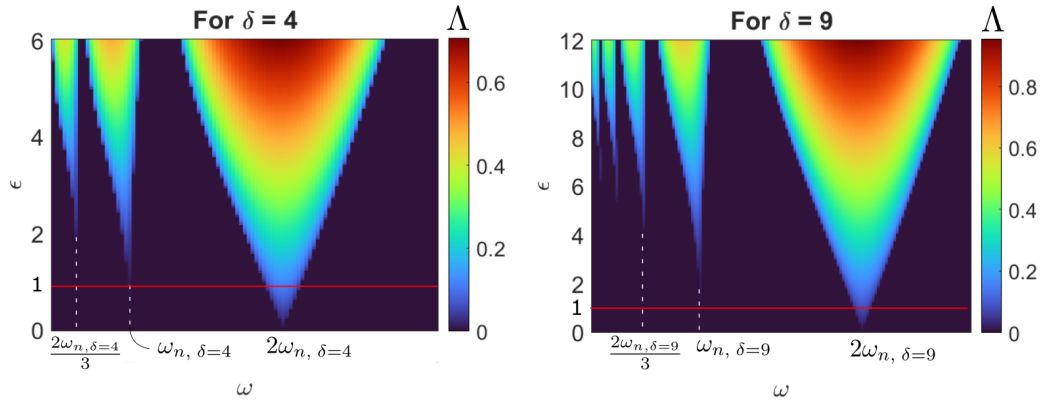

Figure 4.2: Stability maps using Λ for the undamped Mathieu's equation for $\delta = 4$ and 9, respectively.

By fixing values of ϵ as well as of δ, it is possible to obtain the Λ as function of the excitation frequency ω, provided by figure 4.3 for $\epsilon = 1$ and

the same values of $\delta = 4$ and 9. It is possible to notice the predominance of the first critical frequency between the other ones, fact already mentioned in section 3.3.1. The peaks of instability, meaning the intervals where Λ is higher then zero, appear exactly where expected by figure 4.2, once we are simply taking a "cut" from the previous stability maps. Critical frequency of lower orders do not appear in this plot due to the chosen section of figure 4.2 and the used grid in the simulations. If a smaller grid and/or a higher value of ϵ were used, these peaks could be seen in the $\omega \times \Lambda$ plot.

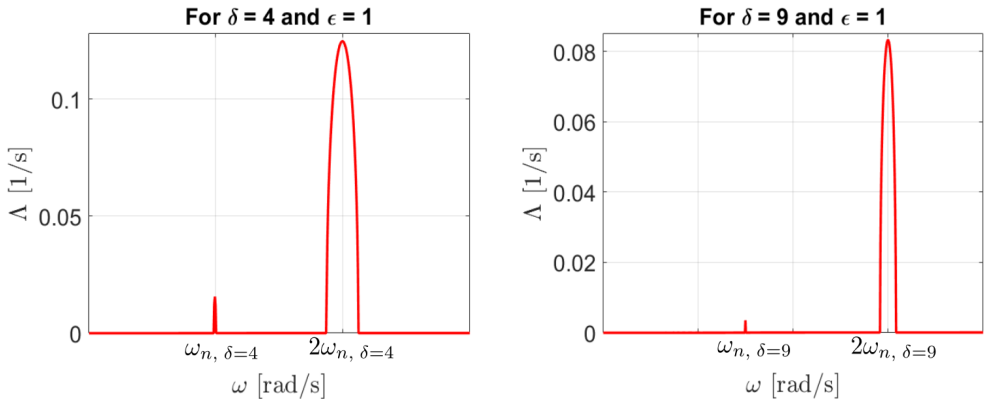

Figure 4.3: The maximum value of the LCEs Λ for the undamped Mathieu's equation with $\epsilon = 1$ and $\delta = 4$ and 9, respectively.

The influence of the excitation frequency on the stability of the trivial solution is analyzed next by making use of stability maps in the $\delta \times \epsilon$. Four different values of ω were used in a simulation and for each one of them a stability map of this type was plotted. The $\delta \times \epsilon$ planes were plotted with a grid of size 0.02, given in figure 4.4. These stability maps for the undamped Mathieu's equation were plotted for $\omega = 1,\ 2,\ 3$ and 4 rad/s, where the dark blue areas represent once again the unstable regions according to Floquet theory. The first important observation about these stability maps is that if a smaller grid was used, the instability "tongues" would all be touching the δ-axis. This was not done because it would imply in longer simulations times.

It is possible to observe through the stability maps that, with the increase of the frequency ω, the unstable regions are shifted to the right direction of the δ-axis. This means that there are less instability "tongues" for the same range of values of the parameters δ and ϵ. However, the remaining unstable regions are wider, as if the map was being zoomed in (or enlarged).

It is also possible to use the maximum value of LCEs (Λ) to obtain stability maps in this same plane. Figure 4.5 shows these maps with a grid of 0.1. The more red is the region of the map, higher the value of Λ and more

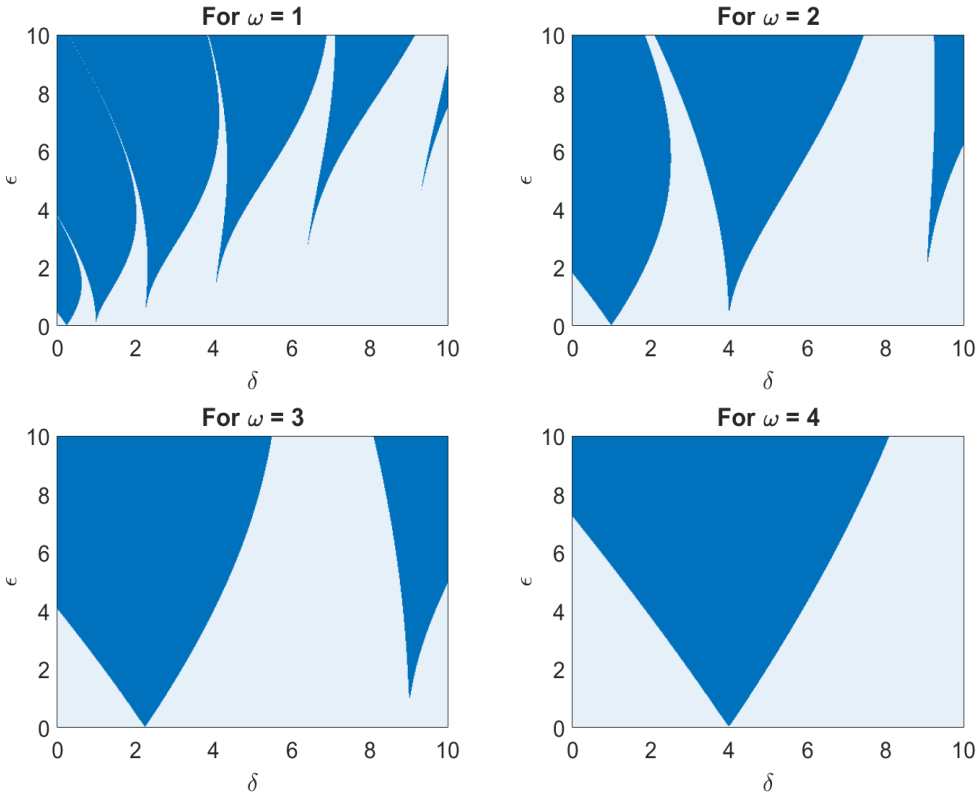

Figure 4.4: Stability maps for the undamped Mathieu's equation for $\omega = 1, 2, 3$ and 4, respectively.

unstable the trivial solution is for the given pair of parameters, as seen through the color-bars on the right-hand side of the stability maps.

Phase diagrams can also be plotted to evaluate the behaviour around the trivial solution. The chosen parameters values are $\delta = 4$ and $\epsilon = 2$. The simulations were done for 0 s to 100 s with a grid of 0.002 and with initial conditions $y(0) = 0.001,\ \dot{y}(0) = 0$ to represent a small deviation from the zero solution. These phase diagrams are shown in figure 4.6, where the motions' start points are marked with a red dot and the numerical approximations at the final time are marked with a black dot. The numerical approximations for $\omega = 1$ and 3 with the chosen parameters and initial conditions are stable, but not asymptotically stable. The amplitudes of the numerical approximations for a slight change from the zero solution do not increase indefinitely with time, but neither they tend to the zero solution. This does not hold for the other phase diagrams with $\omega = 2$ and 4, cases where the amplitudes only increase with time, being then unstable.

A great advantage of using Floquet theory is that conclusions can be taken about the zero solution's stability by solving the equations for only one period T. Without using this theory, it would be necessary to obtain numerical

approximations for larger periods of time to evaluate this behaviour.

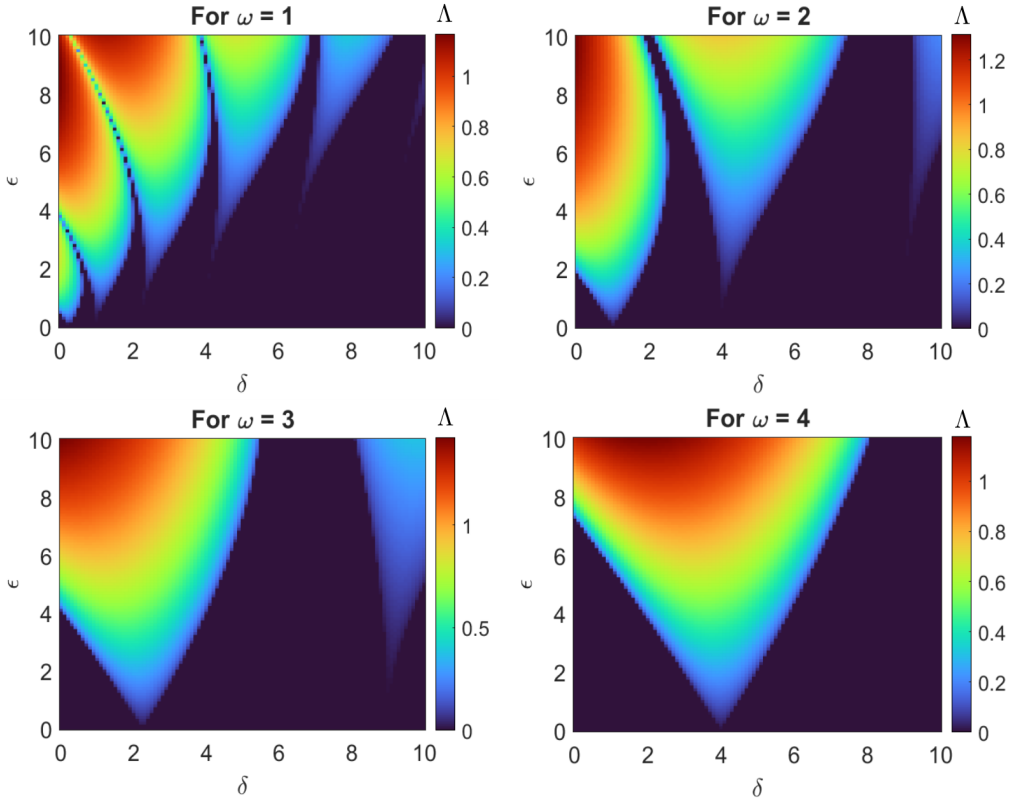

Figure 4.5: Stability maps using Λ for the undamped Mathieu's equation for $\omega = 1, 2, 3$ and 4, respectively.

4.1.2 Case II: damped system

For further analysis of the systems that can be described by the general form of equation (3-1), one may analyze the damped Mathieu's equation [22; 32; 33], given by

$$\ddot{y} + b\,\dot{y} + (\delta + \epsilon\,\cos(\omega\,t))\;\; y = 0, \tag{4-2}$$

where δ, ϵ and ω are the same parameters as the ones used for the undamped case. Since we are dealing now with the damped Mathieu's equation, a damping coefficient is present, taken as a constant b. Once again the equation is written in its two-dimensional first order form

$$\begin{bmatrix} \dot{y} \\ \ddot{y} \end{bmatrix} = \begin{bmatrix} 0 & 1 \\ -[\delta + \epsilon\,\cos(\omega\,t)] & -b \end{bmatrix} \begin{bmatrix} y \\ \dot{y} \end{bmatrix}. \tag{4-3}$$

The goal now is to analyze the influence of damping on stability maps, as mentioned in section 3.3.1. To compare it with the undamped case, the range

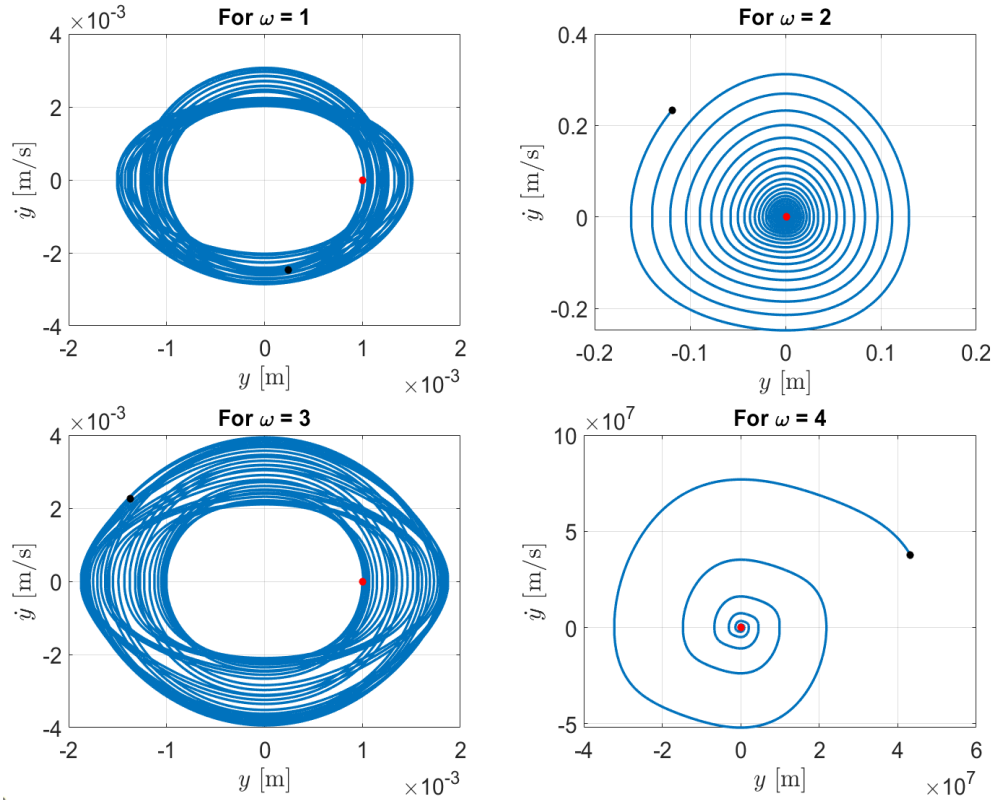

Figure 4.6: Phase diagrams for the undamped Mathieu's equation for $\omega = 1, 2, 3$ and 4, respectively, for $\delta = 4$ and $\epsilon = 2$.

of the parameters δ and ϵ is as in figures 4.4 and 4.5. The numerical procedure is followed as described in appendix E.

Stability maps for $\omega = 1$ and 3 can be seen in figures 4.7 and 4.8, where the dark blue area represents the unstable regions in the $\delta \times \epsilon$ plane plotted with a grid of 0.02 for different values of damping b. One can observe in these stability maps that the unstable regions have smoother borders when compared to the undamped cases for these values of excitation frequency in figure 4.4. It is also possible to notice that increasing the damping coefficient reduces the unstable regions of the stability maps, that are shrunken as this happens.

Just as it was done for the undamped case, it is possible to make use of the maximum value of the Lyapunov characteristic exponents (Λ). The same stability maps just analyzed are now plotted by making use of the Λ values for each pair of δ and ϵ, shown in figures 4.9 and 4.10. The regions of instability are the same for both ways of plotting this map. Thus, the difference between these maps and the ones in figure 4.5 for the chosen frequencies is provided by the color-bar. In the damped cases, there are negative values of Λ, resulting in the sharp "tongues" of stability in those maps. By only evaluating directly the magnitude of the Floquet multipliers as in figure 4.5, these information

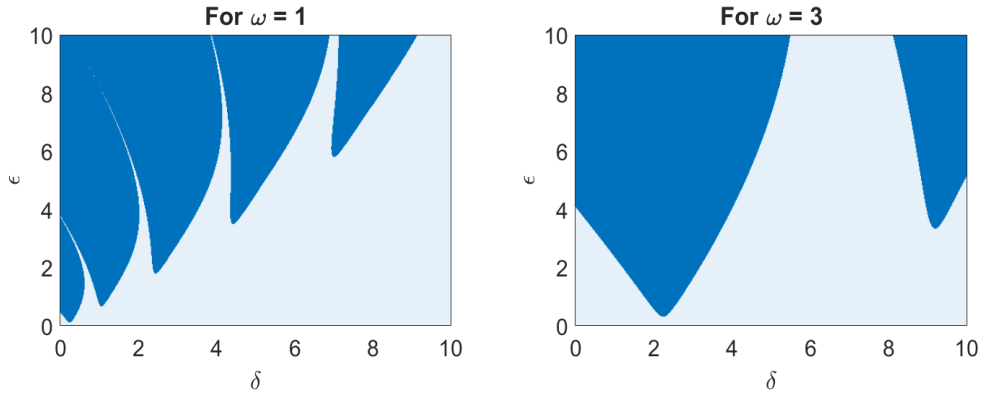

Figure 4.7: Stability maps for the damped Mathieu's equation with $b = 0.1$ and $\omega = 1$ and 3, respectively.

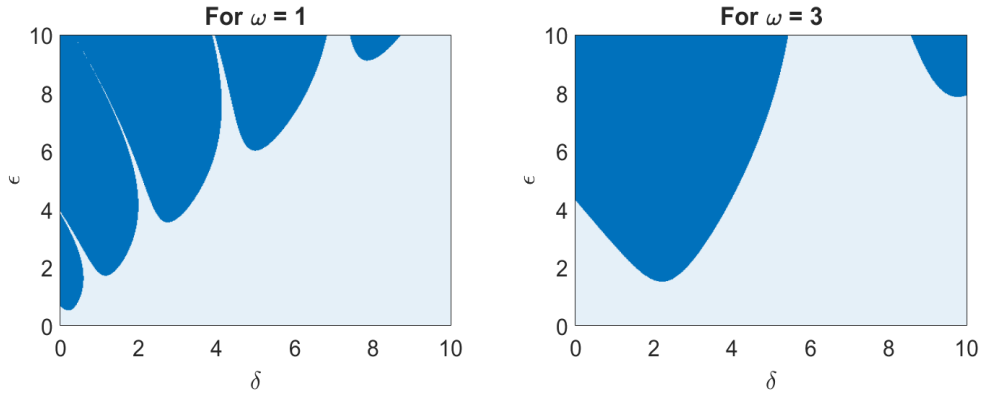

Figure 4.8: Stability maps for the damped Mathieu's equation with $b = 0.5$ and $\omega = 1$ and 3, respectively.

are not shown, since the regions are restricted to stable/unstable areas. This is a great advantage of using Λ in stability maps. Furthermore, it is possible to notice that for greater damping values, the Λs assume more negative values. Recalling section 3.3, this corresponds to asymptotic stability.

4.2 2DoF examples: mechanical and electromagnetic systems

In this section, several examples of 2DoF systems are going to be analyzed. The goal is to discuss the stability of the trivial solution of these 2DoF systems using Floquet theory and see how parametric excitation influences their stability. A purely mechanical system and a purely electromagnetic system that can be described by the same differential equations are shown. Appendix C briefly discusses how to obtain the equations of motion of purely electromagnetic systems, where an example is given so the reader can compare the found dynamics with the examples given next.

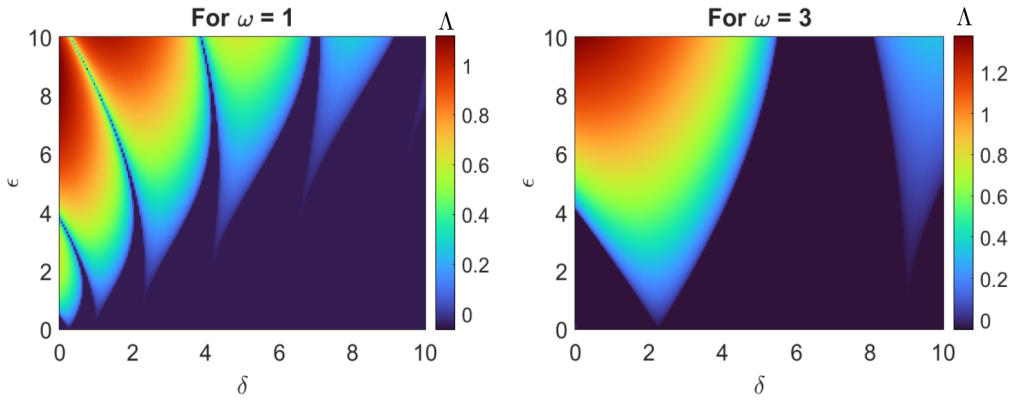

Figure 4.9: Stability maps using Λ for the damped Mathieu's equation with $b = 0.1$ and $\omega = 1$ and 3, respectively.

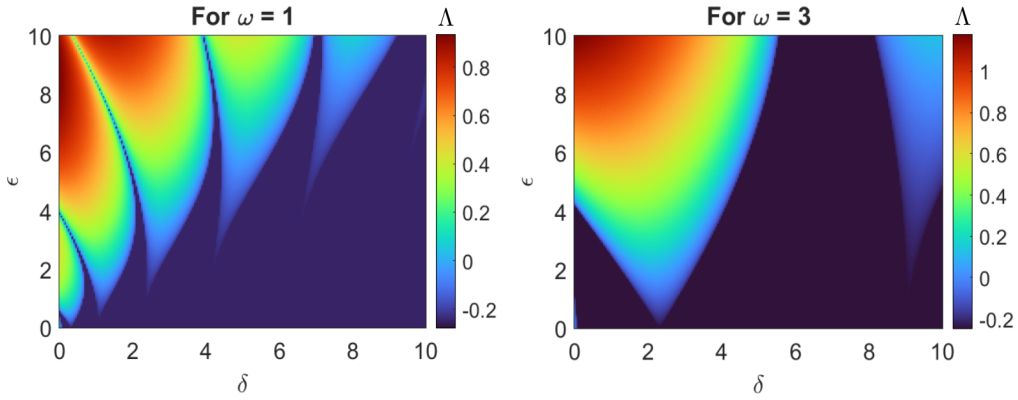

Figure 4.10: Stability maps using Λ for the damped Mathieu's equation with $b = 0.5$ and $\omega = 1$ and 3, respectively.

4.2.1 Case I: undamped system with one time-periodic coefficient

Two systems that can be described by similar differential equations are depicted in figure 4.11. On the left, a 2DoF mechanical system is shown, composed by two masses m_1, m_2 and three springs with stiffness coefficient k_1, k_2 and k_3. Meanwhile, on the right in the same figure, an electromagnetic system is seen, another system that can be described by the previous differential equations. It is composed by two inductors l_1, l_2 and three capacitors with capacitance c_1, c_2 and c_3.

Since the intuition for mechanical systems is more clear, only this system is going to be treated next. However, it is important to highlight that the same conclusions about stability of the trivial solution can be made for the electromagnetic system as well for the same used parameters. The differences would lie in the physical interpretations of the system's behaviour.

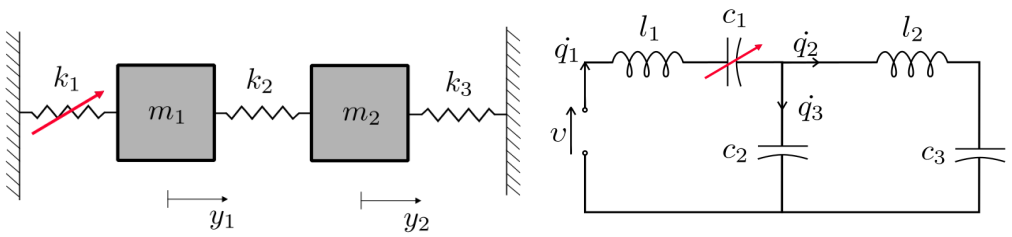

Figure 4.11: 2DoF mechanical system with its electromagnetic equivalent system for case I.

Parametric excitation can be introduced to the proposed mechanical system in the spring connecting m_1 to the wall. Thus, take $k_1 = k + \epsilon\cos(\omega t)$. The dynamics of this non-autonomous system for unit masses ($m_1 = m_2 = 1$) in matrix form is

$$\begin{bmatrix} \ddot{y}_1 \\ \ddot{y}_2 \end{bmatrix} + \begin{bmatrix} [k + \epsilon\cos(\omega t)] + k_2 & -k_2 \\ -k_2 & k_2 + k_3 \end{bmatrix} \begin{bmatrix} y_1 \\ y_2 \end{bmatrix} = \begin{bmatrix} 0 \\ 0 \end{bmatrix}. \tag{4-4}$$

The natural frequencies of this undamped system when there is no parametric excitation for $k = k_2 = k_3 = 1$ are, in rad/s,

$$\omega_1 = 1 \;\text{ and }\; \omega_2 = \sqrt{3} \approx 1.732. \tag{4-5}$$

By making use of equations (3-20) and (3-21), the critical frequencies can be obtained, where the phenomenon of parametric resonance occurs. They are of interest so the frequency intervals where instability takes place are known. Using first equation (3-20), these frequencies are obtained, in rad/s, as

$$2\,\omega_1 = 2,\quad \frac{2\,\omega_1}{2} = 1,\quad \frac{2\,\omega_1}{3} = \frac{2}{3},\ \ldots$$
$$2\,\omega_2 \approx 3.464,\quad \frac{2\,\omega_2}{2} \approx 1.732,\quad \frac{2\,\omega_2}{3} \approx 1.155,\ \ldots$$

By making use of equation (3-21), these frequencies are, also in rad/s,

$$\Sigma \approx 2.732,\quad \frac{\Sigma}{2} \approx 1.366,\quad \frac{\Sigma}{3} \approx 0.911,\ \ldots$$
$$\Delta = 0.732,\quad \frac{\Delta}{2} = 0.366,\quad \frac{\Delta}{3} = 0.244,\ \ldots$$

where $\Delta = \omega_2 - \omega_1$ and $\Sigma = \omega_1 + \omega_2$.

The goal now is to use Floquet theory to evaluate the stability of the trivial solution of this 2DoF system. Take then the dynamics in its two-dimensional first order form

$$\begin{bmatrix} \dot{y}_1 \\ \dot{y}_2 \\ \ddot{y}_1 \\ \ddot{y}_2 \end{bmatrix} = \begin{bmatrix} 0 & 0 & 1 & 0 \\ 0 & 0 & 0 & 1 \\ -(k + \epsilon\cos(\omega t) + k_2) & k_2 & 0 & 0 \\ k_2 & -(k_2 + k_3) & 0 & 0 \end{bmatrix} \begin{bmatrix} y_1 \\ y_2 \\ \dot{y}_1 \\ \dot{y}_2 \end{bmatrix}.$$

By using the numerical procedure described in appendix E, a stability map on the $\omega \times \epsilon$ plane is plotted, shown in figure 4.12 and plotted with a grid of 0.001. The dark blue area represents the unstable cases for each pair (ω, ϵ) for the fixed values of k, k_2 and k_3. Figure 4.12 shows that the unstable behaviour occurs where expected: at the vicinities of the obtained critical frequencies.

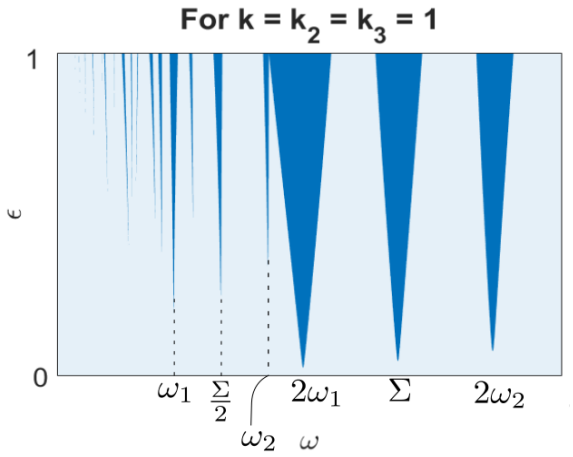

Figure 4.12: Stability map for the 2DoF system with $k = k_2 = k_3 = 1$.

The same can be seen in figure 4.13, that shows the stability maps in terms of Λ in the same range of the $\omega \times \epsilon$ plane, plotted with a grid of 0.005. For each one of the pairs (ω, ϵ), the respective Λ is disposed in different colors for different values of these exponents: the more red is the region of the map, the more unstable, once the more positive is Λ the more unstable is the trivial solution for that point in the map. This values can be seen through the color-bars on the right side of the map.

Nonetheless, the predominance of the first order critical frequency is not obvious by analyzing these maps. Thus, let us fix a value of ϵ so the plane $\omega \times \Lambda$ can be plotted. Using a grid of 0.001 and a chosen fixed value of $\epsilon = 0.3$, this plot is given in figure 4.14. It is possible to notice that the values of Λ are positive in the vicinities of the critical frequencies, shown in the ω-axis in figure 4.14. As expected, the color scale in figure 4.14 that provides the values of Λ match with the values in figure 4.13. The predominance of the first order critical frequency at $2\omega_1$ can be clearly seen in this plot on the $\omega \times \Lambda$ plane, that is easier to see and faster to compute.

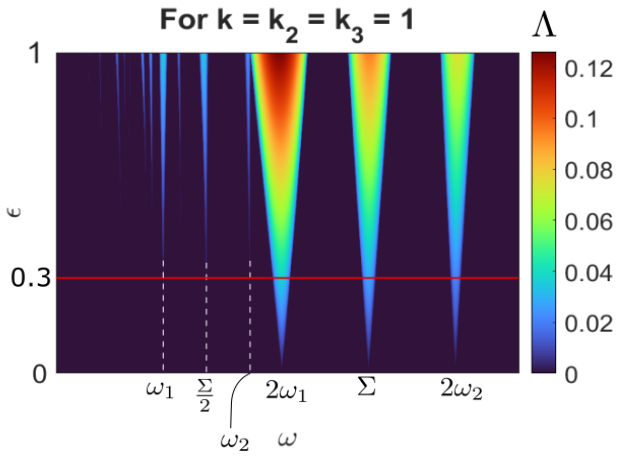

Figure 4.13: Stability map for the 2DoF system with $k = k_2 = k_3 = 1$ using Λ.

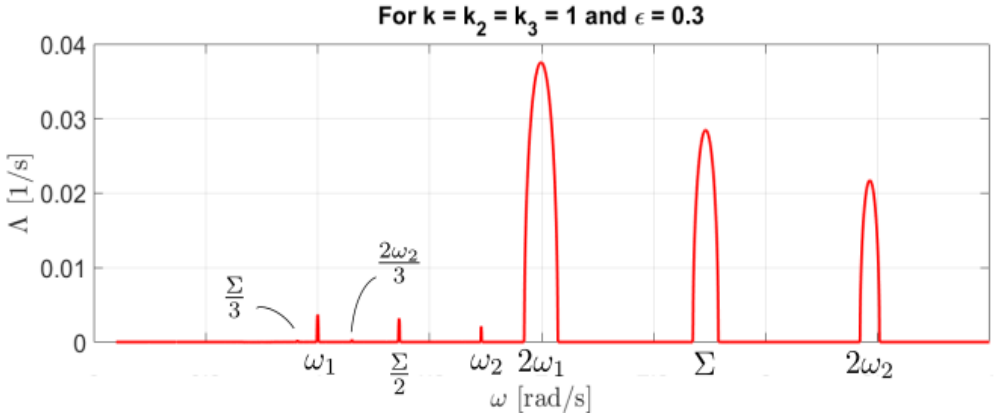

Figure 4.14: $\omega \times \Lambda$ plot for the system with $k = k_2 = k_3 = 1$.

To make a complete analysis, figures 4.15 and 4.16 show different phase diagrams of $y_1 \times \dot{y}_1$ and $y_2 \times \dot{y}_2$, respectively, with a grid of 0.002 and during 100 s. The frequency $\omega = 1.5$ was taken so a stable case could be discussed. For each figure, the first row of figures 4.15 and 4.16 was plotted for the initial conditions $y_1(0) = 1$, $y_2(0) = 0$, $\dot{y}_1(0) = 0$, $\dot{y}_2(0) = 0$ and $y_1(0) = 0$, $y_2(0) = 1$, $\dot{y}_1(0) = 0$, $\dot{y}_2(0) = 0$, respectively. Meanwhile, their second row was plotted for $y_1(0) = 0$, $y_2(0) = 0$, $\dot{y}_1(0) = 1$, $\dot{y}_2(0) = 0$ and $y_1(0) = 0$, $y_2(0) = 0$, $\dot{y}_1(0) = 0$, $\dot{y}_2(0) = 1$, respectively.

As mentioned in section 2.2.2, phase diagrams for time-varying systems can be challenging to analyze due to the explicit dependency of time on the equations of motion. To make it easier to understand them, the motions' start points are marked with a red dot and the numerical approximations at the final time are marked with a black dot. Figures 4.15 and 4.16 are showing stable motions around the origin, but the general behaviour is quite complex.

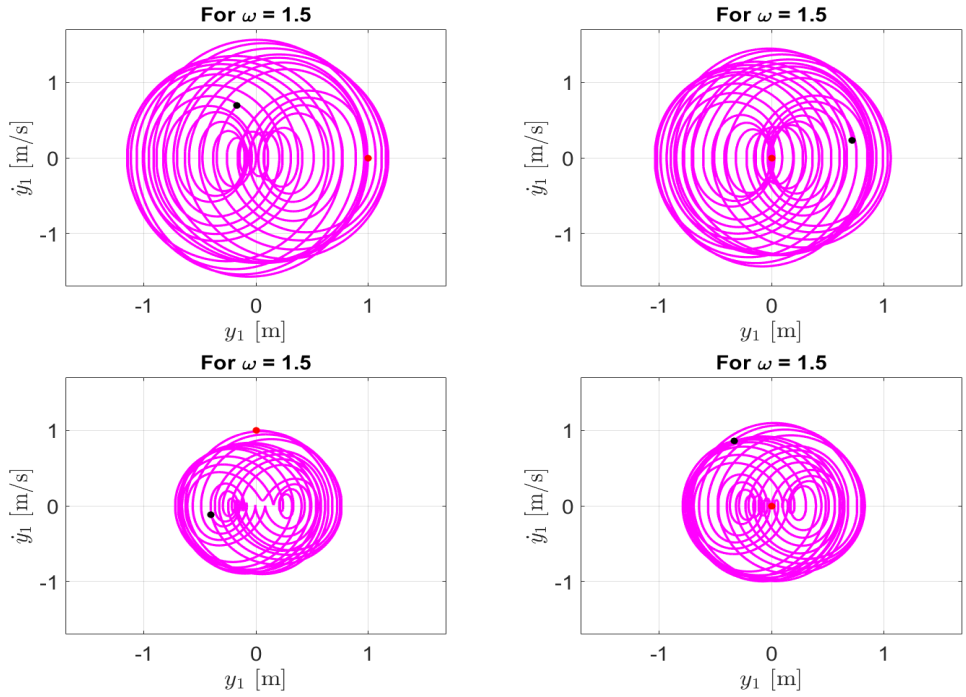

Figure 4.15: Phase diagrams for $y_1 \times \dot{y}_1$ with $\omega = 1.5$, $k = k_2 = k_3 = 1$ and $\epsilon = 0.3$, where the start points are marked with red dots and the numerical approximations at the final time are marked with black dots.

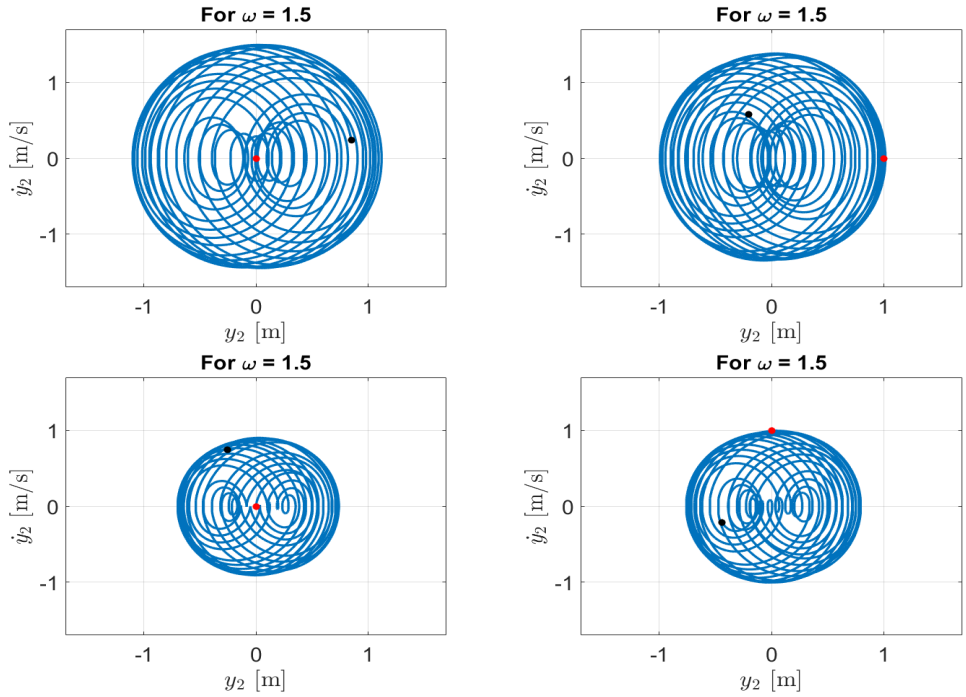

Figure 4.16: Phase diagrams for $y_2 \times \dot{y}_2$ with $\omega = 1.5$, $k = k_2 = k_3 = 1$ and $\epsilon = 0.3$, where the start points are marked with red dots and the numerical approximations at the final time are marked with black dots.

4.2.2
Case II: damped system with two time-periodic coefficients

The two systems that can be described by similar differential equations are now depicted in figure 4.17. The differences between this example and the previous one are: a second time-periodic parameter is introduced to the system (on the stiffness coefficient k_3 for the purely mechanical system or on the capacitance c_3 for the purely electromagnetic one) and the presence of dissipation (through two dampers with constant damping coefficients $b_1,\ b_2$ for the purely mechanical system or two resistors with resistance $r_1,\ r_2$ for the purely electromagnetic one).

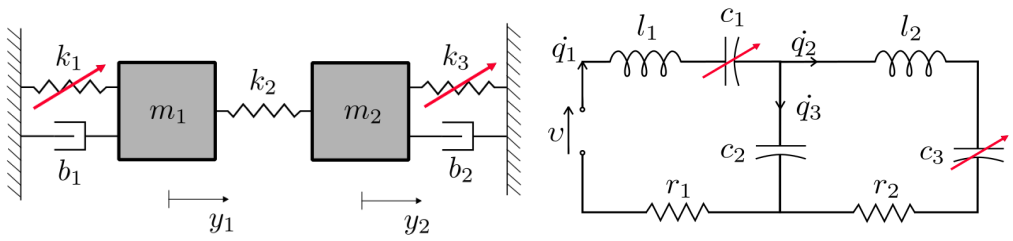

Figure 4.17: 2DoF mechanical system with its electromagnetic equivalent system for case II.

Just as for the previous example, we are going to continue by addressing the mechanical system. Taking $k_1 = k_3 = k + \epsilon\cos(\omega t)$, the system's dynamics for unit masses is

$$\begin{bmatrix} \ddot{y}_1 \\ \ddot{y}_2 \end{bmatrix} + \begin{bmatrix} b_1 & 0 \\ 0 & b_2 \end{bmatrix} \begin{bmatrix} \dot{y}_1 \\ \dot{y}_2 \end{bmatrix} + \\ + \begin{bmatrix} [k + \epsilon\cos(\omega t)] + k_2 & -k_2 \\ -k_2 & k_2 + [k + \epsilon\cos(\omega t)] \end{bmatrix} \begin{bmatrix} y_1 \\ y_2 \end{bmatrix} = \begin{bmatrix} 0 \\ 0 \end{bmatrix}, \qquad (4\text{-}6)$$

that in its two-dimensional first order form is

$$\begin{bmatrix} \dot{y}_1 \\ \dot{y}_2 \\ \ddot{y}_1 \\ \ddot{y}_2 \end{bmatrix} = \begin{bmatrix} 0 & 0 & 1 & 0 \\ 0 & 0 & 0 & 1 \\ -(k + \epsilon\cos(\omega t) + k_2) & k_2 & -b_1 & 0 \\ k_2 & -(k_2 + k + \epsilon\cos(\omega t)) & 0 & -b_2 \end{bmatrix} \begin{bmatrix} y_1 \\ y_2 \\ \dot{y}_1 \\ \dot{y}_2 \end{bmatrix}.$$

The goal is to analyze how the introduction of a second time-periodic coefficient and damping to the system influence the stability of the zero solution. Notice first that the natural frequencies of the undamped system without the parametric excitation are also the ones given in equation (4-5) for the same parameters $k = k_2 = 1$.

The stability map in the $\omega \times \epsilon$ plane is provided in figure 4.18, plotted with a grid of 0.001. The dark blue area represents the unstable areas for fixed parameters $k = k_2 = 1$, $b_1 = b_2 = 0.1$. Moreover, figure 4.19 shows the stability maps in terms of Λ in the same interval of the $\omega \times \epsilon$ plane, plotted with a grid of 0.005.

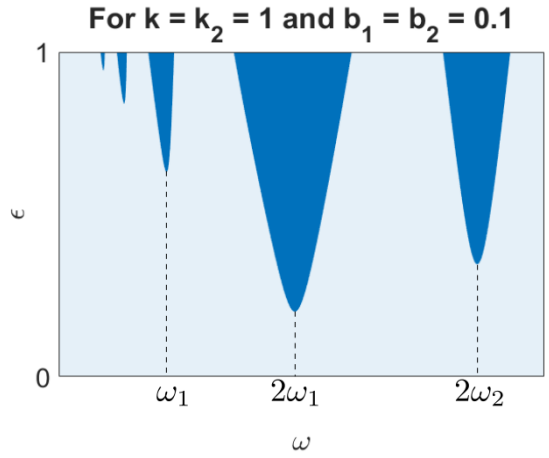

Figure 4.18: Stability map for the 2DoF system with $k = k_2 = 1$ and $b_1 = b_2 = 0.1$.

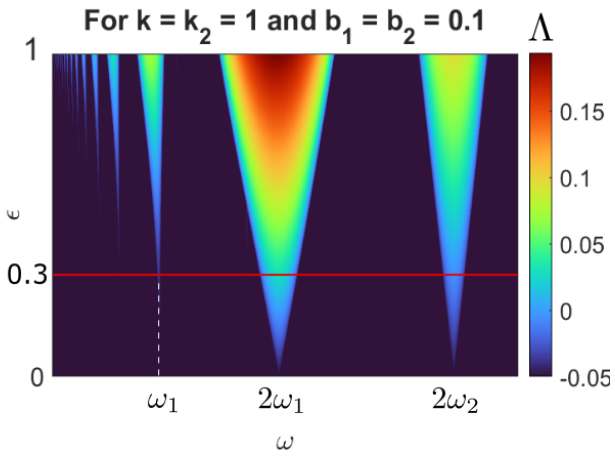

Figure 4.19: Stability map for the 2DoF system with $k = k_2 = 1$ and $b_1 = b_2 = 0.1$ using Λ.

When comparing figures 4.18 and 4.19, it might seem odd that they are different, once the maps using Λ values has sharp "tongues". If one notices the color bar in figure 4.19, it is possible to see that the difference is due to the fact that this stability map presents negative values for Λ, just as discussed in the stability analysis of the damped Mathieu's equation. These negative Λs are a consequence of the present dissipation, that result in sharp "tongues" in

the stability map that do not appear when only using Floquet multipliers in figure 4.18, once this is restricted to the classification of stable/unstable areas.

Furthermore, by comparing figures 4.12 and 4.18 as well as figures 4.13 and 4.19, one can notice that the unstable intervals in the vicinities of the critical frequencies that depend on Σ do not appear. This is a consequence of the addition of a second time-periodic parameter that is equal to the already existent one. However, even though some instability "tongues" disappear, the remaining unstable areas are wider then with one time-periodic coefficient and the values of Λ reach higher values.

Fixing $\epsilon = 0.3$, the plane $\omega \times \Lambda$ is plotted with a grid of 0.001 in figure 4.20, where it is possible to see the predominance of first order critical frequencies. By comparing figures 4.14 and 4.20, it is possible to notice that the addition of damping to system for the same fixed parameters shifts the curve to lower values in the Λ-axis, only being higher than zero in the vicinity of $2\omega_1$. Notice that this is the case for when both dampers have the same damping coefficient.

Moreover, one can notice that the critical frequencies corresponding to Σ, $\Sigma/2$ and $\Sigma/3$ are not present in the plot. This is due to the two equal time-periodic coefficients and was expected from the stability maps. This means that adding time-periodic coefficients to the already parametrically excited system is a way of cancelling instability areas, a type of vibration control for this kind of system.

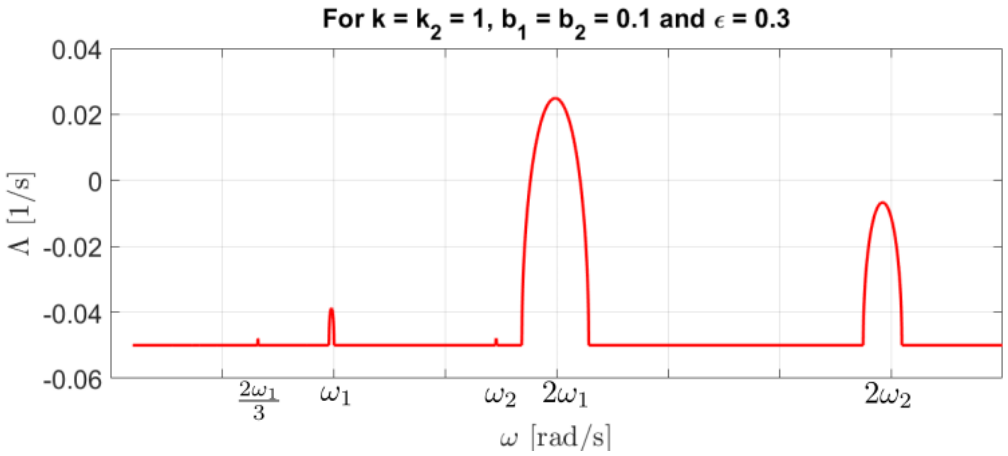

Figure 4.20: $\omega \times \Lambda$ plot for the system with $k = k_2 = 1$ and $b_1 = b_2 = 0.1$.

Furthermore, figure 4.21 shows the numerical approximations through time with $\epsilon = 0.3$, $\omega = 4$ and initial conditions $y_1(0) = 0.001$, $y_2(0) = 0$, $\dot{y}_1(0) = 0$, $\dot{y}_2(0) = 0$. It is possible to see that both approximations for a slight change from the trivial solution return to the origin, making this case

not only stable, but asymptotically stable. This was expected for the chosen parameters once the Λ value is negative.

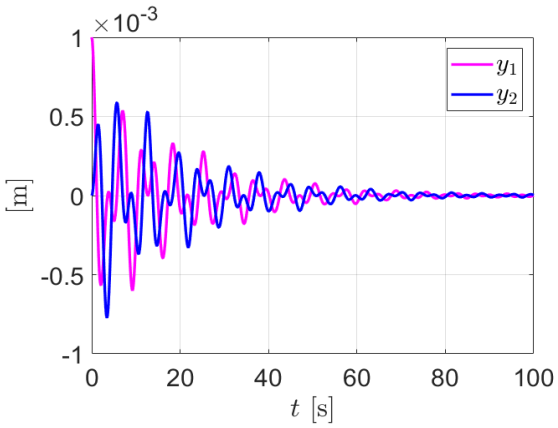

Figure 4.21: Numerical approximations with $\epsilon = 0.3$ and $\omega = 4$.

One can also plot the phase diagrams, shown in figure 4.22, where the beginning of the motion is marked with a red dot and the numerical approximation at the final time (100 s) is marked with a black dot. The expected behaviour from the former analysis of approaching the origin as time increases can be seen. Notice that in the phase diagram for $y_2 \times \dot{y}_2$ the motion starts and finishes at the origin and that is why only the red dot can be seen.

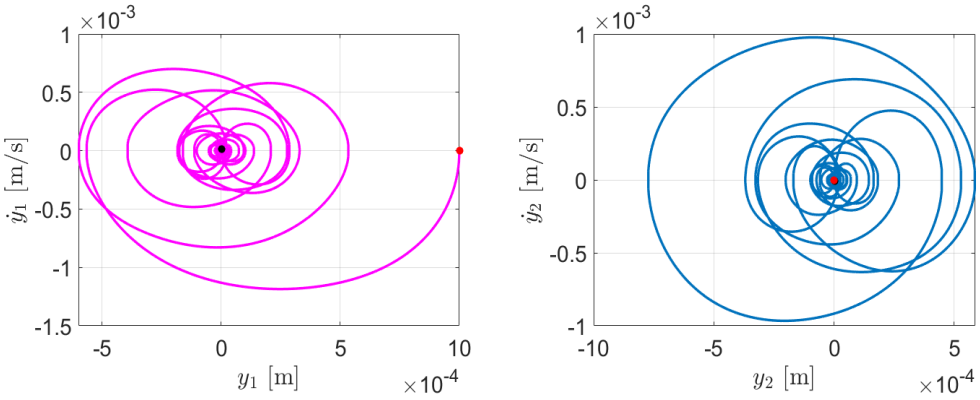

Figure 4.22: Phase diagrams with $\epsilon = 0.3$ and $\omega = 4$.

4.2.3
Case III: damped system with one time-periodic coefficient

In this example, take the 2DoF mechanical system on the left of figure 4.23. It is composed by two masses m_1, m_2, a spring k_1 and a damper b connecting the first mass to a wall and one spring connecting both masses with stiffness k_2, a time-periodic coefficient taken as $k_2 = k + \epsilon \cos(\omega t)$.

This results in a parametric excitation occurring in all terms of the stiffness matrix, including on the off-diagonal elements, differently from the previous examples. An electromagnetic system that can be described in a similar matter is depicted on the right in figure 4.23. It is composed by two inductors l_1, l_2, two capacitors (one with constant capacitance c_2 and another one with time-periodic capacitance c_1) and a resistor with resistance r.

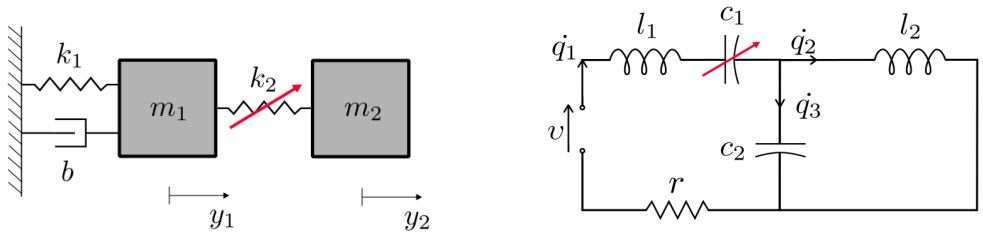

Figure 4.23: 2DoF mechanical system with its electromagnetic equivalent system for case IV.

Both of this systems can be described by similar differential equations, but, just as for the previous examples, the mechanical system is going to be addressed next. This system's dynamics in matrix form for unit masses is

$$\begin{bmatrix} \ddot{y}_1 \\ \ddot{y}_2 \end{bmatrix} + \begin{bmatrix} b & 0 \\ 0 & 0 \end{bmatrix} \begin{bmatrix} \dot{y}_1 \\ \dot{y}_2 \end{bmatrix} + \\ + \begin{bmatrix} k_1 + [k + \epsilon\cos(\omega t)] & -[k + \epsilon\cos(\omega t)] \\ -[k + \epsilon\cos(\omega t)] & k + \epsilon\cos(\omega t) \end{bmatrix} \begin{bmatrix} y_1 \\ y_2 \end{bmatrix} = \begin{bmatrix} 0 \\ 0 \end{bmatrix},$$

The natural frequencies for the undamped system without parametric excitation with $m_1 = m_2 = 1$, $k_1 = 3$ and $k = 1$ are, in rad/s,

$$\omega_1 = \sqrt{\frac{5 + \sqrt{13}}{2}} \approx 2.074 \text{ and } \omega_2 = \sqrt{\frac{5 - \sqrt{13}}{2}} \approx 0.835.$$

Let us now obtain the critical frequencies. Using equation (3-20) they are, in rad/s,

$$2\,\omega_1 \approx 4.149, \quad \frac{2\,\omega_1}{2} \approx 2.074, \quad \frac{2\,\omega_1}{3} \approx 1.383, \ \ldots$$
$$2\,\omega_2 \approx 1.67, \quad \frac{2\,\omega_2}{2} \approx 0.835, \quad \frac{2\,\omega_2}{3} \approx 0.557, \ \ldots$$

By making use of equation (3-21), the obtained frequencies are, also in

rad/s,

$$\Sigma \approx 2.909, \quad \frac{\Sigma}{2} \approx 1.455, \quad \frac{\Sigma}{3} \approx 0.97, \ \ldots$$
$$\Delta \approx 1.239, \quad \frac{\Delta}{2} \approx 0.62, \quad \frac{\Delta}{3} \approx 0.413, \ \ldots$$

where $\Delta = \omega_1 - \omega_2$ and $\Sigma = \omega_1 + \omega_2$. Furthermore, the dynamics can be written in its two-dimensional first order form

$$\begin{bmatrix} \dot{y}_1 \\ \dot{y}_2 \\ \ddot{y}_1 \\ \ddot{y}_2 \end{bmatrix} = \begin{bmatrix} 0 & 0 & 1 & 0 \\ 0 & 0 & 0 & 1 \\ -(k_1 + k + \epsilon\cos(\omega t)) & k + \epsilon\cos(\omega t) & -b & 0 \\ k + \epsilon\cos(\omega t) & -(k + \epsilon\cos(\omega t)) & 0 & 0 \end{bmatrix} \begin{bmatrix} y_1 \\ y_2 \\ \dot{y}_1 \\ \dot{y}_2 \end{bmatrix}.$$

After writing the equations of motion in its state-space form, a stability map obtained by using Floquet theory can be plotted through the numerical procedure in appendix E. This stability map is given in figure 4.24, where the $\omega \times \epsilon$ plane was plotted with a grid of 0.005. The dark blue area represents once again the regions where instability takes place for fixed values $k_1 = 3$, $k = 1$ and $b = 0.2$. Since there is a dissipative term, the instability "tongues" in the stability maps are not sharp.

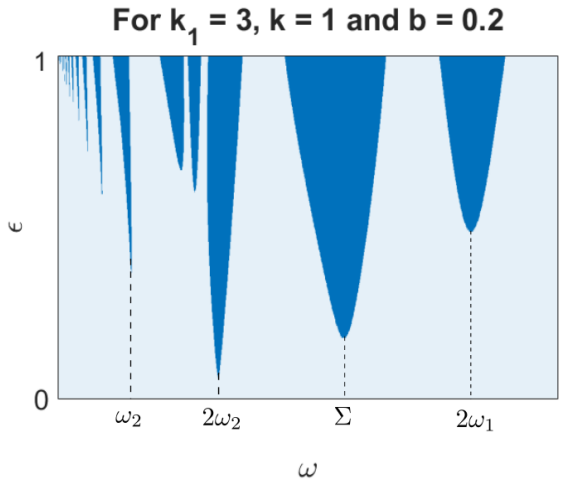

Figure 4.24: Stability map in the $\omega \times \epsilon$ plane for the 2DoF system with $k_1 = 3$, $k = 1$ and $b = 0.2$.

The stability maps in terms of Λ can also be obtained. The $\omega \times \epsilon$ plane was plotted with a grid of 0.005, given in figure 4.25. By comparing figures 4.24 and 4.25, it is possible to notice that they differ in some important aspects as a result of the gradient of Λ values. Figure 4.25 provides information about the stability of the trivial solution by a classification of only stable or unstable. One may also wonder why the stability map in figure 4.19 differs so profoundly from

the one in figure 4.25. Even though the range of Λ values is not that different, the heatmap plot used in the software *MatLab* provided the color gradient on its on, making the lower values of Λ assume the dark blue color.

Furthermore, by making use of this stability map, it is also possible to notice the existence of what is known as *parametric anti-resonance*, shown as the dark blue area of stability in figure 4.25. It corresponds to the critical frequency Δ, obtained by the subtraction of the found natural frequencies. This phenomenon was briefly discussed in section 3.3.1 and is going to be analyzed in more details next.

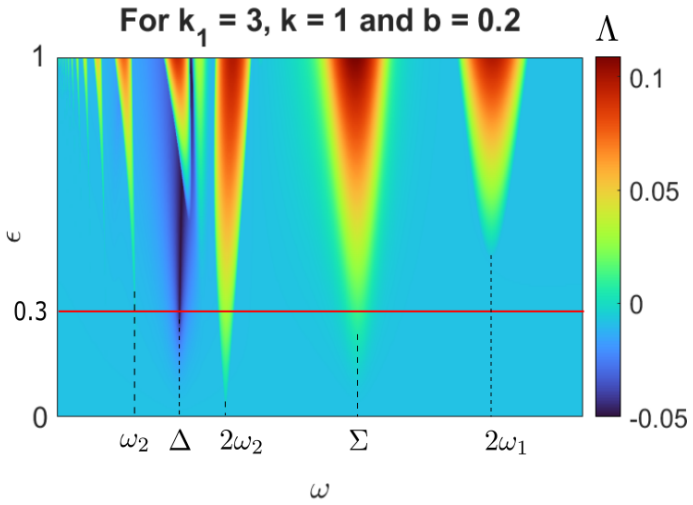

Figure 4.25: Stability map in the $\omega \times \epsilon$ plane for the 2DoF system with $k_1 = 3$, $k = 1$ and $b = 0.2$ using Λ.

Let us fix the value of ϵ as 0.3 to obtain the plot $\omega \times \Lambda$, just as it was done for the previous examples. Using a grid of 0.001, this graphic is given in figure 4.26. One may notice that a destabilizing effect only occurs for the critical frequencies $2\omega_2$ and Σ for the fixed amplitude ϵ. Meanwhile, the critical frequencies ω_2, $2\omega_2/3$ and $\Sigma/2$ are associated to negative values of Λ, being then a region of asymptotically stability of the trivial solution. This means that, as a result of the existing damping, these critical frequencies do not result in instability for the chosen value of ϵ. Furthermore, the critical frequency Δ has a stabilizing effect. As said previously, this frequency is associated with the parametric anti-resonance phenomenon and results in an abrupt decrease in the values of Λ. While the other critical frequencies result in rounded curves at their neighbourhood, the curve around Δ has a sharp form.

It is of interest at this moment to analyze the just seen facts with a little more depth. By using the chosen value of ϵ, phase diagrams can be obtained. This is done for different values of excitation frequency ω so it is

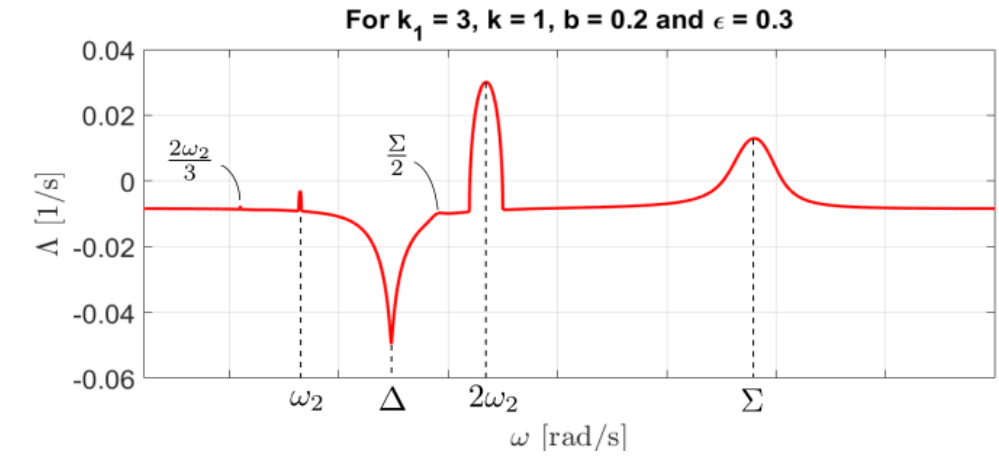

Figure 4.26: $\omega \times \Lambda$ plot for the system with $k_1 = 3$, $k = 1$ and $b = 0.2$.

possible to compare the numerical approximations for each case. The used parameters are $k_1 = 3$, $k = 1$, $b = 0.2$ and $\epsilon = 0.3$, with initial conditions $y_1(0) = 0.001, y_2(0) = 0, \dot{y}_1(0) = 0, \dot{y}_2(0) = 0$.

Let us first compare a stable case where $\omega = 1$ with the excitation frequency where the parametric anti-resonance occurs $\omega = \Delta$. Figures 4.27 and 4.28 show the phase diagrams for $\omega = 1$ and $\omega = \Delta$, respectively, where once again the beginning of the motion is marked as a red dot and the end as a black one. It is possible to see that for both cases the numerical approximations are approaching the zero value, making the trivial solution for both excitation frequencies asymptotically stable.

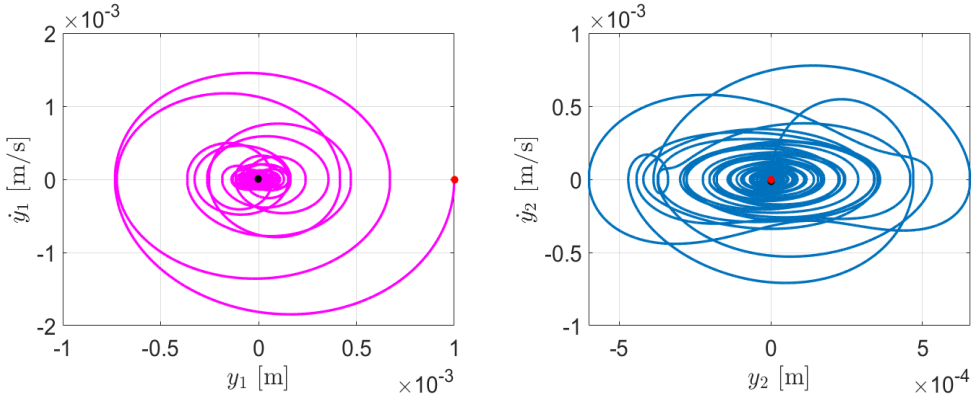

Figure 4.27: Phase diagrams with $\omega = 1$.

However, there is no evident discrepancy between these phase diagrams. After all, what is the difference between these cases? This can be graphically answered by plotting the numerical approximations through time for both excitation frequencies. Figures 4.29 and 4.30 show these plots for $\omega = 1$ and $\omega = \Delta$, respectively. It is also possible to notice the asymptotic stable

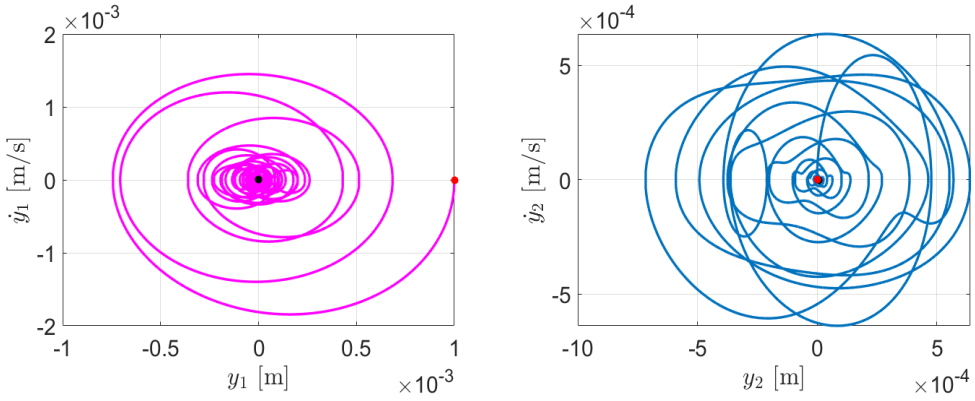

Figure 4.28: Phase diagrams with $\omega = \Delta$.

behaviour, where the difference between them relies on how fast the trivial solution approaches zero. The numerical approximations with $\omega = \Delta$ for a small deviation from the trivial solution approach zero for a shorter period of time then with $\omega = 1$.

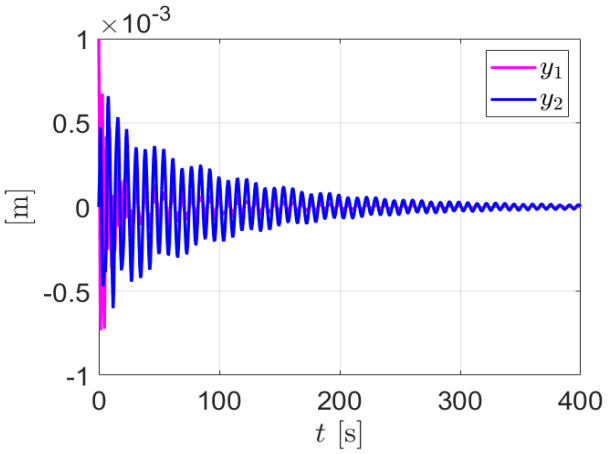

Figure 4.29: Numerical approximations of the system's response with $\epsilon = 0.3$ and $\omega = 1$.

Therefore, by strategically choosing the excitation frequency as the frequency correspondent to the parametric anti-resonance phenomenon, it allows one to make a vibration control of the analyzed system. Parametric excitation can thus be used as a way of controlling vibration due to its stabilizing effect on the system.

For a final analysis of this example, take the case where $\omega = 2\omega_2$. Through figure 4.26 it is possible to see that this corresponds to an unstable situation. Since this is the case, one expects that the numerical approximations diverge from the zero solution as time goes by. This behaviour can be seen in figure 4.31, that provides us the system's phase diagrams from 0 s to 150 s of simulation.

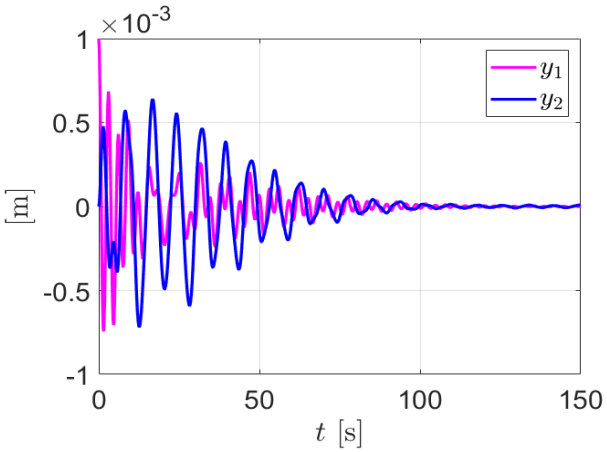

Figure 4.30: Numerical approximations of the system's response with $\epsilon = 0.3$ and $\omega = \Delta$.

However, a different effect occurs for this excitation frequency that can be seen through figure 4.32. This is a clear example of the importance of Floquet analysis: if only a short period of time was taken in consideration for the simulation, let us say until 30 s, the response would appear to be only decaying with time, when it is clear by figure 4.32 that this is not the case for longer periods of time. By solving IVPs for only one period T, one can use Floquet analysis to analyze the stability of the trivial solution.

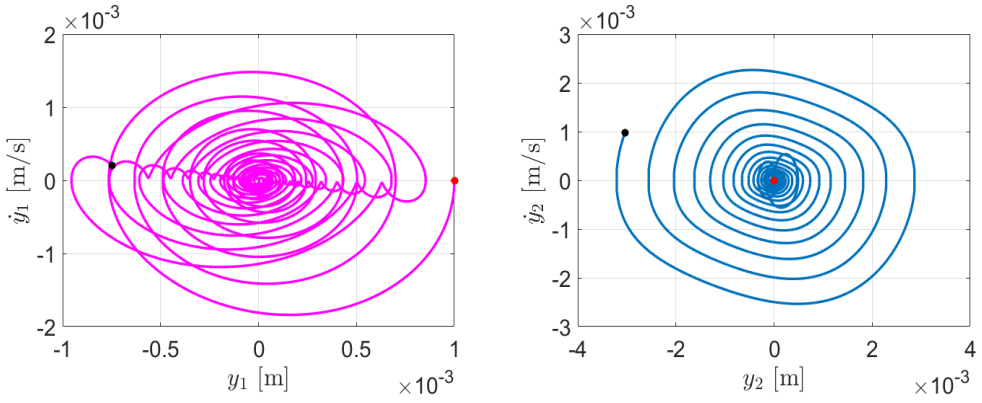

Figure 4.31: Phase diagrams with $\omega = 2\omega_2$.

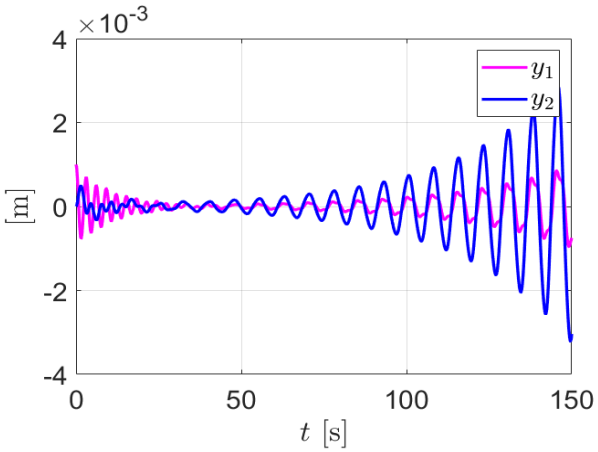

Figure 4.32: Numerical approximations of the system's response with $\epsilon = 0.3$ and $\omega = 2\omega_2$.

This last example of the use of Floquet theory to evaluate the stability of a 2DoF system also clearly shows the advantages of using the maximum value of the LCEs Λ as used in the numerical procedure provided in this dissertation. This is due to the fact that the phenomenon of parametric anti-resonance could not be perceived by only making use of Floquet multipliers as proposed by the numerical procedure in appendix E.

5
Electromechanical systems

As introduced in chapter 1, electromechanical systems are systems composed by two different natures: one mechanical and another electromagnetic [7; 8; 9; 10]. Thus, the energies present in this type of system also have distinct origins: some are mechanical energies (such as kinetic and potential energies) while others are electromagnetic energies (like magnetic and electrical energies) [11; 12].

Electromechanical systems are characterized by the interaction between their subsystems, meaning that the mechanical subsystem influences the electromagnetic subsystem as well as the inverse [13; 14; 15; 16; 17]. Due to this mutual influence, it is not sufficient to describe each subsystem separately for an accurate description of their dynamics. One must take into account parameters of both mechanical and electromagnetic natures [18; 19].

The mutual interaction between the subsystems is only possible through coupling elements that provide a way of exchanging energy among them [11; 12]. In general, for linear electromechanical systems, these coupling terms appear in the equations of motion through gyroscopic and circulatory terms, matrices G and N, respectively.

Knowing the dynamics of this kind of system enables one to take a step further by introducing parametric excitation through time-periodic coefficients. This makes it possible to use Floquet theory to make a stability analysis. Since the simplest example of an electromechanical system must have at least two coordinates (one mechanical and one electromagnetic), for this first approach into stability analysis of the trivial solution of electromechanical systems, a 2DoF system called electromagnetic loudspeaker is going to be analyzed. Appendix D provides a brief introduction into how to obtain the equations of motion of electromechanical systems, using the loudspeaker to exemplify this [9; 18].

5.1 Stability analysis for time-periodic electromechanical systems

As said previously, this type of system has two distinct origins: one mechanical and another electromagnetic. With the used parametrization, their natural frequencies are *hybrid frequencies*, once they are dependent on parameters with both origins [37]. This also means that stability maps can be obtained by varying a mechanical parameter and an electromagnetic one.

This chapter analyzes different models of an electromagnetic loudspeaker, which dynamics is known [12; 9], given in more details in appendix D. First, a general view of this system is presented, providing the elements that compose it. The usual linear differential equations with constant coefficients that describe the loudspeaker's motion are then used to obtain the natural frequencies and mode shapes for the undamped case. After that, the forced response is going to be briefly analyzed. Thereafter, parametric excitation is introduced to the system through a time-periodic stiffness parameter, making it possible to make a stability analysis through Floquet theory for the undamped and damped cases. Stability maps are also used to evaluate the stability of the trivial solution.

5.1.1 Electromagnetic loudspeaker

Figure 5.1 provides an illustrative representation of an electromagnetic loudspeaker [9; 12]. This system is composed by a mass m, a spring with stiffness coefficient k, a damper with damping coefficient b, a voltage source v in series with a RL circuit (which means an inductor of inductance l and a resistor of resistance r) and a moving-coil transducer with transducer constant ρ. The parametrization used to describe the system's configuration is the displacement z of the mass from the mechanical subsystem's equilibrium point and the charge q passing through the circuit.

It is important to highlight that z is merely the displacement of the mass m from the chosen equilibrium point. The spring and damper simulate a membrane in the loudspeaker. The coupling enabling energy to flow between the two subsystems is provided by the moving-coil transducer, an element composed by a permanent magnet and a coil that can move in the z direction. This element converts electrical power into mechanical power or vice versa and cannot store energy [10; 18].

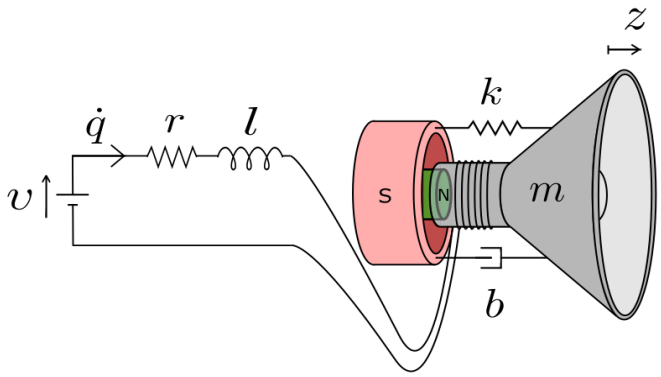

Figure 5.1: Electromagnetic loudspeaker.

The general form of a system's dynamics is given by equation (2-1), that for this linear system with constant coefficients is, as developed in appendix D,

$$\begin{bmatrix} m & 0 \\ 0 & l \end{bmatrix} \begin{bmatrix} \ddot{z} \\ \ddot{q} \end{bmatrix} + \left\{ \begin{bmatrix} b & 0 \\ 0 & r \end{bmatrix} + \begin{bmatrix} 0 & -\rho \\ \rho & 0 \end{bmatrix} \right\} \begin{bmatrix} \dot{z} \\ \dot{q} \end{bmatrix} + \begin{bmatrix} k & 0 \\ 0 & 0 \end{bmatrix} \begin{bmatrix} z \\ q \end{bmatrix} = \begin{bmatrix} 0 \\ \upsilon \end{bmatrix}, \tag{5-1}$$

where the dependence on time was omitted for notation simplification. Taking the general form of equation (2-1), the matrices present in the system's dynamics are

$$M = \begin{bmatrix} m & 0 \\ 0 & l \end{bmatrix},\ D = \begin{bmatrix} b & 0 \\ 0 & r \end{bmatrix},\ G = \begin{bmatrix} 0 & -\rho \\ \rho & 0 \end{bmatrix},\ K = \begin{bmatrix} k & 0 \\ 0 & 0 \end{bmatrix},$$

recalling that in the present system no coefficient matrix varies with time. It is possible to notice that the coupling between the mechanical and electromagnetic subsystems is provided by gyroscopic terms and that circulatory terms are not present in the dynamics.

Next, several cases of the loudspeaker dynamics are going to be analyzed.

5.1.1.1
Case I: undamped autonomous model

First it is of interest to find the system's natural frequencies [38; 39]. Taking equation (5-1) without a voltage source ($\upsilon = 0$) and considering the system with no dissipative terms ($b = 0,\ r = 0$), it is possible to rewrite the equations of motion as

$$E\dot{x} + Hx = 0, \tag{5-2}$$

where $x(t) = [z(t)\ q(t)\ \dot{z}(t)\ \dot{q}(t)]^T$, $E = \begin{bmatrix} G & M \\ M & 0 \end{bmatrix}$ and $H = \begin{bmatrix} K & 0 \\ 0 & -M \end{bmatrix}$.
The solutions of equation (5-2) are in the form

$$x(t) = u\, e^{\lambda t} = \begin{bmatrix} \psi \\ \lambda\psi \end{bmatrix} e^{\lambda t} \tag{5-3}$$

where λ is a scalar that represents the eigenvalues and u the respective eigenvectors. The second half of these eigenvectors has a multiplication by λ as a result of how vector x is written: its lower half is the derivative of the upper half. The eigenvalue problem (EVP) that must be solved is

$$(\lambda\, E + H)u = 0. \tag{5-4}$$

Since u should be a non-null vector for a non-trivial solution, matrix $(\lambda\, E + H)$ must be singular and thus have a null determinant, resuming the EVP for this case with no dissipation to

$$\det[\lambda\, E + H] = \det \begin{bmatrix} k & -\rho\lambda & m\lambda & 0 \\ \rho\lambda & 0 & 0 & l\lambda \\ m\lambda & 0 & -m & 0 \\ 0 & l\lambda & 0 & -l \end{bmatrix} = 0.$$

The characteristic function derived from it is thus

$$\begin{aligned} m^2l^2\lambda^4 + (\rho^2ml + kml^2)\lambda^2 &= 0, \\ \lambda^2(m^2l^2\lambda^2 + \rho^2ml + kml^2) &= 0. \end{aligned}$$

The wanted eigenvalues are roots of this characteristic function. Solving for λ leads to

$$\lambda_1 = \sqrt{\frac{k}{m} + \frac{\rho^2}{ml}}\; i, \;\; \lambda_2 = -\sqrt{\frac{k}{m} + \frac{\rho^2}{ml}}\; i \text{ and } \lambda_{3,4} = 0,$$

where $i = \sqrt{-1}$ and $\lambda_{3,4}$ is a double root. To obtain the eigenvectors corresponding to each one of them, one must substitute the just found eigenvalues into equation (5-4), where the vector u is now wanted.

For the first eigenvalue λ_1, the EVP is $(\lambda_1\, E + H)u_1 = 0$, that leads to the system

$$\begin{bmatrix} k & -\rho\lambda_1 & m\lambda_1 & 0 \\ \rho\lambda_1 & 0 & 0 & l\lambda_1 \\ m\lambda_1 & 0 & -m & 0 \\ 0 & l\lambda_1 & 0 & -l \end{bmatrix} \begin{bmatrix} u_{11} \\ u_{12} \\ u_{13} \\ u_{14} \end{bmatrix} = \begin{bmatrix} 0 \\ 0 \\ 0 \\ 0 \end{bmatrix},$$

where the constants $u_{11},\ u_{12},\ u_{13},\ u_{14}$ are the unknown elements of the wanted eigenvector u_1. This system can be written as

$$
\begin{aligned}
k u_{11} - \rho\lambda_1 u_{12} + m\lambda_1 u_{13} &= 0, && (5\text{-}5)\\
\rho\lambda_1 u_{11} + l\lambda_1 u_{14} &= 0, && (5\text{-}6)\\
\lambda_1 u_{11} - m u_{13} &= 0, && (5\text{-}7)\\
l\lambda_1 u_{12} - l u_{14} &= 0. && (5\text{-}8)
\end{aligned}
$$

By the last two equalities (5-7) and (5-8), $u_{13} = \lambda_1 u_{11}$ and $u_{14} = \lambda_1 u_{12}$. One can then substitute u_{13} and u_{14} into equations (5-5) and (5-6) to obtain

$$
\begin{aligned}
(k + m\lambda_1^2)u_{11} - \rho\lambda_1 u_{12} &= 0,\\
\rho\lambda_1 u_{11} + l\lambda_1^2 u_{12} &= 0,\\
u_{12} &= -\frac{\rho}{l\,\lambda_1} u_{11}.
\end{aligned}
$$

Therefore,

$$
\begin{aligned}
\left(k + m\lambda_1^2 + \frac{\rho^2}{l}\right) u_{11} &= 0,\\
\left[k - m\left(\frac{k}{m} + \frac{\rho^2}{ml}\right) + \frac{\rho^2}{l}\right] u_{11} &= 0,\\
0\; u_{11} &= 0.
\end{aligned}
$$

This leads to $u_{11} \in \mathbb{R}^*$ and $u_{12} = -\dfrac{\rho}{l\,\lambda_1} u_{11}$. Thus, the eigenvector u_1 corresponding to the eigenvalue λ_1 is

$$
u_1 = \begin{bmatrix} 1 \\ -\rho/(l\,\lambda_1) \\ \lambda_1 \\ -\rho/l \end{bmatrix} \alpha, \quad \alpha \in \mathbb{R}^*.
$$

For λ_2, this same procedure can be done, obtaining

$$
(\lambda_2\, A + B)u_2 = 0 \;\; \rightarrow \;\; u_2 = \begin{bmatrix} 1 \\ -\rho/(l\,\lambda_2) \\ \lambda_2 \\ -\rho/l \end{bmatrix} \zeta, \;\; \zeta \in \mathbb{R}^*.
$$

Finally, for $\lambda_{3,4}$ the EVP is $(\lambda_{3,4}\, E + H)u_3 = 0$, that results in

$$
\begin{bmatrix} k & 0 & 0 & 0 \\ 0 & 0 & 0 & 0 \\ 0 & 0 & -m & 0 \\ 0 & 0 & 0 & -l \end{bmatrix} \begin{bmatrix} u_{31} \\ u_{32} \\ u_{33} \\ u_{34} \end{bmatrix} = \begin{bmatrix} 0 \\ 0 \\ 0 \\ 0 \end{bmatrix}.
$$

where the constants $u_{31},\ u_{32},\ u_{33},\ u_{34}$ are once again the unknowns. By solving this system one gets

$$\begin{array}{c} ku_{31}=0 \rightarrow u_{31}=0 \\ u_{32}\in\mathbb{R}^* \\ -mu_{33}=0 \rightarrow u_{33}=0 \\ -lu_{34}=0 \rightarrow u_{34}=0 \end{array} \quad \rightarrow \quad u_3 = \begin{bmatrix} 0 \\ 1 \\ 0 \\ 0 \end{bmatrix} \iota, \quad \iota \in \mathbb{R}^*.$$

The eigenvectors and their respective eigenvalues were just obtained. In summary, these eigenpairs are

$$\begin{aligned} \lambda_1 &= \sqrt{\frac{k}{m}+\frac{\rho^2}{ml}}\, i, & u_1 &= \begin{bmatrix} 1 & -\rho/(l\,\lambda_1) & \lambda_1 & -\rho/l \end{bmatrix}^T, \\ \lambda_2 &= -\sqrt{\frac{k}{m}+\frac{\rho^2}{ml}}\, i, & u_2 &= \begin{bmatrix} 1 & -\rho/(l\,\lambda_2) & \lambda_2 & -\rho/l \end{bmatrix}^T, \\ \lambda_{3,4} &= 0, & u_3 &= \begin{bmatrix} 0 & 1 & 0 & 0 \end{bmatrix}^T. \end{aligned}$$

The eigenvalues $\lambda_{1,2}$ and $\lambda_{3,4}$ result, respectively, in the natural frequencies

$$\omega_{1,2} = \sqrt{\frac{k}{m}+\frac{\rho^2}{ml}} \ \text{ and } \ \omega_{3,4}=0, \tag{5-9}$$

while the normal modes are taken as the upper half of the found eigenvectors.

The natural frequency $\omega_{1,2}$ in (5-9) is a *hybrid frequency*, once it depends on mechanical as well as electromagnetic coordinates, two variables with different natures. It is also possible to notice that $\omega_{1,2}$ is composed of two portions: k/m and $\rho^2/(ml)$. The former portion appears in the natural frequency of a purely mechanical mass-spring system. Meanwhile, the latter portion involves both mechanical and electromagnetic parameters.

The general solution for this system is given by a linear combination involving the found eigenvalues and eigenvector, as in equation (5-3). The solution can thus be written as

$$x(t) = (b_1+a_1 t)\begin{bmatrix} 0 \\ 1 \\ 0 \\ 0 \end{bmatrix} + a_2\, e^{i\,\omega_{1,2}\,t}\begin{bmatrix} 1 \\ -\rho/(l\,\omega_{1,2}\,i) \\ \omega_{1,2}\,i \\ -\rho/l \end{bmatrix} + a_3\, e^{-i\,\omega_{1,2}\,t}\begin{bmatrix} 1 \\ \rho/(l\,\omega_{1,2}\,i) \\ -\omega_{1,2}\,i \\ -\rho/l \end{bmatrix}, \tag{5-10}$$

where the constants $b_1,\ a_1,\ a_2,\ a_3$ are obtained by making use of initial conditions.

In systems described simply by the mass and stiffness matrices, the eigenvectors are composed by real elements and have a clear physical meaning. However, the eigenvectors can be complex ones for other cases, providing the interpretation that, even though they have the same oscillation frequency, they do not pass through their equilibrium points at the same time. The nodal points

are not fixed, unlike the case of real eigenvalues. Eigenvectors are complex when at least one of the coefficient matrices is not symmetric or when it is not possible to diagonalize the damping matrix through undamped mode shapes [40]. Even though the loudspeaker system was taken in such a way that it has no dissipative terms, the presence of the gyroscopic matrix, a skew-symmetric matrix, leads to complex mode shapes.

It is of interest now to analyze in more details what these pairs of natural frequencies and mode shapes mean. The first point that stands out is that the null natural frequency $\omega_{3,4}$ is a consequence of a double root and it corresponds to a real eigenvector u_3 that does not depend on the system's parameters, differently from the other two eigenvectors. The solution regarding this frequency cannot be given as the others and must be in the form of a linear relation with time, as in equation (5-10).

Furthermore, the only coordinate present is u_3 (the eigenvector corresponding to the null natural frequency) is q, meaning that the portion of the system's solution that corresponds to a non-oscillatory response that increases linearly with time involves only the charge of the circuit.

5.1.1.2
Case II: undamped non-autonomous model with a voltage source

Now that the free vibration model of the electromagnetic loudspeaker was analyzed in more details, one may use the results from the previous section to evaluate the forced response. The voltage source is no longer null and is taken as harmonic in the form $v(t) = v_0 \sin(\omega t)$. Fixing the system's parameters as $l = 1$, $m = 1$, $\kappa = 8$ and $\rho = 1$, the non-null loudspeaker's natural frequency found in equation (5-9) is

$$\omega_{1,2} = \sqrt{\frac{8}{1} + \frac{1^2}{1\ .\ 1}} = 3.$$

By solving the IVP with initial conditions $z(0) = 1,\ q(0) = 0,\ \dot{z}(0) = 0,\ \dot{q}(0) = 0$ one can obtain numerical approximations of the system's response to the forced excitation. The goal is to show what happens to the system when the excitation frequency equals the system's natural frequency. Taking $v_0 = 1$ and $\omega = \omega_{1,2} = 3$, the numerical approximations for z and $\dot{q}$ are obtained, plotted in figure 5.2. The amplitudes of both coordinates are increasing indefinitely with time, an expected behaviour discussed in section 2.1 and appendix A, corresponding to the resonance phenomenon.

Resonance and parametric resonance occur due to distinct types of excitations. Let us now analyze the situation where the system's excitation is due to time-varying coefficients.

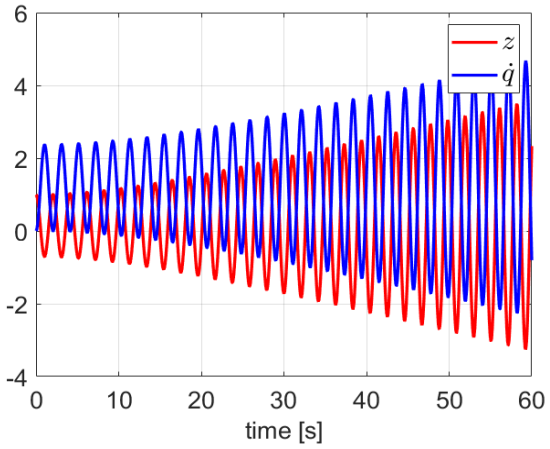

Figure 5.2: Numerical approximations when $\omega = \omega_{1,2} = 3$.

5.1.1.3 Case III: undamped non-autonomous model with parametric excitation

Until now only the loudspeaker with constant coefficients was dealt with so a few details regarding this electromechanical system's dynamics could be discussed without further complications. To continue with the stability analysis, let us introduce parametric excitation to the system. Take $k = \kappa + \epsilon \cos(\omega t)$, meaning that this model of the system has a time-periodic coefficient in the stiffness term. It is thus being parametrically excited.

The equations of motion when there is no voltage source ($v = 0$) or dissipation ($b = 0,\ r = 0$) are, in matrix form,

$$\begin{bmatrix} m & 0 \\ 0 & l \end{bmatrix} \begin{bmatrix} \ddot{z} \\ \ddot{q} \end{bmatrix} + \begin{bmatrix} 0 & -\rho \\ \rho & 0 \end{bmatrix} \begin{bmatrix} \dot{z} \\ \dot{q} \end{bmatrix} + \begin{bmatrix} \kappa + \epsilon \cos(\omega t) & 0 \\ 0 & 0 \end{bmatrix} \begin{bmatrix} z \\ q \end{bmatrix} = \begin{bmatrix} 0 \\ 0 \end{bmatrix},$$

that in its two-dimensional first order form is

$$\begin{bmatrix} \dot{z} \\ \dot{q} \\ \ddot{z} \\ \ddot{q} \end{bmatrix} = \begin{bmatrix} 0 & 0 & 1 & 0 \\ 0 & 0 & 0 & 1 \\ -[\kappa + \epsilon \cos(\omega t)]/m & 0 & 0 & \rho/m \\ 0 & 0 & -\rho/l & 0 \end{bmatrix} \begin{bmatrix} z \\ q \\ \dot{z} \\ \dot{q} \end{bmatrix}.$$

Notice that the natural frequencies of the undamped system without parametric excitation are just as obtained previously, given in equation (5-9), where k is replaced by κ. Fixing the parameters as in the last section ($l = 1$, $m = 1$, $\kappa = 8$ and $\rho = 1$), they are

$$\omega_{1,2} = 3 \ \text{ and } \ \omega_{3,4} = 0.$$

Equations (3-20) and (3-21) can be used to obtain the critical frequencies

just as it was done in chapter 4. Since one of the natural frequencies is equal to zero, only the non-null natural frequency is needed to find the critical frequencies. The relations obtained with (3-21) are already included in (3-20) for this case. Therefore, using equation (3-20), the critical frequencies are, in rad/s,

$$2\,\omega_{1,2} = 6, \quad \omega_{1,2} = 3, \quad \frac{2\,\omega_{1,2}}{3} = 2, \quad \frac{\omega_{1,2}}{2} = 1.5, \quad \ldots$$

The goal is to again make a stability analysis by using Floquet theory, but now to evaluate stability of the trivial solution of this 2DoF electromechanical system. A stability map in the $\omega \times \epsilon$ plane is given in figure 5.3, plotted with a grid of size 0.01 for this case with no dissipation terms. The dark blue area represents where instability of the trivial solution takes place according to Floquet theory. In figure 5.3 is possible to see that instability occurs around the found critical frequencies. The same can be seen in figure 5.4, that shows the stability map in terms of Λ, plotted with a grid of 0.01. It is clearly seen through this maps the dominance of the first order critical frequency.

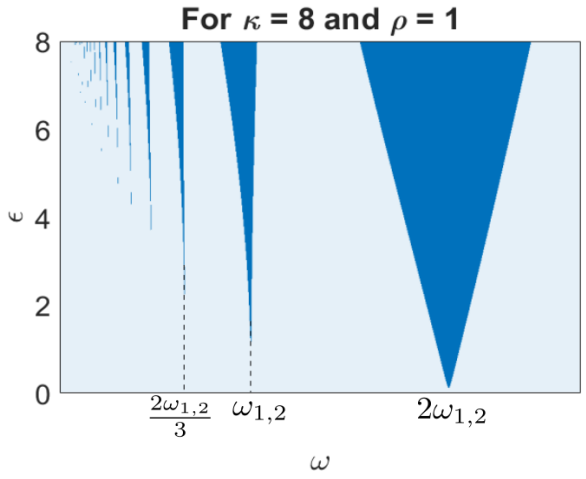

Figure 5.3: Electromagnetic loudspeaker's stability map in the $\omega \times \epsilon$ plane.

By fixing the excitation's amplitude as $\epsilon = 0.3$, it is possible to obtain Λ while varying the excitation's frequency ω. The main frequency that appears in the $\omega \times \Lambda$ plot for the chosen parameters is $2\omega_{1,2}$, as shown in figure 5.5. This means that, for small values of ϵ, instability is of most interest in the loudspeaker when the excitation frequency approaches the double value of the natural frequency of the undamped system without parametric excitation, the already mentioned critical frequency of first order. For purely mechanical systems as well as for purely electromagnetic ones, the higher effect of this first order critical frequency is well known (as discussed, for example, in [2; 3]) and it was addressed throughout chapter 4.

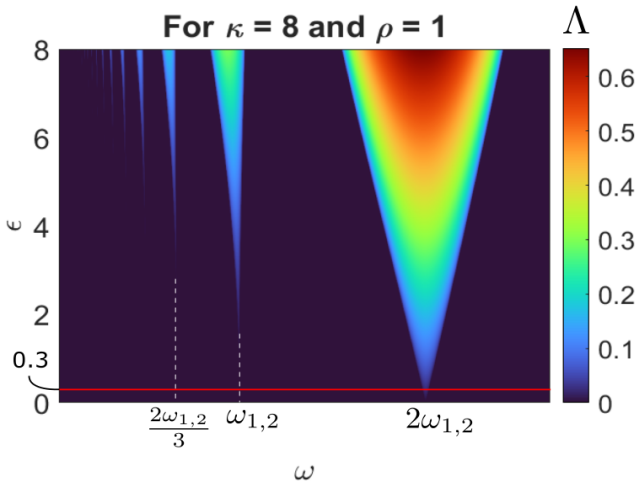

Figure 5.4: Electromagnetic loudspeaker's stability map in the $\omega \times \epsilon$ plane using Λ.

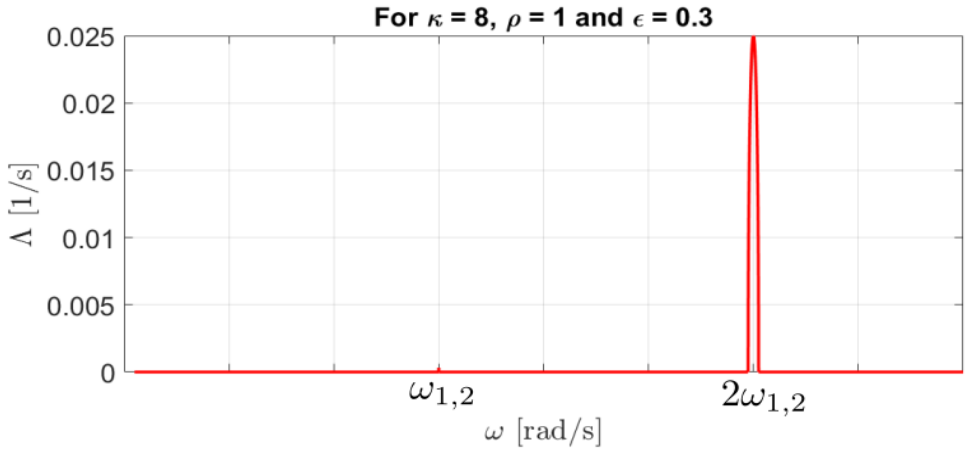

Figure 5.5: $\omega \times \Lambda$ plot for the electromagnetic loudspeaker with $\kappa = 8$, $\rho = 1$ and $\epsilon = 0.3$.

Another plot of interest to discuss is the stability map in the $\omega \times \rho$ plane using Λ, shown in figure 5.6 for $\epsilon = 0.3$. Through this figure it is possible to notice that the excitation frequency may result in instability of the trivial solution depending on the chosen value of ρ. The unstable "path" present in this stability map occurs due to the change in the loudspeaker's natural frequency, once this dynamic property is dependent on the parameter value ρ, clearly seen in (5-9).

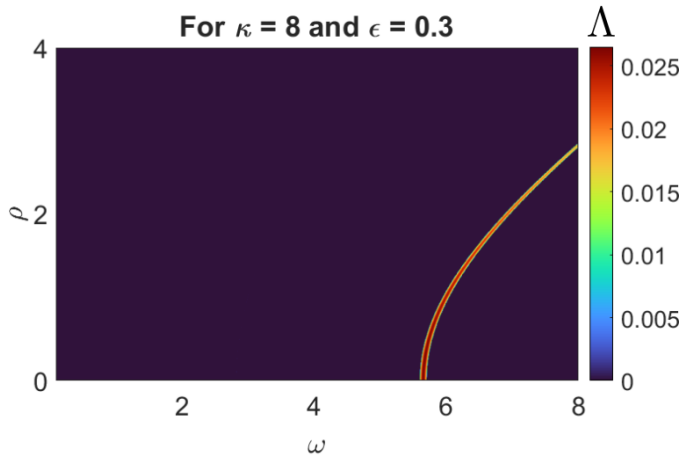

Figure 5.6: Electromagnetic loudspeaker's stability map in the $\omega \times \rho$ plane using Λ for $\epsilon = 0.3$.

5.1.1.4 Case IV: damped non-autonomous model with parametric excitation

By introducing terms of dissipation, the equations of motion when there is no voltage source ($\upsilon = 0$) are, in matrix form,

$$\begin{bmatrix} m & 0 \\ 0 & l \end{bmatrix} \begin{bmatrix} \ddot{z} \\ \ddot{q} \end{bmatrix} + \begin{bmatrix} b & -\rho \\ \rho & r \end{bmatrix} \begin{bmatrix} \dot{z} \\ \dot{q} \end{bmatrix} + \begin{bmatrix} \kappa + \epsilon\cos(\omega t) & 0 \\ 0 & 0 \end{bmatrix} \begin{bmatrix} z \\ q \end{bmatrix} = \begin{bmatrix} 0 \\ 0 \end{bmatrix},$$

that in its two-dimensional first order form is

$$\begin{bmatrix} \dot{z} \\ \dot{q} \\ \ddot{z} \\ \ddot{q} \end{bmatrix} = \begin{bmatrix} 0 & 0 & 1 & 0 \\ 0 & 0 & 0 & 1 \\ -[\kappa + \epsilon\cos(\omega t)]/m & 0 & -b/m & \rho/m \\ 0 & 0 & -\rho/l & -r/l \end{bmatrix} \begin{bmatrix} z \\ q \\ \dot{z} \\ \dot{q} \end{bmatrix}.$$

At this first moment, let us introduce dissipation to the system by making only the damping coefficient b non-null. Thus, the resistance in the circuit remains zero ($r = 0$). The goal is to see how the damping influences the stability of the trivial solution of the electromagnetic loudspeaker by making use of stability maps not used previously in this dissertation.

Taking $\epsilon = 0.3$ and the same parameters used before ($l = 1$, $m = 1$, $\kappa = 8$ and $\rho = 1$), one can plot a stability map in the $\omega \times b$ plane, as depicted in figure 5.7. It is possible to see that instability takes place only at a small neighbourhood of $\omega = 2\omega_{1,2} = 6$, showing once again the higher effect of the first order critical frequency in terms of instability of the trivial solution.

Taking a step further to introduce resistance into the electromagnetic subsystem (now, $r \neq 0$ as well as $b \neq 0$), a stability map of interest is given in the $r \times b$ plane. Figure 5.8 provides this plot for $\epsilon = 0.3$ and $\omega = 2\omega_{1,2} = 6$.

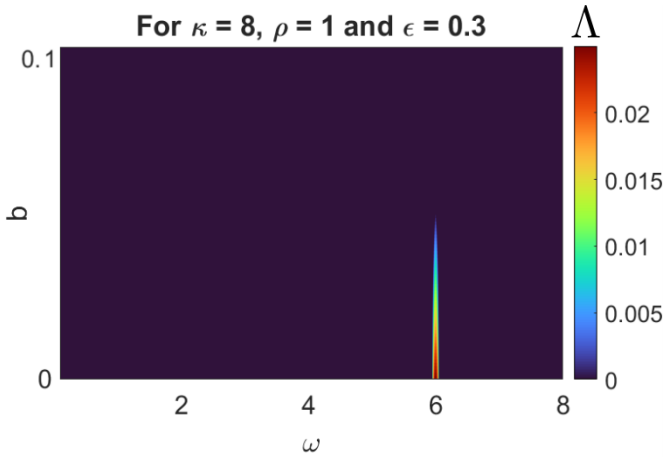

Figure 5.7: Electromagnetic loudspeaker's stability map in the $\omega \times b$ plane using Λ.

This frequency was chosen so the effects of damping could be discussed in more details for a situation where the excitation frequency is equal to the first order critical frequency.

The stability map in figure 5.8 provides stability information in terms of parameters of both mechanical and electromagnetic natures. It also shows that instability takes place at the chosen excitation frequency $\omega = 2\omega_{1,2}$ only for very small values of both damping and resistance. For higher values of this coefficients, the trivial solution is stable, showing that instability at this first order critical frequency can be suppressed.

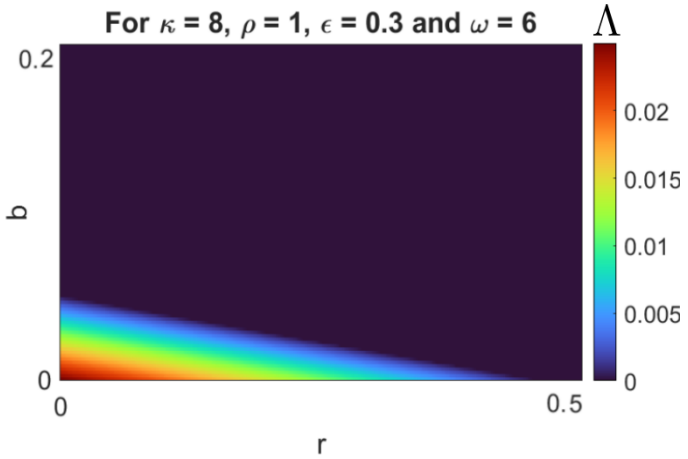

Figure 5.8: Electromagnetic loudspeaker's stability map in the $r \times b$ plane using Λ.

6
Conclusions

Stability analysis is applicable to many fields of knowledge, from mechanics to electronics and fluid dynamics. To fully comprehend its applications, one must first be familiarized with basic concepts that lead not only to a formal understanding of this topic, but also to an intuition of what it means for a motion to be stable or unstable. To achieve this, the dissertation provided the needed background to start stability analysis studies. The presented theory encompassed: resonance; stability; what an equilibrium position is; examples of phase diagrams and how to analyze them so a system's motion can be evaluated; linearization of differential equations around equilibrium points. After that, the difference between autonomous and non-autonomous systems was given.

To continue, stability in the sense of Lyapunov was introduced. The dissertation's main topic of interest was to analyze stability of the trivial solution of linear systems with time-periodic coefficients, thus Floquet theory was presented. This theory enables one to make stability statements about the trivial solution of this type of system. Then, stability maps, transition curves obtained through a perturbation method and the phenomenon of parametric resonance were discussed by making use of the example of Mathieu's equation.

Afterwords, Mathieu's equation was studied in more details. The trivial solution's stability was analyzed for the undamped and damped cases while making use of stability maps and phase portraits. After that, several examples of two degrees of freedom systems with parametric excitation that encompass mechanical as well as electromagnetic systems were given to exemplify the use of Floquet theory and evaluate how parametric excitation influences the stability of their trivial solution. To do so, stability maps, phase diagrams and the plane $\omega \times \Lambda$ were discussed throughout this dissertation.

Each example was approached so different features could be presented and analyzed in more details. The advantages of using Floquet theory became clear, that allows one to make stability statements about the trivial solution by only solving the dynamics for one period T. Without using this theory, it would be necessary to obtain numerical approximations for larger periods of time to evaluate the behaviour. The phenomenon of parametric anti-resonance

and its capability of controlling vibration were also discussed. Furthermore, the advantages of using the maximum value of the Lyapunov characteristic exponents Λ became clear: stabilizing and destabilizing effects can be seen by making use of such values, providing important information about stability of the trivial solution that would be lost if only the magnitude of the Floquet multipliers were directly analyzed.

After these examples, electromechanical systems were introduced. A brief explanation of how to obtain their equations of motion was given so then stability could be addressed. Then, a specific example was used to analyze stability of several different cases: an electromagnetic loudspeaker. The undamped system's natural frequencies were obtained, that are hybrid frequencies for the used parametrization, once they depend on parameters of both natures (mechanical and electromagnetic). By making use of different stability maps, the stability of the trivial solution was discussed.

The numerical procedure used throughout the dissertation was provided in a step by step procedure. Its disadvantages and difficulties were also discussed as well as ways to overcome them so satisfactory results in stability maps are obtained. In resume, one of the goals of this dissertation was to provide a numerical procedure to evaluate the stability of the trivial solution of linear time-periodic systems through Floquet theory. Also, several examples were analyzed by making use of this procedure. Another goal of this dissertation was to introduce stability analysis for electromechanical systems.

At this point, one may have noticed that the seen theory for linear time-periodic systems was used only for systems with parametric excitation present in stiffness coefficients. A possible way of continuing this study would be to evaluate stability when the time-periodic coefficient is given, for example, in gyroscopic terms. The same path followed throughout this dissertation could be used (obtaining approximations of the transition curves, plotting stability maps and phase portraits, etc). The electromechanical system of a DC motor would be an example of interest, once its standard form has no stiffness terms and the coupling between the mechanical and electromagnetic subsystems is given by gyroscopic terms.

Another possible way of continuing this stability study would be to make stability analysis for more examples of electromechanical systems. This would be a step further into the comprehension of this type of system.

A
Free vibration and harmonic excitation of a SDoF system

A.1
Response to free vibration

Take figure 2.3, a simple single degree of freedom (SDoF) system with free vibration [20]. This system is composed by a mass m, a spring with stiffness coefficient k and a damper with coefficient b. For this example, equation (2-1) becomes

$$m\ddot{y}(t) + b\dot{y}(t) + ky(t) = 0, \tag{A-1}$$

with initial conditions $y(0) = y_0,\ \dot{y}(0) = v_0$. For a first approach, take the undamped case ($b = 0$), that resumes equation (A-1) to

$$\ddot{y}(t) + \omega_n^2 y(t) = 0. \tag{A-2}$$

where ω_n is known as the system's *natural frequency*, given by

$$\omega_n = \sqrt{\frac{k}{m}}.$$

The proposed solution to solve this equation of motion is taken in the form

$$y(t) = e^{\lambda t}, \tag{A-3}$$

where λ is an unknown scalar that is wanted. Substituting (A-3) into the equation of motion (A-2),

$$\begin{aligned} \lambda^2\, e^{\lambda t} + \omega_n^2\, e^{\lambda t} &= 0, \\ (\lambda^2 + \omega_n^2)\, e^{\lambda t} &= 0. \end{aligned}$$

Since $e^{\lambda t}$ cannot be zero, this leads to

$$\begin{aligned} \lambda^2 + \omega_n^2 &= 0, \\ \lambda_{1,2} &= \pm\, \omega_n\, i. \end{aligned}$$

Two values of λ were found, resulting in two possible solutions. Now it is possible to obtain the general solution by substituting the found values $\lambda_{1,2}$ into (A-3). Since equation (A-2) is linear, the system's response is given by a linear combination of both possible solutions, that in its general form is

$$y(t) = b_1 e^{i\,\omega_n\,t} + b_2 e^{-i\,\omega_n\,t},$$

where $i = \sqrt{-1}$ and b_1, b_2 are complex constants that can be obtained by making use of the initial conditions. This represents a purely oscillatory solution, also called *simple harmonic motion*. It is possible to rearrange it and substitute the complex exponential by sines and cosines functions to express the solution as

$$y(t) = a\,\sin(\omega_n t + \phi),$$

where a and ϕ are real constants. This can also be written as

$$y(t) = a_1\,\cos(\omega_n t) + a_2\,\sin(\omega_n t),$$

where a_1 and a_2 are real constants that are obtained by making use of the provided initial conditions. Deriving $y(t)$ and evaluating at $t = 0$,

$$\begin{aligned} y(0) = y_0 \quad &\rightarrow \quad a_1\,\cos(0) + a_2\,\sin(0) = y_0, \\ \dot{y}(0) = v_0 \quad &\rightarrow \quad -a_1\,\omega_n\,\sin(0) + a_2\,\omega_n\,\cos(0) = v_0. \end{aligned}$$

Solving this system, the constants a_1 and a_2 can be found in terms of the generic initial conditions. They are

$$a_1 = y_0 \;\text{ and }\; a_2 = \frac{v_0}{\omega_n}.$$

The system's solution is then given by

$$y(t) = y_0\,\cos(\omega_n t) + \frac{v_0}{\omega_n}\,\sin(\omega_n t).$$

Taking, for example, the natural frequency as $\omega_n = 2$ and the initial conditions $y_0 = 1$ and $v_0 = 0$, it is possible to plot the solution $y(t)$ over time, given in figure A.1.

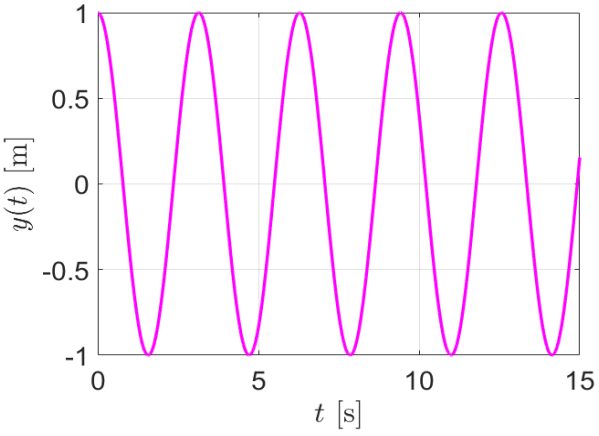

Figure A.1: Solution of the undamped SDoF system.

Let us now analyze the damped case. Equation (A-1) can be rewritten as

$$\ddot{y}(t) + 2\xi\omega_n\dot{y}(t) + \omega_n^2 y(t) = 0, \tag{A-4}$$

where ω_n is the natural frequency of the undamped system and ξ is

$$\xi = \frac{b}{2\sqrt{km}},$$

known as the *damping ratio*.

Substituting the same proposed solution (A-3) into the equation of motion (A-4), one gets

$$\begin{aligned} \lambda^2\, e^{\lambda t} + 2\xi\omega_n\, \lambda\, e^{\lambda t} + \omega_n^2\, e^{\lambda t} &= 0, \\ (\lambda^2 + 2\xi\omega_n\lambda + \omega_n^2)\, e^{\lambda t} &= 0. \end{aligned}$$

Since $e^{\lambda t}$ cannot be zero,

$$\lambda^2 + 2\xi\omega_n\lambda + \omega_n^2 = 0.$$

Solving for λ, the roots of this equation are

$$\begin{aligned} \lambda_{1,2} &= \frac{-2\xi\omega_n \pm \sqrt{(2\xi\omega_n)^2 - 4\omega_n^2}}{2}, \\ \lambda_{1,2} &= \omega_n(-\xi \pm \sqrt{\xi^2 - 1}). \end{aligned}$$

Depending on the damping ratio, the values of λ can be real or complex. Therefore, it is possible to classify the system's response due respect to its damping ratio: if $0 < \xi < 1$ the motion is said to be *underdamped*; if $\xi > 1$ it is *overdamped* and when $\xi = 1$, is said to be *critically damped*. Also, when $\xi = 0$, the system has no damping, corresponding to the *undamped* case. Each one of these cases are going to be discussed next.

For the underdamped case, the eigenvalues assume complex conjugate values, resulting in a solution of the form

$$y(t) = e^{-\xi\omega_n t}\left[a_1 e^{i\,\omega_n\,\sqrt{1-\xi^2}\,t} + a_2 e^{-i\,\omega_n\,\sqrt{1-\xi^2}\,t}\right],$$

where a_1 and a_2 are complex constants that can be obtained by making use of the initial conditions. This can also be written as

$$y(t) = a\, e^{-\xi\omega_n t}\sin\left(\omega_d\, t + \phi\right),$$

where a and ϕ are constants corresponding to the amplitude and phase shift, respectively, and $\omega_d = \omega_n\sqrt{1-\xi^2}$. Making use of the initial conditions, one can find that

$$a = \sqrt{\frac{(v_0 + \omega_n\, \xi\, y_0)^2 + (\omega_d\, y_0)^2}{\omega_d^2}} \text{ and } \phi = \tan^1\left(\frac{\omega_d\, y_0}{v_0 + \omega_n\, \xi\, y_0}\right).$$

The solution $y(t)$ for the underdamped case is shown in figure A.2 with damping ratio $\xi = 0.1$ and the same initial conditions and natural frequency as the ones used for the undamped case. The dashed black curves represent the "envelope" of this decaying oscillatory motion, given by $e^{-\xi\omega_n t}$.

Now analyzing the overdamped case, the eigenvalues assume distinct real values, resulting in a solution of the form

$$y(t) = e^{-\xi\omega_n t}\left[a_1 e^{-\omega_n\sqrt{\xi^2-1}\,t} + a_2 e^{\omega_n\sqrt{\xi^2-1}\,t}\right],$$

where a_1 and a_2 are, once again, constants obtained by using initial conditions. One can find that these constants are

$$a_1 = \frac{-v_0 + \left(-\xi + \sqrt{\xi^2-1}\right)\omega_n y_0}{2\omega_n\sqrt{\xi^2-1}} \text{ and } a_2 = \frac{v_0 + \left(\xi + \sqrt{\xi^2-1}\right)\omega_n y_0}{2\omega_n\sqrt{\xi^2-1}}.$$

The solution $y(t)$ for the overdamped case can also be seen in figure A.2 with the same initial values and natural frequency as before and damping ratio $\xi = 2$. This solution returns to the rest position without oscillation.

Let us analyze now the last case, the critically damped motion. Its solution cannot be given in the same way as for the other two damped cases, once this results in two equal eigenvalues $\lambda_{1,2} = -\omega_n$. The solution for this case must be in the form

$$y(t) = (a_1 + a_2 t)\, e^{-\omega_n t}.$$

where a_1 and a_2 are again constants obtained by using the initial conditions. By doing so, one obtains

$$a_1 = y_0 \text{ and } a_2 = v_0 + \omega_n y_0.$$

Figure A.2 shows this solution with the same initial values and natural frequency of the previous cases, but now with $\xi = 1$. This value of damping ratio can be thought as the one that separates the oscillatory response from the non-oscillatory one. Also, for the used initial conditions, the critically damped solution returns to the rest position faster then the overdamped one.

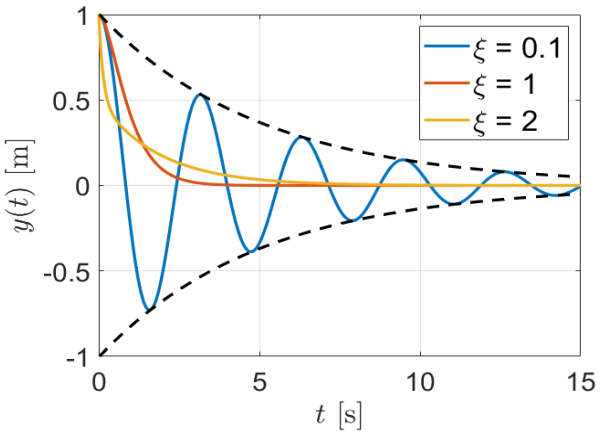

Figure A.2: Effect of damping on the solution for free vibration.

A.2
Response to harmonic excitation

After this initial analysis of a SDoF system with free vibration, an applied external force is introduced to it, depicted in figure A.3. The external force is taken as harmonic of the form $f(t) = f_0 \cos(\omega t)$, where f_0 is the amplitude and ω, its frequency. The analysis can also be made if the force was in the form $f_0 \sin(\omega t)$ or $f_0\, e^{i\omega t}$.

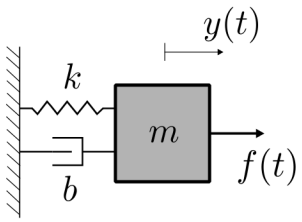

Figure A.3: SDoF system with an applied external force.

The system's equation of motion is

$$\ddot{y}(t) + 2\xi\omega_n\dot{y}(t) + \omega_n^2 y(t) = F_0 \cos(\omega t), \tag{A-5}$$

where $F_0 = f_0/m$. The initial conditions are taken as $y(0) = y_0,\ \dot{y}(0) = v_0$. The total response $y(t)$ is a sum of a homogeneous solution $y_h(t)$, found by using the system with free vibration as in the previous section, and by a particular solution $y_p(t)$, found by considering the applied external force. The response $y(t) = y_h(t) + y_p(t)$ can be fully obtained by making use of the initial conditions provided to the system.

Evaluating first the undamped case ($\xi = 0$), the equation of motion is

$$\ddot{y}(t) + \omega_n^2 y(t) = F_0 \cos(\omega t), \tag{A-6}$$

The particular solution is proposed to be in the same form of the forcing term. Thus, it is taken as

$$y_p(t) = Y_0 \cos(\omega t), \tag{A-7}$$

where Y_0 is the amplitude of the forced response. Substituting this into the equation of motion (A-6),

$$\begin{aligned} -\omega^2 Y_0 \cos(\omega t) + \omega_n^2 Y_0 \cos(\omega t) &= F_0 \cos(\omega t), \\ (-\omega^2 Y_0 + \omega_n^2 Y_0 - F_0)\cos(\omega t) &= 0, \end{aligned}$$

implying that

$$\begin{aligned} -\omega^2 Y_0 + \omega_n^2 Y_0 - F_0 = 0, \\ Y_0 = \frac{F_0}{\omega_n^2 - \omega^2}, \end{aligned}$$

with $\omega \neq \omega_n$. This means that the particular solution for the case where the natural frequency and the excitation frequency are not the same is

$$y_p(t) = \frac{F_0}{\omega_n^2 - \omega^2} \cos(\omega t).$$

The total solution $y(t)$ is a sum of the homogeneous and particular solutions, that in this cases results in

$$y(t) = a_1 \sin(\omega_n t) + a_2 \cos(\omega_n t) + \frac{F_0}{\omega_n^2 - \omega^2} \cos(\omega t),$$

where a_1 and a_2 are found by making use of the initial conditions. Deriving $y(t)$ and evaluating at $t = 0$,

$$\begin{aligned} y(0) = y_0 \quad &\rightarrow \quad a_1 \sin(0) + a_2 \cos(0) + \frac{F_0}{\omega_n^2 - \omega^2} \cos(0) = y_0, \\ \dot{y}(0) = v_0 \quad &\rightarrow \quad a_1\, \omega_n \cos(0) - a_2\, \omega_n \cos(0) - \frac{F_0 \omega}{\omega_n^2 - \omega^2} \sin(0) = v_0. \end{aligned}$$

The constants a_1 and a_2 are then

$$a_1 = \frac{v_0}{\omega_n} \text{ and } a_2 = y_0 - \frac{F_0}{\omega_n^2 - \omega^2}.$$

The system's solution is thus given by

$$y(t) = \frac{v_0}{\omega_n} \sin(\omega_n t) + \left(y_0 - \frac{F_0}{\omega_n^2 - \omega^2} \right) \cos(\omega_n t) + \frac{F_0}{\omega_n^2 - \omega^2} \cos(\omega t). \tag{A-8}$$

Notice that if $f_0 = 0$, meaning there is no external force, the values of

a_1 and a_2 are the same as for the undamped free vibration case discussed previously, as expected. It is also possible to see through equation (A-8) that the response's amplitude becomes larger as the excitation frequency approaches the natural frequency, once the denominator of $\frac{F_0}{\omega_n^2 - \omega^2}$ becomes very small. When these values are equal ($\omega = \omega_n$), the found solution does not apply anymore. For this case, the particular solution must be in the form

$$y_p(t) = t\, Y_0 \sin(\omega t),$$

once the proposed particular solution in equation (A-7) is also a solution for the homogeneous solution when both frequencies are equal. The term $t \sin(\omega t)$ in the proposed solution foresees that the response will be unbounded independently of the homogeneous portion. By substituting this in the equation of motion, the constant Y_0 is obtained by doing

$$\begin{aligned} \omega Y_0 \cos(\omega t) + \omega Y_0 \cos(\omega t) - t\omega^2 Y_0 \sin(\omega t) + t\omega_n^2 Y_0 \sin(\omega t) &= F_0 \cos(\omega t), \\ (2\omega Y_0 - F_0)\cos(\omega t) + (-t\omega^2 Y_0 + t\omega_n^2 Y_0)\sin(\omega t) &= 0. \end{aligned}$$

Since $\omega = \omega_n$,

$$\begin{aligned} 2\omega Y_0 - F_0 &= 0, \\ Y_0 &= \frac{F_0}{2\omega}, \end{aligned}$$

The particular solution is then

$$y_p(t) = \frac{F_0}{2\omega}\, t \sin(\omega t)$$

and the total solution is in the form

$$y(t) = a_1 \sin(\omega_n t) + a_2 \cos(\omega_n t) + \frac{F_0}{2\omega}\, t \sin(\omega t).$$

By making use of the initial conditions and the fact that in this situation $\omega = \omega_n$, the solution is

$$y(t) = \frac{v_0}{\omega} \sin(\omega t) + y_0 \cos(\omega t) + \frac{F_0}{2\omega}\, t \sin(\omega t).$$

By analyzing this result, one can see that for this given frequency the solution's amplitude grows indefinitely as times passes. This is the definition of the *resonance phenomenon*. Figure A.4 provides this response, where the dashed black lines show the "envelop" in which the response's amplitude grows without bound, given by $\frac{F_0}{2\omega}\, t$.

Let us now discuss the damped case, where the equation of motion is given by equation (A-5). For this case, the proposed particular solution is in

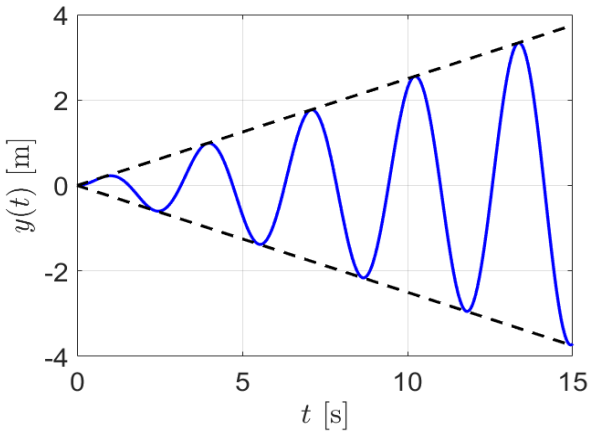

Figure A.4: Solution of the undamped SDoF system with an external harmonic force, where $y_0 = v_0 = 0$, $\omega = \omega_n = 2$ and $f_0 = 1$.

the form

$$y_p(t) = Y_0 \cos(\omega t - \theta),$$

that can also be written as

$$\begin{aligned} y_p(t) &= Y_0 \cos(\theta)\cos(\omega t) + Y_0 \sin(\theta)\sin(\omega t). \\ y_p(t) &= d_1 \cos(\omega t) + d_2 \sin(\omega t). \end{aligned}$$

Therefore, d_1 and d_2 are constants that satisfy

$$Y_0 = \sqrt{d_1^2 + d_2^2} \quad \text{and} \quad \theta = \tan^{-1}\left(\frac{d_2}{d_1}\right).$$

Substituting the proposed solution into the equation of motion,

$$(-\omega^2 d_1 + 2\xi\omega\omega_n d_2 + \omega_n^2 d_1 - F_0)\cos(\omega t) + (-\omega^2 d_2 + 2\xi\omega\omega_n d_1 + \omega_n^2 d_2)\sin(\omega t) = 0,$$

implying that

$$\begin{aligned} -\omega^2 d_1 + 2\xi\omega\omega_n d_2 + \omega_n^2 d_1 &= F_0, \\ -\omega^2 d_2 + 2\xi\omega\omega_n d_1 + \omega_n^2 d_2 &= 0. \end{aligned} \tag{A-9}$$

These constants are then

$$d_1 = \frac{(\omega_n^2 - \omega^2)F_0}{(\omega_n^2 - \omega^2)^2 + (2\xi\omega\omega_n)^2} \quad \text{and} \quad d_2 = \frac{2\xi\omega\omega_n F_0}{(\omega_n^2 - \omega^2)^2 + (2\xi\omega\omega_n)^2}$$

and the amplitude and phase shift of the particular solution are

$$Y_0 = \frac{F_0/k}{\sqrt{\left[1 - \left(\frac{\omega}{\omega_n}\right)^2\right]^2 + \left[2\xi\left(\frac{\omega}{\omega_n}\right)\right]^2}} \quad \text{and} \quad \theta = \tan^{-1}\left(\frac{-2\xi\frac{\omega}{\omega_n}}{1 - \left(\frac{\omega}{\omega_n}\right)^2}\right). \tag{A-10}$$

Now it is possible to obtain the full solution. For the underdamped case it is

$$y(t) = a\ e^{-\xi\omega_n t}\sin(\omega_d t - \phi) + Y_0\cos(\omega t - \theta),$$

where the constants a and ϕ of the homogeneous solution can be obtained by making use of the initial conditions provided to the system.

Through the total solution is possible to notice that, for large values of t, the homogeneous solution approaches zero due to the exponential with the negative exponent ($e^{-\xi\omega_n t}$). Even more: the greater the value of the damping ratio ξ, the faster the solution's amplitude tends to zero. With this transient stage of damped decaying motion, the particular solution becomes the main part of the total solution for long periods of time, taking a steady-state harmonic oscillation form with frequency ω [6; 20].

The effect of damping in the steady-state response can be discussed by analyzing figure A.5, that shows plots of $\omega/\omega_n \times Y_0 k/F_0$ and $\omega/\omega_n \times \theta$. For low damping ratios the amplitude is overly large at specific frequencies, seen when the amplitude is at its maximum value. By differentiating the relation of Y_0 in equation (A-10) in terms of the ratio ω/ω_n, one can conclude that this maximum occurs at

$$\frac{\omega}{\omega_n} = \sqrt{1 - 2\xi^2}.$$

The term inside the square root must be positive for the amplitude to achieve a maximum value, implying that this is valid only for damping ratios ξ lower than $1/\sqrt{2}$ (or 70.7%). In the limiting case where ξ approaches 0, then $\omega/\omega_n \to 1$, where the phase shift is $\pi/2$. The applied external force and the system's velocity are then at phase. They do not oppose each other, making the response reach great amplitudes.

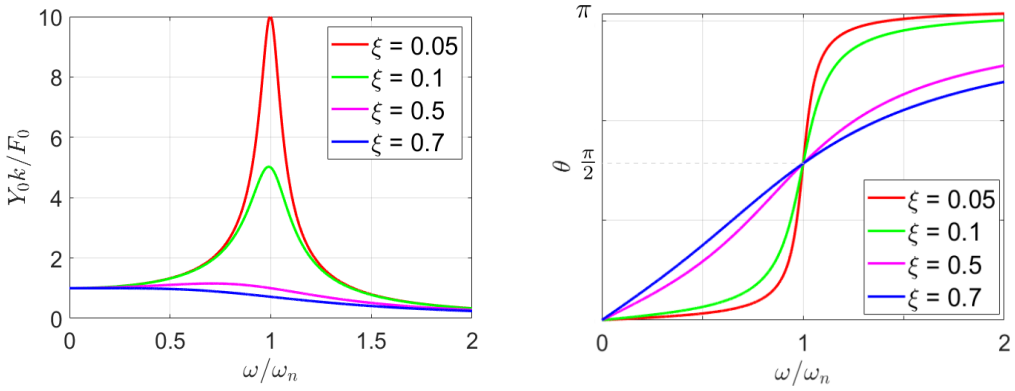

Figure A.5: Effect of damping on the particular solution.

B
Floquet's theorem

The goal here it to prove the Floquet's theorem, enunciated in theorem 3.1 in section 3.3 [27]. To achieve this, several lemmas must be first addressed and they are proven next. Consider the first order linear differential equation

$$\dot{x}(t) = A(t)\, x(t), \tag{B-1}$$

where $x(t) = [y \quad \dot{y}]^T \in \mathbb{R}^{2n}$ is the system's solution. $A(t) \in \mathbb{C}^{2n\times 2n}$ is the coefficient matrix, that is time-periodic with period T, which means that for $T > 0$, $A(t) = A(t+T)$ for every $t \in \mathbb{R}$. For a set of n linear independent solutions $(x_1(t), x_2(t), ..., x_{2n}(t))$ of this equation, it is possible to define

$$\Phi(t) = [\ x_1(t) \quad x_2(t) \quad ... \quad x_{2n}(t)\ ],$$

the *fundamental matrix*, a non-singular matrix where it's columns are the linear independent solutions of (B-1). Notice that, if a $x(t)$ satisfies equation (3-4), then $w(t) = x(t+T)$ also does [35; 27], as it is possible to conclude by doing

$$\dot{w}(t) = \dot{x}(t+T) = A(t+T)x(t+T) = A(t)w(t), \quad t \in \mathbb{R}.$$

Lemma 1 *Let $\Phi(t)$ be a fundamental matrix of equation* (B-1)*. Then any non-singular constant matrix B makes $\Psi(t) = \Phi(t)B$ also a fundamental matrix of* (B-1)*.*

Proof. $\Phi(t)$ is a non-singular matrix by definition, implying that $\Psi(t)$ is also a non-singular matrix. Thus it is possible to derive and obtain

$$\dot{\Psi} = \dot{\Phi}B = A\Phi B = A\Psi,$$

meaning that $\Psi(t)$ is indeed a fundamental matrix of equation (B-1). ■

Lemma 2 *Let $\Phi(t)$ be a fundamental matrix of equation* (B-1)*. Then $\Upsilon(t) = \Phi(t+T)$ is also a fundamental matrix of* (B-1)*.*

Proof. By deriving $\Upsilon(t) = \Phi(t+T)$ one gets

$$\dot{\Upsilon}(t) = \dot{\Phi}(t+T) = A(t+T)\Phi(t+T) = A(t)\Upsilon(t),$$

meaning that $\Upsilon(t)$ is indeed a fundamental matrix of equation (B-1). ■

Lemma 3 *Let $\Phi(t)$ be a fundamental matrix of equation* (B-1)*. Then there exists a non-singular matrix R such that $\Phi(t+T) = \Phi(t)R$.*

Proof. By lemma 2, one knows that $\Upsilon(t) = \Phi(t+T)$ is also a fundamental matrix of equation (B-1). Defining, for all t,

$$R^*(t) = \Phi^{-1}(t)\Upsilon(t),$$

one gets that

$$\begin{aligned} \Upsilon(t) &= \Phi(t)\Phi^{-1}(t)\Upsilon(t), \\ &= \Phi(t)R^*(t). \end{aligned} \tag{B-2}$$

Now, fixing a time t_0 and taking $R = R^*(t_0)$,

$$\Upsilon(t_0) = \Phi(t_0)R. \tag{B-3}$$

By lemma 1, one can also take $\Upsilon_0(t) = \Phi(t)R$, that by fixing the time t_0 leads to

$$\Upsilon_0(t_0) = \Phi(t_0)R. \tag{B-4}$$

Two fundamental matrices were just obtained: $\Upsilon(t)$ and $\Upsilon_0(t)$. Through equations (B-3) and (B-4), it must follow that $\Upsilon(t_0) = \Upsilon_0(t_0)$. Thus, by uniqueness of solutions, $\Upsilon(t) = \Upsilon_0(t)$. This means that matrix $R^*(t)$ must equal R for all t.

Recalling that $\Upsilon(t) = \Phi(t+T)$, it is possible to obtain by equation (B-2)

$$\begin{aligned} \Upsilon(t) &= \Phi(t)R^*(t), \\ \Phi(t+T) &= \Phi(t)R. \end{aligned}$$

Therefore, R is a non-singular constant matrix such that $\Phi(t+T) = \Phi(t)R$. ■

Also, since matrix R is independent of time, by setting $t = 0$ and using lemma 2, one gets

$$R = \Phi^{-1}(0)\Upsilon(0) = \Phi^{-1}(0)\Phi(T).$$

Taking $\Phi(0) = I$, it follows from this last relation that $R = \Phi(T)$, making it possible to use lemma 3 to obtain

$$\Phi(t+T) = \Phi(t)\Phi(T). \tag{B-5}$$

After these initial ideas, one can enunciate the *Floquet' theorem.*

Floquet's theorem: *The fundamental matrix* $\Phi(t)$ *with* $\Phi(0) = I$ *has a Floquet normal form*

$$\Phi(t) = Q(t)e^{Bt}$$

where $Q \in C^1(\mathbb{R})$ *is a* T*-periodic* $(Q(t) = Q(t+T))$ *invertible matrix for all* t *and* $B \in \mathbb{C}^{2n\times 2n}$ *is a constant matrix given by* $B = \frac{1}{T}\, ln(\Phi(T))$.

Proof. It follows from lemma 3 that there exists a matrix R such that

$$\Phi(t+T) = \Phi(t)\ R.$$

By also knowing that that there exists a complex matrix B such that $e^{BT} = R$ for a non-singular square matrix R (as proved, for example, in [27]) and using equation (B-5), one gets that

$$R = \Phi(T) = e^{BT}.$$

If $Q(t) = \Phi(t)\ e^{-Bt}$ is taken, for all t one has

$$\begin{aligned} Q(t+T) &= \Phi(t+T)\ e^{-B(t+T)} \\ &= \Phi(t)\ R\, e^{-Bt}\ e^{-BT} \\ &= \Phi(t)\ e^{BT}\ e^{-Bt}\ e^{-BT} \\ &= \Phi(t)\ e^{-Bt} \\ &= Q(t). \end{aligned}$$

This result leads to

$$\Phi(t) = Q(t)e^{Bt}.$$

meaning that $Q(t)$ is T-periodic as well as that $Q(0) = \Phi(0)e^0 = I$. Since exponentials of square matrices are invertible, the matrix e^{-Bt} is invertible, which means that $Q(t)$ also is.

■

C
Dynamics of electromagnetic systems

The goal here is to obtain the dynamics of a purely electromagnetic system by making use of the Lagrangian method. The used notation is as follow:

- E_m is the magnetic energy;
- E_e is the electric energy;
- E_m^*, E_e^* are the respective co-energies, meaning the magnetic co-energy and the electric co-energy;
- Z is the Lagrangian function for an electromagnetic system.

The Lagrangian function for a purely electromagnetic system is

$$Z = E_m^* - E_e. \tag{C-1}$$

Being q_i a generalized coordinate of the system, each differential equation for an electromagnetic system dynamics can be found by applying the formula

$$\frac{d}{dt}\left(\frac{\partial Z}{\partial \dot{q}_i}\right) - \frac{\partial Z}{\partial q_i} = \frac{d\delta W}{d\delta q_i}. \tag{C-2}$$

Therefore, to obtain the equations of motion through this method, one must first find the energies that can be present in the system [9; 10]. Take the case of a capacitor, an element composed by two plates that transfer charge from one to another. Its capacity to store electric energy is known as a capacitance c. The constitutive relation for an ideal and linear capacitor is

$$q = c\, e,$$

where q is the charge and e, the difference of potential between the capacitor's plates. The electric energy stored in an ideal capacitor is obtained by calculating the work done by this element. Integrating the power inserted in the circuit to obtain this work leads to

$$\begin{aligned} E_e(q) &= \int_0^t e\dot{q}\, dt = \int_0^q e\, dq, \\ &= \frac{q^2}{2c}. \end{aligned}$$

The electric co-energy can be obtained by doing

$$\begin{aligned} E_e^*(e) &= eq - E_e(q), \\ &= \frac{c\ e^2}{2}. \end{aligned}$$

Thus, the general forms for the electrical energy and co-energy are

$$\begin{aligned} E_e(q) &= \frac{1}{2}\sum_{i,r}^{s}\left(\frac{1}{c_{ir}}\ q_i\ q_r\right), \\ E_e^*(e) &= \frac{1}{2}\sum_{i,r}^{s}\left(c_{ir}\ e_i\ e_r\right). \end{aligned}$$

where s is the number of capacitors and c_{ir} is the mutual capacitance between two capacitors with capacitances c_i and c_r, that in some cases cannot be neglected.

Now, take the case of an inductor, element that stores energy in the form of a magnetic field. The constitutive law for linear inductors is

$$\vartheta = l\ \dot{q},$$

where l is the inductance and ϑ is known as the flux linkage. It is possible to do the same process done for the capacitor to obtain the energy provided to the system by this element. Thus, by knowing that $e = d\vartheta/dt$, the magnetic energy in a circuit is

$$\begin{aligned} E_m(\vartheta) &= \int_0^t e\dot{q}\ dt = \int_0^{\vartheta} \dot{q}\ d\vartheta, \\ &= \frac{\vartheta^2}{2l}. \end{aligned}$$

To obtain the magnetic co-energy, it is sufficient to do as before, getting

$$\begin{aligned} E_m^*(\dot{q}) &= \vartheta\ \dot{q} - E_m(\vartheta), \\ &= \frac{l\ \dot{q}^2}{2}. \end{aligned}$$

The general forms of the magnetic energy and co-energy are

$$\begin{aligned} E_m(\vartheta) &= \frac{1}{2}\sum_{i,r}^{s}\left(\frac{1}{l_{ir}}\ \vartheta_i\ \vartheta_r\right), \\ E_m^*(\dot{q}) &= \frac{1}{2}\sum_{i,r}^{s}(l_{ir}\ \dot{q}_i\ \dot{q}_r). \end{aligned}$$

For non-conservative elements such as voltage sources and resistors, the

concept of virtual work (δW) is used. For voltage sources, it is given by

$$\delta_{f_i} = \upsilon_i \, \delta q_i,$$

while for resistors it is given by

$$\delta_d = r_i \, \dot{q}_i \, \delta q_i.$$

To exemplify how to obtain the dynamics of an electromagnetic system, take figure C.1. This circuit is composed by two inductors with inductances $l_1,\ l_2$, three capacitors with capacitance $c_1,\ c_3,\ c_2$, two resistors with resistance $r_1,\ r_2$ and a voltage source υ. Notice that this example has two degrees of freedom (three distinct currents, but only two are independent from the others). The equation with the existent constraint is $q_3 = q_1 - q_2$.

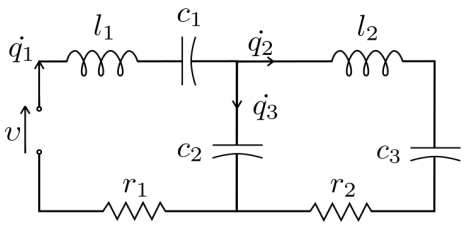

Figure C.1: 2DoF electromagnetic system.

The energies necessary for the construction of the Lagrangian function are

$$\begin{aligned} E_m^* &= \frac{l_1}{2}\,\dot{q}_1^2 + \frac{l_2}{2}\,\dot{q}_2^2, \\ E_e &= \frac{q_1^2}{2c_1} + \frac{q_2^2}{2c_3} + \frac{q_3^2}{2c_2} = \frac{q_1^2}{2c_1} + \frac{q_2^2}{2c_3} + \frac{(q_1 - q_2)^2}{2c_2}, \end{aligned}$$

By equation (C-1), the Lagrangian function for this system is

$$\begin{aligned} Z &= E_m^* - E_e \\ &= \frac{l_1}{2}\,\dot{q}_1^2 + \frac{l_2}{2}\,\dot{q}_2^2 - \left[\frac{q_1^2}{2c_1} + \frac{q_2^2}{2c_3} + \frac{(q_1 - q_2)^2}{2c_2}\right]. \end{aligned}$$

Since there are non-conservative elements in the system, the virtual work must be obtained. It is

$$\begin{aligned} \delta W &= \delta_f - \delta_d \\ &= \upsilon \, \delta q_1 - (r_1 \, \dot{q}_1 \, \delta q_1 + r_2 \, \dot{q}_2 \, \delta q_2)\,. \end{aligned}$$

By calculating the partial derivatives of the Lagrangian function the

equations of motion can be found. Thus, for q_1,

$$\begin{aligned} \frac{\partial Z}{\partial q_1} &= -\frac{q_1}{c_1} - \frac{q_1 - q_2}{c_2}, \\ \frac{d}{dt}\left(\frac{\partial Z}{\partial \dot{q}_1}\right) &= l_1 \ddot{q}_1, \\ \frac{d\delta W}{d\delta q_1} &= \upsilon - r_1 \dot{q}_1. \end{aligned}$$

For the coordinate q_2,

$$\begin{aligned} \frac{\partial Z}{\partial q_2} &= -\frac{q_2}{c_3} + \frac{q_1 - q_2}{c_2}, \\ \frac{d}{dt}\left(\frac{\partial Z}{\partial \dot{q}_2}\right) &= l_2 \ddot{q}_2, \\ \frac{d\delta W}{d\delta q_2} &= -r_2 \dot{q}_2. \end{aligned}$$

The equations of motion are obtained by using the formula in equation (C-2). The equations of motion are

$$\frac{d}{dt}\left(\frac{\partial Z}{\partial \dot{q}_1}\right) - \frac{\partial Z}{\partial q_1} = \frac{d\delta W}{d\delta q_1} \rightarrow l_1 \ddot{q}_1 + r_1 \dot{q}_1 + \left(\frac{1}{c_1} + \frac{1}{c_3}\right) q_1 - \frac{1}{c_2} q_2 = \upsilon,$$

$$\frac{d}{dt}\left(\frac{\partial Z}{\partial \dot{q}_2}\right) - \frac{\partial Z}{\partial q_2} = \frac{d\delta W}{d\delta q_2} \rightarrow l_2 \ddot{q}_2 + r_2 \dot{q}_2 + \left(\frac{1}{c_3} + \frac{1}{c_2}\right) q_2 - \frac{1}{c_2} q_1 = 0.$$

Writing in matrix form,

$$\begin{bmatrix} l_1 & 0 \\ 0 & l_2 \end{bmatrix} \begin{bmatrix} \ddot{q}_1 \\ \ddot{q}_2 \end{bmatrix} + \begin{bmatrix} r_1 & 0 \\ 0 & r_2 \end{bmatrix} \begin{bmatrix} \dot{q}_1 \\ \dot{q}_2 \end{bmatrix} + \begin{bmatrix} \left(\frac{1}{c_1} + \frac{1}{c_3}\right) & -\frac{1}{c_2} \\ -\frac{1}{c_2} & \left(\frac{1}{c_2} + \frac{1}{c_3}\right) \end{bmatrix} \begin{bmatrix} q_1 \\ q_2 \end{bmatrix} = \begin{bmatrix} \upsilon \\ 0 \end{bmatrix}.$$

D
Dynamics of electromechanical systems

When dealing with electromechanical systems, it is necessary to take into account parameters of both mechanical and electromagnetic origins. It is not sufficient to describe each one of its subsystems separately and thus a method to achieve this is needed. The Lagrangian method is chosen to approach this problem, an energetic method that allows a formulation in a way that makes it possible to obtain the system's dynamics as a whole. The Lagrangian function for an electromechanical system [8; 9; 18] is

$$\Gamma = T^* - V + E_m^* - E_e \pm U^*, \tag{D-1}$$

where U^* is a possible coupling term that can have an electric or magnetic origin. The signal depends on its origin: if it is magnetic (U_m^*) the signal is positive and if it is electric (U_e^*) the signal is negative. The other energies present in this Lagrangian function (the magnetic co-energy E_m^* and the electric energy E_e) were discussed in appendix C.

Being z_i a generalized coordinate of the system, each differential equation for the electromechanical system dynamics can be found by applying the formula

$$\frac{d}{dt}\left(\frac{\partial \Gamma}{\partial \dot{z}_i}\right) - \frac{\partial \Gamma}{\partial z_i} = \frac{d\ \delta W}{d\ \delta z_i}. \tag{D-2}$$

D.1
Example: electromagnetic loudspeaker

To exemplify this, take the electromechanical system in figure 5.1, known as electromagnetic loudspeaker [9; 11; 12]. This system is composed by a mass m, a spring with stiffness coefficient k, a damper with damping coefficient b, a voltage source v in series with a RL circuit (which means an inductor of inductance l and a resistor of resistance r) and a moving-coil transducer with transducer constant ρ. The coupling enabling energy to flow between the two subsystems is provided by the moving-coil transducer. The spring and damper simulate a membrane in the loudspeaker.

The parametrization used to describe the system's configuration is the displacement z of the mass from the mechanical subsystem's equilibrium point and the charge q passing through the circuit. Also, it is important to highlight

that z is merely the displacement of the mass m from the chosen equilibrium point.

The Lagrangian method is now going to be used to find the equations that describe the system's dynamics. The energies present in the system are

$$\begin{aligned} T^* &= \frac{m\dot{z}^2}{2}, \\ V &= \frac{kz^2}{2}, \\ E_m^* &= \frac{l\dot{q}^2}{2}, \\ E_e &= 0, \end{aligned}$$

where the electric energy is null because there is no capacitor present in the system. For further information about the electromagnetic part see appendix C. Also, as said before, the coupling term is given by the moving-coil transducer. The energy provided by this element is

$$U_m^* = \rho\dot{q}z.$$

Notice that this energy is dependent of both variables z and q.

The Lagrangian function given in equation (D-1) for this system is

$$\begin{aligned} \Gamma &= T^* - V + E_m^* - E_e \pm U^*, \\ &= \frac{m\dot{z}^2}{2} - \frac{kz^2}{2} + \frac{l\dot{q}^2}{2} + \rho\dot{q}z. \end{aligned}$$

Since there are non-conservative elements in the system, the virtual work must be found. It is given by

$$\begin{aligned} \delta W &= \delta_f - \delta_d \\ &= \upsilon\, \delta q - (r\, \dot{q}\, \delta q + b\, \dot{z}\, \delta z)\,. \end{aligned}$$

By obtaining the partial derivatives of the Lagrangian function the equations of motion can be found. Thus, for the mechanical coordinate z,

$$\begin{aligned} \frac{\partial \Gamma}{\partial z} &= -kz + \rho\dot{q}, \\ \frac{d}{dt}\left(\frac{\partial \Gamma}{\partial \dot{z}}\right) &= m\ddot{z}, \\ \frac{d\, \delta W}{d\, \delta z} &= -b\dot{z}. \end{aligned}$$

For the electromagnetic coordinate q, one has

$$\begin{aligned} \frac{\partial \Gamma}{\partial q} &= 0, \\ \frac{d}{dt}\left(\frac{\partial \Gamma}{\partial \dot{q}}\right) &= l\ddot{q} + \rho\dot{z}, \\ \frac{d\ \delta W}{d\ \delta q} &= \upsilon - r\dot{q}. \end{aligned}$$

The equations of motion for the electromagnetic loudspeaker are obtained by using the formula in equation (D-2). They are

$$\frac{d}{dt}\left(\frac{\partial \Gamma}{\partial \dot{z}}\right) - \frac{\partial \Gamma}{\partial z} = \frac{d\ \delta W}{d\ \delta z} \quad \rightarrow \quad m\ddot{z} + b\dot{z} + kz - \rho\dot{q} = 0,$$

$$\frac{d}{dt}\left(\frac{\partial \Gamma}{\partial \dot{q}}\right) - \frac{\partial \Gamma}{\partial q} = \frac{d\ \delta W}{d\ \delta q} \quad \rightarrow \quad l\ddot{q} + r\dot{q} + \rho\dot{z} = \upsilon.$$

E
Numerical procedure

After understanding the needed theory for a stability analysis approach seen throughout this dissertation, it is of interest to make a general step by step procedure of how to apply Floquet theory in numerical simulations. The first step is to write the system's equations of motion in its state space form and make a function out of it, where the time-varying parameters must be present in the inputs. Take, for example, a function *system(t, x, ω, a, b)* describing a generic system's dynamics. Here, t represents time, x is the state vector, ω represents the frequency of the time-periodic coefficient and a, b are parameters of the system.

Define a function *system* where the analyzed equations of motion are written in their state space form.
The **output** should be the state vector's derivative.

The goal is to plot stability maps. This type of map allows one to obtain regions of stability and instability for given range of parameters composing the system. To make a stability map, it is necessary to define the varying parameters and the wished interval for each one of them, that will be the axis of the stability map.

As an example, let us fix the value of the parameter b and vary the parametric excitation frequency ω as well as the parameter a. This means that b is taken as a scalar, while the other two are taken as vectors, called here ω_{vec} and a_{vec}, respectively. Take length(ω_{vec}) and length(a_{vec}) as the size of each vector.

Define scalar b
Define vector ω_{vec}, where each element is $\omega_{vec}(i)$, for $i = 1, \ldots, \text{length}(\omega_{vec})$
Define vector a_{vec}, where each element is $a_{vec}(j)$, for $j = 1, \ldots, \text{length}(a_{vec})$

One loop for each one of the parameters being varied is needed to plot the map. It is important to notice that, since the frequency is varying in this example, the period $T = 2\pi/\omega_{vec}(i)$ is also varying in each loop. Furthermore, it is not possible to start the interval of ω_{vec} at zero, once it would result in

a division by zero when obtaining T. If instead of the excitation frequency, the parameter b was being varied, the period T term inside the loop could be placed outside it.

In this case, for each pair $\omega_{vec}(i)$ and $a_{vec}(j)$ numerical approximations of the fundamental matrix must be obtained. The monodromy matrix can thus be obtained for the present pair of parameters. Afterwords, one may use directly the Floquet multipliers to evaluate the stability of the trivial solution or make use of the maximum value of the Lyapunov characteristic exponents (Λ).

Start loop for every element $\omega_{vec}(i)$, with $i = 1, \ldots, \text{length}(\omega_{vec})$

$T = 2 * \pi / \omega_{vec}(i)$

tspan = period from 0 to T

Start loop for every element $a_{vec}(j)$, with $j = 1, \ldots, \text{length}(a_{vec})$

Numerical integrations

Obtain the monodromy matrix

Evaluate the **Floquet multipliers** or use Λ

End loop for every element $a_{vec}(j)$

End loop for every element $\omega_{vec}(i)$

Now, each one of the steps inside both loops are going to be dealt with in more details. This means that, from this point on, every step is done for each pair $\omega_{vec}(i)$ and $a_{vec}(j)$.

First, it is possible to obtain numerical approximations of the system's solutions for each pair $\omega_{vec}(i)$ and $a_{vec}(j)$ by solving initial value problems (IVPs), where the initial conditions must be chosen to go accordingly to theorem 3.1.

For a nDoF system, $2n$ IVPs must be solved here. Thus, for every pair $\omega_{vec}(i)$ and $a_{vec}(j)$, $2n$ numerical integrations of *system* are done for one period T. The result of a single IVP is a matrix with $2n$ columns and a number of rows that depends on the step of the numerical integrator or of a step predefined by the user to do this numerical integration.

Without lost of generality, take a two degrees of freedom (2DoF) example. For this case, four IVPs must be solved. Since the fundamental matrix must be equal to the identity matrix for time zero, the initial conditions are taken as the columns of the identity matrix. For each one of the IVPs one gets a vector of time and a matrix with four columns and number of rows equal to the size of the time vector.

For each pair $\omega_{vec}(i)$ and $a_{vec}(j)$:

First **IVP** of *system*

Initial conditions: $[1\ 0\ 0\ 0]^{\mathrm{T}}$

Interval of integration: tspan

Result of the **numerical integration**:

vector t_1 of time and matrix X_1 with size length$(t_1) \times 4$

Second **IVP** of *system*

Initial conditions: $[0\ 1\ 0\ 0]^{\mathrm{T}}$

Interval of integration: tspan

Result of the **numerical integration**:

vector t_2 of time and matrix X_2 with size length$(t_2) \times 4$

Third **IVP** of *system*

Initial conditions: $[0\ 0\ 1\ 0]^{\mathrm{T}}$

Interval of integration: tspan

Result of the **numerical integration**:

vector t_3 of time and matrix X_3 with size length$(t_3) \times 4$

Fourth **IVP** of *system*

Initial conditions: $[0\ 0\ 0\ 1]^{\mathrm{T}}$

Interval of integration: tspan

Result of the **numerical integration**:

vector t_4 of time and matrix X_4 with size length$(t_4) \times 4$

By recalling equation (3-11), that shows that the monodromy matrix R equals the fundamental matrix at time T for $\Phi(0) = I$, one must allocate the last row (called here $lastrow_{X_s}$, for $s = 1, 2, 3, 4$) of each one of the obtained matrices $X_1,\ X_2,\ X_3,\ X_4$ as columns of R. This follows because the numerical integrations were done for an interval from 0 to T, meaning that the last rows of the obtained matrices correspond to the numerical approximations at time T. Afterwords, the Floquet multipliers γ can be obtained by solving the eigenvalue problem (EVP) $Ru = \gamma u$.

For the example of a 2DoF system being carried out here, R is a 4×4 matrix and thus four Floquet multipliers are found.

$x_1(T) = X_1(lastrow_{X_1},\ :)^{\mathrm{T}}$

$x_2(T) = X_2(lastrow_{X_2},\ :)^{\mathrm{T}}$

$x_3(T) = X_3(lastrow_{X_3},\ :)^{\mathrm{T}}$

$x_4(T) = X_4(lastrow_{X_4},\ :)^{\mathrm{T}}$

Monodromy matrix $R = \begin{bmatrix} | & | & | & | \\ x_1(T) & x_2(T) & x_3(T) & x_4(T) \\ | & | & | & | \end{bmatrix}$

Solve the EVP $Ru = \gamma u$ to obtain the **Floquet multipliers** γ_p, $p = 1, 2, 3, 4$

Now it is possible to make stability statements about the trivial solution as discussed in chapter 3.3. The first possibility is by evaluating directly the magnitude of the obtained Floquet multipliers. For the trivial solution to be considered unstable, it is sufficient for one of the Floquet multipliers to have magnitude greater than one. The classification regarding stability is restrained here to simply stable or unstable.

For the 2DoF example used until this point, at least one of the four Floquet multipliers need to have magnitude higher than one to consider the trivial solution as unstable.

If at least one $|\gamma_p| > 1$, for $p = 1, 2, 3, 4$, the trivial solution is **unstable**

Save in a matrix *result(j,i)* the value 1

If all $|\gamma_p| \leq 1$, for $p = 1, 2, 3, 4$, the trivial solution is **stable**

Save in a matrix *result(j,i)* the value 0

The matrix *result* as used here will have size length(a_{vec}) × length(ω_{vec}) and is forced to assume the value 1 for an unstable case and 0 for a stable case. It is possible to complete this matrix by doing this to every pair $\omega_{vec}(i)$ and $a_{vec}(j)$, obtaining a stability map in the $\omega \times a$ plane when plotting it, for example, with a *heatmap* command in *MatLab*. This would result in a map of only two colors since it is restricted to ones and zeros.

However, one may also evaluate stability using the maximum value of the Lyapunov characteristic exponents (Λ). In this case, after obtaining the Floquet multipliers for a pair $\omega_{vec}(i)$ and $a_{vec}(j)$, equation (3-14) is used. Thus, for the 2DoF example used until this point:

Use equation (3-14) to obtain the LCEs μ_p, $p = 1, 2, 3, 4$
Save the value of $\Lambda = \max(\mu_p)$ in a matrix *result(j,i)*

Then, both loops are closed and the *result* matrix is obtained. Using this second approach, the matrix *result* also has size length(a_{vec}) $\times$ length(ω_{vec}), but now each element equals the value of Λ and not only zeros and ones. It is also possible to plot this *result* matrix by using a *heatmap* command in *MatLab*, that results in a map with a gradient of colors for the values of Λ in the $\omega \times a$ plane.

Furthermore, another way of making use of the LCEs is by plotting the $\omega \times \Lambda$ plane. To achieve this, the only varying parameter (thus, vector) is the excitation frequency and the other parameters are taken as constants, chosen from the start. Therefore, only one loop is needed to obtain the values of Λ. Thus, for the 2DoF example used until this point:

Start loop for every element $\omega_{vec}(i)$, with $i = 1, \ldots,$ length(ω_{vec})
$T = 2 * \pi / \omega_{vec}(i)$
tspan = period from 0 to T
Numerical integrations
Obtain the monodromy matrix
Obtain the Floquet multipliers
Use equation (3-14) to obtain the LCEs μ_p, $p = 1, 2, 3, 4$
Save in a vector $\Lambda_{vec}(i)$ the maximum value of the μ_p, $p = 1, 2, 3, 4$
End loop for every element $\omega_{vec}(i)$

Where the numerical integrations, obtaining the monodromy matrix, finding the Floquet multipliers and obtaining the LCEs are the same as previously explained. Afterwords it is possible to use the vectors ω_{vec} and Λ_{vec} to obtain a curve in the $\omega \times \Lambda$ plane.

E.1 General discussions

The examples in this dissertation were made using the *MatLab* software. Throughout the examples, the Runge-Kutta method of 4^{th} and 5^{th} order was used, the *ode45* function in *MatLab*, with the default relative error tolerance of 10^{-3} and absolute tolerance of 10^{-6} of the *ode45* function.

Moreover, it is important to highlight the following: when using the

Floquet multipliers γ to obtain stability maps, the criterion that $\gamma_p > 1$ for all p to be considered unstable does not always provide satisfactory results. Due to numerical truncation/approximations used by the software itself when finding the Floquet multipliers [3], at times it is needed to increase the criterion to $|\gamma_p| > 1.01$ for all p to obtain accurate stability maps.

Furthermore, two different *heatmap* plots were proposed in this section: one that uses only Floquet multipliers and another one that makes use of the maximum value of the Lyapunov characteristic exponents Λ. The former forces the map to assume the value 1 for unstable cases and 0 otherwise, thus in the examples throughout this dissertation a dark blue color is chosen to represent unstable regions and a light blue color to represent stable ones. Meanwhile, the latter provides a map with a gradient of the maximum values of LCEs, Λ. It would also be possible to force 0 and 1 values when using the LCEs by applying the condition that they should be unstable if at least one of the values of LCEs were higher than zero and stable otherwise. However, the gradient was used as a way of comparing stability maps. The use of Λ also provides some advantages, that are discussed in details in chapter 4.

Notice that taking only the maximum value of Floquet multipliers to create a gradient (as done with Λ) would not be possible, once they are distorted by the period T [28]. Meanwhile, the maximum value of LCEs is not [35] and can be used as done here.

Bibliography

[1] KIRILLOV, O. N. **Nonconservative Stability Problems of Modern Physics**. Walter de Gruyter GmbH, Germany, 2013.

[2] KRYSINSKI, T.; MALBURET, F. **Mechanical Instability**. ISTE Ltd, 2011.

[3] ZAGUARI, B. **Dynamic analysis of a nonlinear parametrically excited system using electromagnets**. Ph.D thesis, University of Southampton, Southampton, England, 2016.

[4] ECKER, H. **Parametric excitation in engineering systems**. In: 20TH INTERNATIONAL CONGRESS OF MECHANICAL ENGINEERING, PROCEEDINGS OF COBEM 2009, 2009.

[5] BARROW, W. L.; SMITH, D. B.; BAUMANN, F. W. **A further study of oscillatory circuits having periodically varying parameters**. Journal of The Franklin Institute, 221(3):403–416, 1936.

[6] THOMSEN, J. J. **Vibrations and Stability: Advanced Theory, Analysis and Tools**. Springer, 2nd edition, 2003.

[7] WELLS, D. A. **Schaum's outline of theory and problems of Lagrangian Dynamics with a treatment of Euler's Equations of Motion, Hamilton's Equations and Hamilton's Principle**. McGraw-Hill, Inc, USA, 1967.

[8] JELTSEMA, D.; SCHERPEN, J. M. A. **Multidomain modeling of nonlinear networks and systems**. IEEE Control Systems, 29:28–59, 2009.

[9] PREUMONT, A. **Mechatronics: Dynamics of Electromechanical and Piezoelectric Systems**, volume 136. Springer, Brussels, Belgium, 2006.

[10] DAQAQ, M. F. **Dynamics of Particles and Rigid Bodies: A Self-learning Approach**. Wiley-ASME Press, New York University, USA, 1st edition, 2018.

[11] HIRSCHFELDT, N.; LIMA, R.; SAMPAIO, R. **Electromagnetic loudspeaker: an energetic approach**. In: XIV ENCONTRO ACADÊMICO DE MODELAGEM COMPUTACIONAL, LNCC, 2021.

[12] HIRSCHFELDT, N.; LIMA, R.; SAMPAIO, R. **Energy analysis of an electromagnetic loudspeaker**. In: CNMAC 2021, PROCEEDING SERIES OF THE BRAZILIAN SOCIETY OF COMPUTATIONAL AND APPLIED MATHEMATICS, 2021.

[13] MANHÃES, W.; LIMA, R.; SAMPAIO, R.; HAGEDORN, P.; DEU, J. **Lagrangians for electromechanical systems**. Mecánica Computacional, XXXVI:1911–1934, 2018.

[14] LIMA, R.; SAMPAIO, R. **Pitfalls in the dynamics of coupled electromechanical systems**. In: CNMAC 2018, PROCEEDING SERIES OF THE BRAZILIAN SOCIETY OF COMPUTATIONAL AND APPLIED MATHEMATICS, 2018.

[15] LIMA, R.; SAMPAIO, R. **Two parametric excited nonlinear systems due to electromechanical coupling**. Journal of the Brazilian Society of Mechanical Sciences and Engineering, 38:931–943, 2016.

[16] LIMA, R.; SAMPAIO, R.; HAGEDORN, P.; DEU, J. **Comments on the paper "on nonlinear dynamics behavior of an electro-mechanical pendulum excited by a nonideal motor and a chaos control taking into account parametric errors" published in this journal**. Journal of the Brazilian Society of Mechanical Sciences and Engineering, 41:552, 2019.

[17] DANTAS, M. J. H.; SAMPAIO, R.; LIMA, R. **Asymptotically stable periodic orbits of a coupled electromechanical system**. Nonlinear Dynamics, 78:29 – 35, 2014.

[18] HIRSCHFELDT, N. **Energetic analysis of electromechanical systems**. Bachelor thesis, Pontifical Catholic University of Rio de Janeiro - PUC-Rio, Rio de Janeiro, Brazil, 2020.

[19] HIRSCHFELDT, N.; LIMA, R.; SAMPAIO, R. **Parametrization of electromechanical systems must acknowledge Newton and Maxwell**. In: CNMAC 2021, PROCEEDING SERIES OF THE BRAZILIAN SOCIETY OF COMPUTATIONAL AND APPLIED MATHEMATICS, 2021.

[20] INMAN, D. **Engineering Vibration**. Pearson Education, Inc, Upper Saddle River, New Jersey 07458, fourth edition edition, 2014.

[21] LEIPHOLZ, H. **Stability Theory: An Introduction to the Stability of Dynamic Systems and Rigid Bodies**. Academic Press, Inc. (London) LTD, 1970.

[22] RAND, R. H. **Lecture Notes on Nonlinear Vibrations**. Ithaca NY 14853, Cornell University, 2014.

[23] ABARBANEL, H.D.I.; RABINOVICH M.I.; SUSHCHIK M.M. **Introduction to nonlinear dynamics for physicists**, volume 53. World Scientific Publishing Co. Pte. Ltd, P O Box 128, Farrer Road, Singapore 9128, 1993.

[24] DING, W. **Self-Excited Vibration: Theory, Paradigms, and Research Methods**. Springer, 2012.

[25] JORDAN, D.W.; SMITH, P. **Nonlinear Ordinary Differential Equations: An Introduction For Scientists And Engineers**. Oxford University Press, 4th edition, 2007.

[26] HAGEDORN, P.; SPELSBERG-KORSPETER, G. **Active and Passive Vibration Control of Structures**, volume 558. CISM International Centre for Mechanical Sciences, Springer, 2014.

[27] FOLKERS, E. **Floquet's theorem**. Bachelor thesis, University of Groningen, Groningen, Netherlands, 2018.

[28] KAREV, A. **Asynchronous Parametric Excitation in Dynamical Systems**. Ph.D thesis, Technische Universität Darmstadt, Darmstadt, Germany, 2020.

[29] FOSSEN, T. I.; NIJMEIJER H. **Parametric Resonance in Dynamical Systems**. Springer Science+Business Media, Norway/Netherlands, 2012.

[30] TONDL, A.; RUIJGROK, T.; VERHULST F.; NABERGOJ, R. **Autoparametric Resonance in Mechanical Systems**. Cambridge University Press, The Pitt Building, Trumpington Street, Cambridge, United Kingdom, 2000.

[31] KURMANN, L. C. **Introduction to parametric and autoparametric resonance**. INTECH, p. 131–152, 2017.

[32] ACAR, G.; FEENY B. F. **Floquet-based analysis of general responses of the Mathieu equation**. Journal of vibration and acoustics, 2016.

[33] KOVACIC, I.; RAND, R.; SAH, S. M. **Mathieu's equation and its generalizations: Overview of stability charts and their features**. ASME, 70, 2018.

[34] ÁVILA, K.M.V. **Pêndulos paramétricos: ponto de suspensão oscilante e comprimento variável**. Bachelor thesis, Centro de Ciências e Tecnologia, Universidade Estadual do Ceará, Ceará, Brazil, 2012.

[35] CODDINGTON, E.A.; CARLSON, R. **Linear Ordinary Differential Equations**. Society for Industrial and Applied Mathematics, 1997.

[36] SIDERIS, T.C. **Ordinary Differential Equations and Dynamical Systems**. Atlantis Press Paris, 1st edition, 2013.

[37] LIMA, R.; SAMPAIO, R. **Modal analysis of an electromechanical system: a hybrid behavior**. In: PROCEEDING SERIES OF THE BRAZILIAN SOCIETY OF COMPUTATIONAL AND APPLIED MATHEMATICS, CNMAC 2022, 2022.

[38] AVITABILE, P. **Modal Testing: A Practitioner's Guide**. The Society for Experimental Mechanics and John Wiley & Sons Ltd, University of Massachusetts Lowell, USA, 2018.

[39] BRANDT, A. **Noise and Vibration Analysis: Signal Analysis and Experimental Procedures**. John Wiley & Sons Ltd, University of Southern Denmark, Denmark, 2011.

[40] HE, J.; FU, Z.F. **Modal Analysis**. Butterworth-Heinemann, Linacre House, Jordan Hill, Oxford, 1st edition, 2001.